Journal of Scientific Computing manuscript No.
(will be inserted by the editor)

Entropy-Stable Multidimensional Summation-by-Parts Discretizations on *hp*-adaptive Curvilinear Grids for Hyperbolic Conservation Laws

Siavosh Shadpey · David W. Zingg

Received: 14 June 2019 / Accepted: 18 February 2020

Abstract We develop high-order entropy-conservative semi-discrete schemes for hyperbolic conservation laws applicable to non-conforming curvilinear grids arising from *h*-, *p*-, or *hp*-adaptivity. More precisely, building on previous work with conforming grids by Crean *et al.* (Journal of Computational Physics, vol. 356, pp. 410-438, Mar. 2018) and Chan *et al.* (SIAM Journal on Scientific Computing, vol. 41, pp. A2938-A2966, Oct. 2019), we present two schemes: the first couples neighbouring elements in a skew-symmetric method, the second in a pointwise fashion. The key ingredients are degree p diagonal-norm summation-by-parts operators equipped with interface quadrature rules of degree $2p$ or higher, a skew-symmetric geometric mapping procedure using suitable polynomial functions, and a numerical flux that conserves mathematical entropy. Furthermore, entropy-stable schemes are obtained when augmenting the original schemes with a stabilization term that dissipates mathematical entropy at element interfaces. We provide both theoretical and numerical analysis for the compressible Euler equations demonstrating the element-wise conservation, entropy conservation/dissipation, and accuracy properties of the schemes. While both methods produce comparable results, our studies suggest that the scheme coupling elements in a pointwise manner is more computationally efficient.

Keywords Summation-by-Parts – Entropy stability – High order – Non-conforming grids – Curvilinear grids

1 Introduction

In computational fluid dynamics, *a posteriori* error estimates can be used to achieve user-requested error tolerances in an automated, reliable, and efficient manner by adaptively refining the mesh [1,2,3]. Discontinuous Galerkin (DG) methods are amenable to error-based *hp*-adaptivity, since they easily handle hanging nodes (*h*-adaptivity) and support local variations in the degree of the domain's polynomial space without affecting neighbouring elements (*p*-adaptivity). The numerical quadrature rules used to perform integration can be independent of these discretization methods and, hence, interface coupling of neighbouring elements of different degree and size is relatively easily achievable. In contrast, in the summation-by-parts (SBP) and collocated finite-element communities, the cubature and quadrature rules are intertwined with the discretization operators. As such, non-conforming interface cubature nodal distributions arise when performing *h*-, *p*-, or *hp*-adaptivity, and thus schemes constructed for conforming grids can not be blindly applied on non-conforming grids. Although the embedding of cubature rules in these discretization methods causes this issue, it has been shown to be of great importance for both linearly and nonlinearly stable schemes [4,5]. The SBP discrete derivative and integration operators are constructed such that integration by parts is satisfied discretely. To the best of the authors' knowledge, *a priori* nonlinear stability proofs (without assuming exact integration) for high-order methods have so far relied on this property – known as the SBP property [6,7,8,9,10,11].

Siavosh Shadpey, Graduate Student
University of Toronto Institute for Aerospace Studies, Toronto, Ontario, M3H 5T6, Canada
E-mail: sia.shadpey@mail.utoronto.ca

David W. Zingg, University of Toronto Distinguished Professor of Computational Aerodynamics and Sustainable Aviation
University of Toronto Institute for Aerospace Studies, Toronto, Ontario, M3H 5T6, Canada
E-mail: dwz@oddjob.utias.utoronto.ca

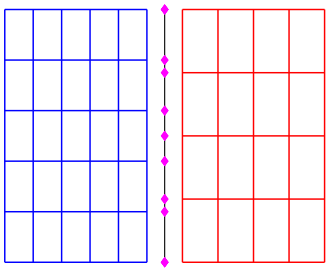

Fig. 1: Pointwise coupling of two non-conforming blocks using an intermediate interface.

Mattsson and Carpenter [12] first introduced interface interpolation operators to construct a finite-difference SBP scheme that is both conservative and energy stable when applied on non-conforming multi-block grids for first-order hyperbolic equations (see also the work of Kopriva [13]). This approach was extended to the second-order wave equation by Wang *et al.* [14]. Kozdon and Wilcox [15] presented a methodology in which the interface coupling is performed in a pointwise manner on an intermediate interface, as illustrated in Figure 1. Their method is also applicable to curved grids with hanging nodes. Lundquist and Nordström [16] noted that SBP schemes suffer from suboptimal convergence rates on non-conforming grids; motivated by this issue, they were able to prove that the accuracy of the schemes is limited by interface interpolation operators which are of degree $p-1$ for degree p discretization operators. In Ref. [17], Friedrich *et al.* proved that an interface quadrature rule of degree $2p$ is needed in order to construct interpolation operators of degree p. Unfortunately, as classical SBP operators are implicitly equipped with quadrature rules of degree $2p-1$ [4], they do not yield degree-preserving interpolation operators. To remedy this issue, the authors constructed finite-difference SBP operators by increasing the boundary stencil size of classical SBP operators such that the norm matrices –which hold the weights of the quadrature rules– are degree $2p$. Their scheme accordingly converged at optimal asymptotic rates on non-conforming grids when coupled with these operators.

The nodal DG method with collocated tensor-product Legendre-Gauss-Lobatto (LGL) solution and cubature nodes has enjoyed much success in the DG and SBP communities since it satisfies the SBP property. We refer the interested reader to Refs. [18,19,20,21,22,23,24,25] for details on energy- and entropy-stable schemes on conforming grids using the LGL operators. These operators, unfortunately, suffer from under-convergence on non-conforming grids since their mass (or norm) matrices are of degree $2p-1$. Carpenter *et al.* [26] and Parsani *et al.* [27] constructed fully-staggered conforming and semi-staggered non-conforming entropy-stable schemes in which the solution was evolved in time on the Legendre-Gauss (LG) nodes whereas the flux computations were performed on the LGL nodes. The semi-staggered technique ensured that the scheme's convergence rate was optimal, since the interface nodes were LG nodes equipped with a degree $2p+1 > 2p$ quadrature rule. Friedrich *et al.* [28] developed an entropy-stable scheme for *hp*-adaptivity on collocated[1], non-conforming affine meshes for which the geometric Jacobian is constant. Their results demonstrated suboptimal convergence rates when using the LGL operators and optimal convergence rates when using the degree-preserving finite-difference SBP operators of Ref. [17].

In Ref. [29], Del Rey Fernández *et al.* developed a framework to construct a first-derivative SBP operator given a quadrature rule in one dimension. This unified many known discretization methods as SBP operators and enabled the construction of novel tensor-product SBP operators using well-known quadrature rules. More recently, this framework has been extended to include multidimensional SBP operators on general elements [30,31] and then used to develop an entropy-stable scheme on curved conforming meshes by Crean *et al.* [11]. This scheme couples neighbouring elements in a skew-symmetric fashion such that it is compatible with operators that do not include boundary nodes, such as the nodal tensor-product DG methods with collocated solution and cubature LG nodes, without the use of staggered grids. In Ref. [32], building on previous work (e.g. Ref. [10]), Chan and coauthors constructed an entropy-stable scheme with the LG operators which couples interior elements in a pointwise manner, again, without the use of staggered grids.

The primary objective of this paper is to develop high-order, entropy-stable, and element-wise conservative semi-discrete schemes for hyperbolic conservation laws applicable to non-conforming curvilinear

[1] The term "collocated mesh" is used here as the opposite of "staggered mesh" and does not refer to a finite-element method with collocated solution and cubature nodes.

(unstructured) grids arising from *h*-, *p*-, or *hp*-adaptivity[2]. We first present an extension of Crean *et al.*'s scheme [11] with the skew-symmetric inter-element coupling term. We also develop a second scheme using the pointwise inter-element coupling procedure of Chan [10]. These schemes can also be viewed as a generalization of the discretization method by Friedrich *et al.* [28] to curved grids and to multidimensional SBP operators on general elements with or without boundary nodes. Furthermore, we numerically compare the efficiency and robustness of both schemes.

The paper is organized as follows. In Section 2, we introduce the notation, and in Section 3, we present the ingredients needed to construct our schemes. After introducing the semi-discrete entropy-stable schemes in Section 4, we demonstrate their properties both theoretically and numerically in Sections 5 and 6, respectively. Finally, in Section 7, we provide our final remarks.

2 Notation

The notation used in this paper closely follows that of the second author's previous papers (e.g. Refs. [30,31,11]).

For a given set of partial differential equations (PDEs) in the domain $\Omega \subset \mathbb{R}^d$, where $d = 1$, 2, or 3 is the spatial dimension, we tessellate Ω into n_e non-overlapping (possibly curved) elements $\mathcal{T}_h \equiv \{\{\Omega_\kappa\}_{\kappa=1}^{n_e} \mid \Omega = \cup_{\kappa=1}^{n_e} \overline{\Omega}_\kappa,\ \Omega_\kappa \cap \Omega_\tau = \emptyset,\ \kappa \neq \tau\}$, where we consider $\overline{\Omega}_\kappa$ the closure of the open element Ω_κ, i.e. $\overline{\Omega}_\kappa \equiv \Omega_\kappa \cup \partial\Omega_\kappa$. The tessellation $\mathcal{T}_h$ is also associated with a boundary set composed of $d-1$ dimensional elements referred to as facets, $\Gamma_h \equiv \{\gamma\}$, which can be subdivided into a boundary facet set, $\Gamma_{h,b} \equiv \{\gamma \in \Gamma_h \mid \gamma \cap \partial\Omega \neq \emptyset\}$, and an interior facet set, $\Gamma_{h,i} \equiv \{\Gamma_h \setminus \Gamma_{h,b}\}$. Each facet $\gamma \in \Gamma_{h,i}$ borders two neighbouring elements (often indicated by κ and ν). In this work, we exclusively deal with scenarios where $\Gamma_{h,b} = \emptyset$ and $\Gamma_{h,i} = \Gamma_h$ through the imposition of periodic boundary conditions. To indicate a sum over all the facets of element κ, i.e. $\Gamma_h^{(\kappa)} \equiv \{\gamma \in \partial\Omega_\kappa\}$, the notation $\sum_{\kappa\gamma} \cdot$ is used. Finally, each physical element is geometrically mapped to a reference element and the symbol $\hat{\cdot}$ is used when referring to the reference domain (e.g. $\hat{\Omega}_\kappa$).

The notation $\vec{\cdot}$ is reserved to denote directional vectors of length d; for instance, $\vec{\xi} \equiv [\xi_1, ..., \xi_d]^{\mathrm{T}}$ and $\vec{x} \equiv [x_1, ..., x_d]^{\mathrm{T}}$ are the vectors of reference and physical spatial coordinates, respectively. We use script type uppercase letters to denote scalar functions, e.g. $\mathcal{S}(\vec{x}) \in \mathbb{R}$, and bold type for vector-valued functions, e.g. $\boldsymbol{\mathcal{U}}(\vec{x}) \in \mathbb{R}^m$. The restriction of an m-vector-valued function $\boldsymbol{\mathcal{U}}(\vec{x})$ on the nodal set $S_{\Omega_\kappa} \equiv \{\vec{x}_j\}_{j=1}^{N_\kappa}$ of element κ is denoted by the lowercase bold type letter $\boldsymbol{u}_\kappa \in \mathbb{R}^{m \cdot N_\kappa}$, where the values of $\boldsymbol{\mathcal{U}}$ evaluated at the first node run first, followed by those of the second node, etc.:

$$\boldsymbol{u}_\kappa = \left[\boldsymbol{\mathcal{U}}(\vec{x}_1)^{\mathrm{T}} \cdots \boldsymbol{\mathcal{U}}(\vec{x}_{N_\kappa})^{\mathrm{T}}\right]^{\mathrm{T}}.$$

Matrices are denoted by sans-serif uppercase letters, e.g. $\mathsf{X} \in \mathbb{R}^{n \times m}$. The symbols $\circ$ and $\otimes$ are used to represent the Hadamard and Kronecker products, respectively. Finally, $\mathcal{P}$ and $\mathcal{Q} \in \mathbb{P}_p(\Omega)$ are reserved for functions spanning the degree p polynomial space defined in the domain Ω; $\boldsymbol{p}$ and $\boldsymbol{q}$ for their restrictions on a nodal set; $\mathbf{1}_n$ and $\mathbf{0}_n$ for column-vectors of length n consisting of all ones and zeros, respectively; and I_n for the $n \times n$ identity matrix.

3 Theoretical Development

In this section, we present the key concepts needed to construct the two entropy-conservative schemes of this paper.

3.1 Multidimensional summation-by-parts operators

The first key concept used to develop the schemes in Section 4 is multidimensional SBP operators on general elements, which were first introduced in Ref. [30]. Their definition is restated here for completeness.

[2] While this paper is concerned with schemes applicable to non-conforming grids, *a posteriori* error estimates are not used here to drive mesh adaptation.

Definition 1 (Multidimensional summation-by-parts operators) The operator $\hat{\mathsf{D}}_{\xi_i} \in \mathbb{R}^{N\times N}$ of degree p is said to be a summation-by-parts approximation of the first-derivative $\frac{\partial}{\partial \xi_i}$ on the nodal set $S_{\hat{\Omega}} \equiv \{\vec{\xi}_j\}_{j=1}^{N}$ of a reference element with domain $\hat{\Omega} \subset \mathbb{R}^d$, if $\hat{\mathsf{D}}_{\xi_i}$, $\hat{\mathsf{Q}}_{\xi_i}$, $\hat{\mathsf{E}}_{\xi_i}$, and $\hat{\mathsf{H}} \in \mathbb{R}^{N\times N}$ satisfy the following conditions:

1. $[\hat{\mathsf{D}}_{\xi_i}\boldsymbol{p}]_j = \frac{\partial \mathcal{P}}{\partial \xi_i}(\vec{\xi}_j),\ \forall\ \mathcal{P} \in \mathbb{P}_p(\hat{\Omega}),\ j \in \{1, ..., N\}$;
2. $\hat{\mathsf{D}}_{\xi_i} = \hat{\mathsf{H}}^{-1}\hat{\mathsf{Q}}_{\xi_i}$, where $\hat{\mathsf{H}} = \hat{\mathsf{H}}^{\mathrm{T}}$, and $\boldsymbol{z}^{\mathrm{T}}\hat{\mathsf{H}}\boldsymbol{z} > 0,\ \forall\ \boldsymbol{z} \neq \boldsymbol{0}$; and
3. $\hat{\mathsf{Q}}_{\xi_i} + \hat{\mathsf{Q}}_{\xi_i}^{\mathrm{T}} = \hat{\mathsf{E}}_{\xi_i}$, and $\boldsymbol{q}^{\mathrm{T}}\hat{\mathsf{E}}_{\xi_i}\boldsymbol{p} = \int_{\partial\hat{\Omega}} \mathcal{P}\mathcal{Q}n_{\xi_i}\ \mathrm{d}\Gamma,\ \forall\ \mathcal{P}, \mathcal{Q} \in \mathbb{P}_r(\hat{\Omega})$,

where n_{ξ_i} is the component of the outward-pointing normal unit vector in the ξ_i-direction and $r \geq p$.

The first condition ensures that the derivative operator $\hat{\mathsf{D}}_{\xi_i} \in \mathbb{R}^{N\times N}$ accurately approximates first-order derivative terms to a given degree. The matrix $\hat{\mathsf{H}} \in \mathbb{R}^{N\times N}$, known as the norm or mass matrix, is symmetric positive-definite. In this paper, we only consider diagonal-norm SBP operators, for which the $\hat{\mathsf{H}}$ matrix is diagonal. The entries of the $\hat{\mathsf{H}}$ matrix along with the nodal set $S_{\hat{\Omega}}$ form a $q \geq 2p-1$ cubature rule. This can be written as

$$\boldsymbol{1}^{\mathrm{T}}\hat{\mathsf{H}}\boldsymbol{p} = \int_{\hat{\Omega}} \mathcal{P}\ \mathrm{d}\Omega,\ \forall \mathcal{P} \in \mathbb{P}_q(\hat{\Omega}).$$

Condition 3 requires that the matrix $\hat{\mathsf{E}}_{\xi_i} \in \mathbb{R}^{N\times N}$ approximates surface integrals in the ξ_i-direction. All 3 conditions of Definition 1 can be combined to show that the SBP operators discretely mimic integration by parts with a one-to-one correspondence between the continuous and discrete terms, i.e.

$$\underbrace{\int_{\hat{\Omega}} \mathcal{V}\frac{\partial \mathcal{U}}{\partial \xi_i}\ \mathrm{d}\Omega}_{\wr\wr} + \underbrace{\int_{\hat{\Omega}} \frac{\partial \mathcal{V}}{\partial \xi_i}\mathcal{U}\ \mathrm{d}\Omega}_{\wr\wr} = \underbrace{\int_{\partial\hat{\Omega}} \mathcal{V}\mathcal{U}n_{\xi_i}\ \mathrm{d}\Gamma}_{\wr\wr}$$
$$\boldsymbol{v}^{\mathrm{T}}\hat{\mathsf{Q}}_{\xi_i}\boldsymbol{u} \quad + \quad \boldsymbol{v}^{\mathrm{T}}\hat{\mathsf{Q}}_{\xi_i}^{\mathrm{T}}\boldsymbol{u} \quad = \quad \boldsymbol{v}^{\mathrm{T}}\hat{\mathsf{E}}_{\xi_i}\boldsymbol{u},$$

$\forall i \in \{1, ..., d\}$. We emphasize that this exact discrete relationship holds for $\boldsymbol{v}, \boldsymbol{u} \in \mathbb{R}^N$ corresponding to any functions $\mathcal{V}$ and $\mathcal{U}$ that are square integrable and whose weak first derivatives are also square integrable (i.e. $\mathcal{V}$,$\mathcal{U} \in H^1(\hat{\Omega})$).

Since boundary and inter-element conditions are generally weakly imposed in a pointwise manner [31], it is important to decompose the surface operators $\hat{\mathsf{E}}_{\xi_i}$ into an interpolation/extrapolation operator, a facet mass matrix, and an outward-pointing normal component for each of the n_f linear and non-overlapping facets $\hat{\gamma}$ of the reference element. Following Ref. [31], this decomposition can be represented as

$$\hat{\mathsf{E}}_{\xi_i} = \sum_{\hat{\gamma}\in\partial\hat{\Omega}} \hat{\mathsf{E}}_{\xi_i}^{\gamma} = \sum_{\hat{\gamma}\in\partial\hat{\Omega}} n_{\gamma,\xi_i}\mathsf{R}_{\gamma}^{\mathrm{T}}\hat{\mathsf{B}}_{\gamma}\mathsf{R}_{\gamma}, \tag{1}$$

where $\mathsf{R}_{\gamma} \in \mathbb{R}^{N_{\gamma}\times N}$ interpolates/extrapolates[3] functions from the volume nodal set $S_{\hat{\Omega}}$ onto the facet nodal set $S_{\hat{\gamma}} \equiv \{\vec{\xi}_{\hat{\gamma},k}\}_{k=1}^{N_{\gamma}}$, and $\hat{\mathsf{B}}_{\gamma} \in \mathbb{R}^{N_{\gamma}\times N_{\gamma}}$ is a diagonal facet mass matrix holding quadrature weights along its diagonal. To comply with the accuracy requirement of condition 3 of Definition 1, we impose individual accuracy conditions on the extrapolation operator and the facet mass matrix. Specifically, we require that[4]

$$[\mathsf{R}_{\gamma}\boldsymbol{p}]_k = [\boldsymbol{p}_{\hat{\gamma}}]_k = \mathcal{P}(\vec{\xi}_{\hat{\gamma},k}),\ \forall \mathcal{P} \in \mathbb{P}_r(\hat{\Omega}),\ k \in \{1, ..., N_{\gamma}\}, \tag{2a}$$
$$\boldsymbol{1}^{\mathrm{T}}\hat{\mathsf{B}}_{\gamma}\boldsymbol{p}_{\hat{\gamma}} = \int_{\partial\hat{\Omega}_{\gamma}} \mathcal{P}\ \mathrm{d}\Gamma,\ \forall \mathcal{P} \in \mathbb{P}_s(\partial\hat{\Omega}_{\gamma}), \tag{2b}$$

where $s \geq 2r$ and, as previously mentioned, $r \geq p$.

[3] For brevity, we will refer to the R_{γ} matrix as the extrapolation operator instead of the interpolation/extrapolation operator for the remainder of this work.

[4] (2b) is sufficient but not necessary to construct SBP operators. For instance, the LGL operators are equipped with a quadrature rule of degree $s = 2p-1 \not\geq 2p$ yet they still satisfy the SBP property. In this work, we exclusively deal with SBP operators that obey (2b).

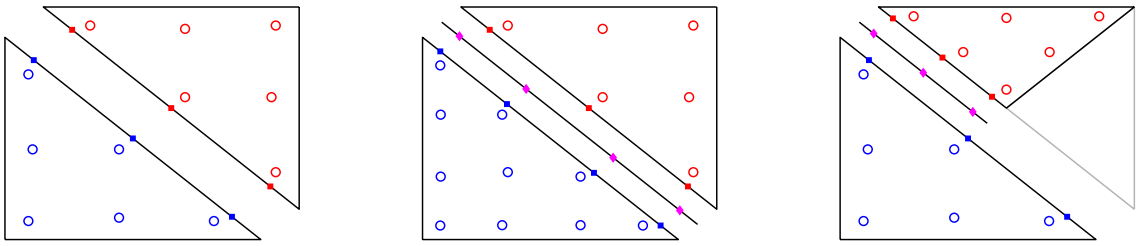

(a) Conforming interface.

(b) Non-conforming interface due to *p*-adaptivity.

(c) Non-conforming interface due to *h*-adaptivity.

Fig. 2: Visualization of coupling of conforming and non-conforming neighbouring elements. Non-conforming elements require an intermediate interface.

3.1.1 Construction of SBP operators

To satisfy (2b), we choose (or construct) a facet quadrature rule of degree $s \geq 2r$, which defines both $\hat{\mathsf{B}}_\gamma$ and $S_{\hat{\gamma}}$ for all the n_f facets of the reference element. Similarly, for the volume cubature rule, we choose (or construct) a cubature rule of degree $q \geq 2p-1$, which defines both $\hat{\mathsf{H}}$ and $S_{\hat{\Omega}}$. Thereafter, we construct R_γ as follows: we define n_r as the cardinality of the monomial basis of total degree r (i.e. the number of linearly independent basis functions spanning the degree r polynomial space), we assume that the volume nodal set $S_{\hat{\Omega}}$ produces a degree r full-column-rank Vandermonde matrix[5] $\hat{\mathsf{V}}_\Omega \in \mathbb{R}^{N\times n_r}$, and we let $\hat{\mathsf{V}}_\gamma \in \mathbb{R}^{N_\gamma \times n_r}$ be the degree r_κ Vandermonde matrix evaluated at the nodal set $S_{\hat{\gamma}}$. We then construct R_γ as

$$\mathsf{R}_\gamma \equiv \hat{\mathsf{V}}_\gamma \hat{\mathsf{V}}_\Omega^\dagger,$$

where $\dagger$ denotes the Moore-Penrose pseudo-inverse, e.g. $\mathsf{A}^\dagger \equiv (\mathsf{A}^\mathrm{T}\mathsf{A})^{-1}\mathsf{A}^\mathrm{T}$ for a non-square matrix A with full column rank. Thus, by construction, this operator satisfies (2a). After constructing $\hat{\mathsf{E}}_{\xi_i}$ from (1), we follow the procedure outlined in Theorem 2 of Ref. [31] to construct $\hat{\mathsf{Q}}_{\xi_i}$ and $\hat{\mathsf{D}}_{\xi_i}$.

In the case of collocated volume and facet SBP nodes, the extrapolation operator simplifies to the delta Kronecker operator, i.e. $[\mathsf{R}_\gamma]_{jl} = \delta_{jl},\ \forall j \in \{1,...,N\},\ l \in \{1,...,N_\gamma\}$, and simply picks the facet nodes that collocate with the volume nodes instead of performing an interpolation or extrapolation. Furthermore, the surface operators $\hat{\mathsf{E}}_{\xi_i}$ are diagonal (accordingly, we refer to this subset of SBP operators as diagonal-E operators). It has been shown that the inter-element coupling of entropy-stable schemes on conforming grids with diagonal-E operators, such as the LGL operators, is less computationally expensive than those with dense-E operators, such as the LG operators (see, for instance, Refs. [33,34,32]). However, in Ref. [35], our numerical studies suggested that dense-E entropy-stable schemes are computationally more efficient than diagonal-E entropy-stable schemes on non-conforming triangular grids primarily due to the higher accuracy properties provided by dense-E operators compared to diagonal-E operators.

3.2 High-order interface operators

The second key concept used to develop the schemes in Section 4 is high-order intermediate interface quadrature rules and interpolation/extrapolation operators used to couple elements with non-conforming interfaces arising from *h*-, *p*-, and *hp*-adaptivity.

3.2.1 Non-conforming elements resulting from p-adaptivity

On conforming grids, neighbouring elements share the same facet nodes, as shown in Figure 2(a) and, hence, inter-element coupling is usually performed in a pointwise manner. When the degree of one of two neighbouring elements is changed, the facet nodes no longer conform. In such a case, we introduce a shared intermediate interface (or mortar element) to enable the pointwise coupling of the elements, as illustrated in Figure 2(b). The conditions that must be satisfied by the quadrature rule on the intermediate interface and the interface interpolation/extrapolation operators is provided in Definition 2.

[5] In the case that this assumption does not hold, a different cubature rule can be chosen or constructed.

Definition 2 (High-order intermediate interface operators) Let $S_{\kappa\hat{\gamma}} \equiv \{\vec{\xi}_{\kappa\hat{\gamma},k}\}_{k=1}^{N_{\kappa\gamma}}$ and $S_{\nu\hat{\gamma}} \equiv \{\vec{\xi}_{\nu\hat{\gamma},l}\}_{l=1}^{N_{\nu\gamma}}$ be the reference facet nodal sets of two different degree neighbouring elements with conforming facet lengths, and $S_{\hat{I}} \equiv \{\vec{\xi}_{\hat{I},m}\}_{m=1}^{N_I}$ be the facet nodal set of the intermediate interface. The intermediate interface preserves the design-order accuracy of the SBP operators and the SBP property if it satisfies the following conditions:

1. $[\mathsf{P}_{\kappa\gamma\to I}\boldsymbol{q}_{\kappa\hat{\gamma}}]_m = \mathcal{Q}(\vec{\xi}_{\hat{I},m}),\ \forall\mathcal{Q}\in\mathbb{P}_{r_\kappa}(\partial\hat{\Omega}_\gamma),\ m\in\{1,...,N_I\}$,
   $[\mathsf{P}_{\nu\gamma\to I}\boldsymbol{q}_{\nu\hat{\gamma}}]_m = \mathcal{Q}(\vec{\xi}_{\hat{I},m}),\ \forall\mathcal{Q}\in\mathbb{P}_{r_\nu}(\partial\hat{\Omega}_\gamma),\ m\in\{1,...,N_I\}$; and
2. $\mathsf{R}_{\kappa\gamma}^{\mathrm{T}}\hat{\mathsf{B}}_{\kappa\gamma}\mathsf{R}_{\kappa\gamma} = \mathsf{R}_{\kappa\gamma}^{\mathrm{T}}\mathsf{P}_{\kappa\gamma\to I}^{\mathrm{T}}\hat{\mathsf{B}}_I\mathsf{P}_{\kappa\gamma\to I}\mathsf{R}_{\kappa\gamma}$,
   $\mathsf{R}_{\nu\gamma}^{\mathrm{T}}\hat{\mathsf{B}}_{\nu\gamma}\mathsf{R}_{\nu\gamma} = \mathsf{R}_{\nu\gamma}^{\mathrm{T}}\mathsf{P}_{\nu\gamma\to I}^{\mathrm{T}}\hat{\mathsf{B}}_I\mathsf{P}_{\nu\gamma\to I}\mathsf{R}_{\nu\gamma}$,

where $r_\kappa \geq p_\kappa$, $r_\nu \geq p_\nu$, $\boldsymbol{q}_{\kappa\hat{\gamma}}$ and $\boldsymbol{q}_{\nu\hat{\gamma}}$ hold the values of polynomial $\mathcal{Q}$ evaluated on the nodal sets $S_{\kappa\hat{\gamma}}$ and $S_{\nu\hat{\gamma}}$ respectively, $\mathsf{P}_{\kappa\gamma\to I}\in\mathbb{R}^{N_I\times N_{\kappa\gamma}}$ and $\mathsf{P}_{\nu\gamma\to I}\in\mathbb{R}^{N_I\times N_{\nu\gamma}}$ interpolate/extrapolate[6] functions from $S_{\kappa\hat{\gamma}}$ and $S_{\nu\hat{\gamma}}$, respectively, to $S_{\hat{I}}$, and $\hat{\mathsf{B}}_{\kappa\gamma}\in\mathbb{R}^{N_{\kappa\gamma}\times N_{\kappa\gamma}}$, $\hat{\mathsf{B}}_{\nu\gamma}\in\mathbb{R}^{N_{\nu\gamma}\times N_{\nu\gamma}}$, and $\hat{\mathsf{B}}_I\in\mathbb{R}^{N_I\times N_I}$ are the diagonal facet mass matrices holding the quadrature weights of the quadrature nodal sets $S_{\kappa\hat{\gamma}}$, $S_{\nu\hat{\gamma}}$, and $S_{\hat{I}}$ respectively.

The first condition ensures that the interface extrapolation operators are design-order accurate. Condition 2 enforces that discrete inner products performed on the intermediate interface be equivalent to discrete inner products performed on the element's facet. For instance, for element κ, this can be mathematically represented as

$$(\mathsf{R}_{\kappa\gamma}\boldsymbol{v}_\kappa)^{\mathrm{T}}\hat{\mathsf{B}}_{\kappa\gamma}(\mathsf{R}_{\kappa\gamma}\boldsymbol{u}_\kappa) = (\mathsf{P}_{\kappa\gamma\to I}\mathsf{R}_{\kappa\gamma}\boldsymbol{v}_\kappa)^{\mathrm{T}}\hat{\mathsf{B}}_I(\mathsf{P}_{\kappa\gamma\to I}\mathsf{R}_{\kappa\gamma}\boldsymbol{u}_\kappa),\ \forall\boldsymbol{v}_\kappa,\ \boldsymbol{u}_\kappa\in\mathbb{R}^{N_\kappa}.$$

The second condition consequently ensures that the SBP property is automatically preserved on non-conforming grids and is key for the conservation and stability properties of the schemes presented in this work.

The interface extrapolation operator $\mathsf{P}_{\kappa\gamma\to I}$ is constructed as follows: we define n_{r_κ} as the cardinality of the monomial basis of total degree r_κ, we assume that the facet nodal set $S_{\kappa\hat{\gamma}}$ produces a degree r_κ full-column-rank Vandermonde matrix $\hat{\mathsf{V}}_{\kappa\gamma}\in\mathbb{R}^{N_{\kappa\gamma}\times n_{r_\kappa}}$, and we let $\hat{\mathsf{V}}_I\in\mathbb{R}^{N_I\times n_{r_\kappa}}$ be the degree r_κ Vandermonde matrix evaluated at the nodal set $S_{\hat{I}}$. We then construct $\mathsf{P}_{\kappa\gamma\to I}$ as

$$\mathsf{P}_{\kappa\gamma\to I} \equiv \hat{\mathsf{V}}_I\hat{\mathsf{V}}_{\kappa\gamma}^{\dagger}.$$

The interface extrapolation operator $\mathsf{P}_{\nu\gamma\to I}$ is constructed in a similar manner. Thus, by construction, these extrapolation operators satisfy condition 1 of Definition 2. To fulfill condition 2, it suffices that the interface's mass matrix $\hat{\mathsf{B}}_I$ be of degree $s_I \geq \max(s_\kappa, s_\nu)$ where $s_\kappa \geq 2r_\kappa$ and $s_\nu \geq 2r_\nu$ are the degrees of the facet mass matrices $\hat{\mathsf{B}}_{\kappa\gamma}$ and $\hat{\mathsf{B}}_{\nu\gamma}$ respectively. The proof is shown in Lemma 1 of Appendix A. In this work, to minimize the floating point operations, we set the intermediate interface's quadrature rule as the more accurate facet quadrature rule of the two neighbouring elements. For instance, if $s_\kappa > s_\nu$, then we have $S_{\hat{I}} = S_{\kappa\hat{\gamma}}$ and $\hat{\mathsf{B}}_I = \hat{\mathsf{B}}_{\kappa\gamma}$.

3.2.2 Non-conforming elements resulting from h- and hp-adaptivity

In the case of neighbouring elements of constant degree with hanging nodes, we subdivide the largest element's facet (parent facet) into subfacets (child facets) that conform in length with the smaller neighbouring element's facets, as shown in Figure 2(c). The parent facet's quadrature rule is then affinely mapped onto the child facets (e.g. $\hat{\mathsf{B}}_{\kappa\gamma} \leftarrow \frac{1}{n_c}\hat{\mathsf{B}}_{\kappa\gamma}$, where n_c is the number of child facets for a given parent facet). Since the lengths of neighbouring facets are now equal, but the nodal distributions of the largest element's parent and child facets are not, we develop high-order intermediate interfaces that satisfy Definition 2. In the case of neighbouring elements of different degrees with hanging nodes, the same procedure is followed.

[6] Similar to R_γ, we will refer to these operators as interface extrapolation operators for brevity.

3.3 Curvilinear transformation

When a curved geometry is represented using a linear mesh, the solution error may be limited to second order independent of the degree of the discretization method. The use of high-order curved elements is thus essential in such cases to benefit from the accuracy properties of high-order discretization methods [36,37]. So far, we have introduced SBP and intermediate interface operators on reference elements. In this subsection, we outline the procedure to construct the SBP and interface operators on a curved physical element given those of the corresponding reference element. Under Assumption 1, this procedure, which follows closely that of Crean *et al.* [11], ensures that the SBP property is preserved, that constant functions are exactly extrapolated and differentiated, and that the physical operators are design-order accurate[7]. These properties are required for conservation, freestream preservation, entropy conservation, and accuracy.

Assumption 1 *First, we assume that we have valid SBP and intermediate interface operators, satisfying Definitions 1 and 2, on the reference element* $\overline{\hat{\Omega}}_\kappa$. *Second, we assume that we have a unique and invertible (time-independent) degree* l *geometric mapping polynomial function* $\mathcal{M}_\kappa : \overline{\hat{\Omega}}_\kappa \to \overline{\Omega}_\kappa$ *which maps any point* $\vec{\xi}_k \in \overline{\hat{\Omega}}_\kappa$ *to the corresponding point* $\vec{x}_k \in \overline{\Omega}_\kappa$, *i.e.* $\vec{x}_k = \mathcal{M}_\kappa(\vec{\xi}_k)$. *Finally, we require that* $l \leq p_{\min} + 1$ *in two dimensions, and* $l \leq \lfloor \frac{p_{\min}}{2} \rfloor + 1$, *in three dimensions, where* $\lfloor \cdot \rfloor$ *is the floor operator and* $p_{\min} \equiv \min_{\Omega_\kappa \in \mathcal{T}_h}\{p_\kappa\}$ *is the lowest degree SBP operator in the tessellated domain.*

Before constructing the physical operators, we define the geometric Jacobian of the transformation in element κ as

$$[\mathcal{J}_\kappa(\vec{\xi}_k)]_{ij} \equiv \frac{\partial x_i}{\partial \xi_j}(\vec{\xi}_k) = \frac{\partial \mathcal{M}_{\kappa,i}}{\partial \xi_j}(\vec{\xi}_k),\ \forall i \in \{1,...,d\},\ j \in \{1,...,d\},\ \vec{\xi}_k \in \overline{\hat{\Omega}}_\kappa.$$

Furthermore, $[\mathcal{J}_\kappa(\vec{\xi}_k)]^{-1}_{ij} = \frac{\partial \xi_i}{\partial x_j}(\vec{\xi}_k)$ and $|\mathcal{J}_\kappa(\vec{\xi}_k)| = |\frac{\partial \vec{x}}{\partial \vec{\xi}}(\vec{\xi}_k)|$ are the inverse Jacobian and the determinant of the Jacobian, respectively.

The physical facet operators are constructed as follows:

$$\begin{aligned}
[\mathsf{B}_I]_{ll} &= [\hat{\mathsf{B}}_I]_{ll} |\mathcal{J}_\kappa(\vec{\xi}_{\hat{I},l})|,\ \forall \vec{\xi}_{\hat{I},l} \in S_{\hat{I}}, \\
[\mathsf{N}^{(\kappa)}_{I,x_j}]_{ll} &= \sum_{i=1}^{d} n_{\gamma,\xi_i} \frac{\partial \xi_i}{\partial x_j}(\vec{\xi}_{\hat{I},l}),\ \forall \vec{\xi}_{\hat{I},l} \in S_{\hat{I}},\ j \in \{1,...,d\},\ \text{and} \\
\mathsf{E}_{x_j} &= \sum_{\kappa\gamma} \mathsf{R}^{\mathrm{T}}_{\kappa\gamma} \mathsf{P}^{\mathrm{T}}_{\kappa\gamma\to I} \mathsf{B}_I \mathsf{N}^{(\kappa)}_{I,x_j} \mathsf{P}_{\kappa\gamma\to I} \mathsf{R}_{\kappa\gamma},\ \forall j \in \{1,...,d\}.
\end{aligned}$$

Note that the normal matrix $\mathsf{N}^{(\kappa)}_{I,x_j} \in \mathbb{R}^{N_I \times N_I}$ is diagonal and that the reference extrapolation operators have been used without modification. The physical element's mass matrix is constructed as

$$[\mathsf{H}]_{kk} = [\hat{\mathsf{H}}]_{kk} |\mathcal{J}_\kappa(\vec{\xi}_k)|,\ \forall \vec{\xi}_k \in S_{\hat{\Omega}}.$$

We then construct $\mathsf{Q}_{x_j},\ \forall j \in \{1,...,d\}$ as $\mathsf{Q}_{x_j} = \mathsf{S}_{x_j} + \frac{1}{2}\mathsf{E}_{x_j}$, where S_{x_j} is a skew-symmetric matrix defined as

$$[\mathsf{S}_{x_j}]_{kl} = \frac{1}{2}\sum_{i=1}^{d}\left(|\mathcal{J}_\kappa(\vec{\xi}_k)|\frac{\partial \xi_i}{\partial x_j}(\vec{\xi}_k)[\hat{\mathsf{Q}}_{\xi_i}]_{kl} - |\mathcal{J}_\kappa(\vec{\xi}_l)|\frac{\partial \xi_i}{\partial x_j}(\vec{\xi}_l)[\hat{\mathsf{Q}}_{\xi_i}]_{lk}\right),\ \forall \vec{\xi}_k, \vec{\xi}_l \in S_{\hat{\Omega}},\ j \in \{1,...,d\}.$$

Finally,

$$\mathsf{D}_{x_j} = \mathsf{H}^{-1}\mathsf{Q}_{x_j},\ \forall j \in \{1,...,d\}. \tag{3}$$

It is important to satisfy the metric identities for freestream preservation [38,39]. For fixed meshes, the metric identities are:

$$\sum_{i=1}^{d} \frac{\partial}{\partial \xi_i}\left(|\mathcal{J}|\frac{\partial \xi_i}{\partial x_j}\right) = 0,\ \forall j \in \{1,...,d\}. \tag{4}$$

Due to the definitions of Q_{x_j} and D_{x_j}, it can be shown that the discrete version of (4) is [11,40]

$$\mathsf{D}_{x_j}\mathbf{1} = \mathbf{0},\ \forall j \in \{1,...,d\}, \tag{5}$$

[7] We refer the interested reader to Ref. [11] for the proofs.

which, unlike its continuous counterpart, is not generally satisfied on curvilinear grids. The underlying reason is that the physical operators are not explicitly constructed in such a way to satisfy an analogous polynomial exactness condition to condition 1 of Definition 1. Consequently, the SBP derivative operators do not exactly differentiate polynomials in $\mathbb{P}_p(\Omega)$ on curvilinear grids and, therefore, (5) – which simply states that the physical derivative operators can exactly differentiate constant functions – might not hold. However, under Assumption 1, (5) is automatically satisfied: by carefully limiting the degree of the geometric transformation function in two and three dimensional spaces, we ensure that the metric terms $|\mathcal{J}|\frac{\partial \xi_i}{\partial x_j}$ are at most degree $p_{\min}$ polynomial functions with respect to $\vec{\xi}$ and, thus, can be exactly extrapolated and differentiated by reference SBP operators of degree $p_{\min}$ or higher. In other words, in such a case, the discrete metric identities follow immediately, since they are equivalent to the continuous ones. If a higher-order mapping function is required than $\lfloor \frac{p_{\min}}{2} \rfloor + 1$ in three-dimensions to represent the geometry of interest, the metric terms can be defined such that the discrete metric identities are enforced, for instance, by using the curl formulation of Ref. [40] (which is based on the work of Refs. [41] and [42]) or by solving local quadratic optimization problems as performed in Ref. [11].

3.4 Euler equations and the entropy inequality

While the theory presented in this paper is applicable to any hyperbolic system of conservation laws endowed with an entropy pair, in this work, we focus on the Euler equations which govern compressible inviscid flows. The d-dimensional Euler equations in (conservative differential form) are

$$\frac{\partial \boldsymbol{\mathcal{U}}}{\partial t} + \sum_{i=1}^{d} \frac{\partial \boldsymbol{\mathcal{F}}_{x_i}}{\partial x_i} = \mathbf{0} \quad \text{in } \Omega \times I \tag{6}$$

with

$$\boldsymbol{\mathcal{U}} = \begin{bmatrix} \rho \\ \rho \vec{u} \\ e \end{bmatrix}, \ \boldsymbol{\mathcal{F}}_{x_i} = \begin{bmatrix} \rho u_i \\ \vec{f}^{(\text{mom})}_{x_i} \\ \rho u_i h \end{bmatrix}, \ \vec{u} = \begin{bmatrix} u_1 \\ \vdots \\ u_d \end{bmatrix}, \text{ and } \vec{f}^{(\text{mom})}_{x_i} = \begin{bmatrix} \rho u_1 u_i + p\delta_{1i} \\ \vdots \\ \rho u_d u_i + p\delta_{di} \end{bmatrix},$$

where $I \equiv (0, T) \subset \mathbb{R}$ is a time interval, ρ is the density, u_i is the velocity in the x_i-direction, e is the total energy per unit volume, p is the pressure, and $h \equiv \frac{e+p}{\rho}$ is the total enthalpy per unit mass of the fluid. The vector $\boldsymbol{\mathcal{U}}(\vec{x}, t) \in \mathcal{H} \in \mathbb{R}^m$ holds the conservative variables which belong to the convex set of physically admissible states denoted by $\mathcal{H}$[8]. The vector $\boldsymbol{\mathcal{F}}_{x_i}(\vec{x}, t, \boldsymbol{\mathcal{U}}) \in \mathbb{R}^m$ holds the inviscid fluxes in the x_i-direction, and $\vec{u}(\boldsymbol{\mathcal{U}}) \in \mathbb{R}^d$ and $\vec{f}^{(\text{mom})}_{x_i}(\boldsymbol{\mathcal{U}}) \in \mathbb{R}^d$ are respectively the velocity and x_i-direction momentum flux vectors, where $m = d+2$ is the number of equations in the system. For calorically perfect gases, the pressure is given by

$$p = (\gamma - 1)(e - \frac{1}{2}\rho \vec{u}^{\mathrm{T}} \vec{u}),$$

where γ is the heat capacity ratio, which is equal to 1.4 for air under standard conditions.

The second law of thermodynamics is a secondary equation that can be derived from the Euler equations. An equivalent mathematical statement, known as the entropy inequality, in the general (integral) form

$$\int_{\Omega} \frac{\partial \mathcal{S}}{\partial t} \, \mathrm{d}\Omega + \sum_{i=1}^{d} \int_{\partial\Omega} \mathcal{G}_{x_i} n_{x_i} \, \mathrm{d}\Gamma \leq 0 \tag{7}$$

can also be cast for the Euler equations and other conservation laws endowed with an entropy-entropy-flux pair $(\mathcal{S}, \mathcal{G}_{x_i})$. The entropy pair satisfies the following conditions:

$$\frac{\partial^2 \mathcal{S}}{\partial \boldsymbol{\mathcal{U}}^2} = \left(\frac{\partial^2 \mathcal{S}}{\partial \boldsymbol{\mathcal{U}}^2} \right)^{\mathrm{T}}, \ \boldsymbol{z}^{\mathrm{T}} \frac{\partial^2 \mathcal{S}}{\partial \boldsymbol{\mathcal{U}}^2} \boldsymbol{z} > 0, \ \forall \boldsymbol{z} \neq \mathbf{0}, \tag{8a}$$

$$\frac{\partial \mathcal{G}_{x_i}}{\partial \boldsymbol{\mathcal{U}}} = \boldsymbol{\mathcal{W}}^{\mathrm{T}} \frac{\partial \boldsymbol{\mathcal{F}}_{x_i}}{\partial \boldsymbol{\mathcal{U}}}, \ \forall i \in \{1, ..., d\}, \tag{8b}$$

[8] For the Euler equations, $\mathcal{H}$ is the set of conservative variables with positive density and pressure.

where $\boldsymbol{\mathcal{W}}(\boldsymbol{\mathcal{U}}) \equiv \frac{\partial \mathcal{S}}{\partial \boldsymbol{\mathcal{U}}} \in \mathbb{R}^m$ is known as the entropy variables. For the Euler and Navier-Stokes equations, the entropy $\mathcal{S} \equiv -\rho s/(\gamma-1)$ and entropy flux $\mathcal{G}_{x_i} \equiv u_i \mathcal{S}$, where $s \equiv \ln(p/\rho^\gamma)$ is the thermodynamic entropy per unit mass and $\boldsymbol{\mathcal{U}} \in \mathcal{H}$, satisfy (8) [43]. For such a pair, the entropy variables are

$$\boldsymbol{\mathcal{W}} = \left[\tfrac{\gamma-s}{\gamma-1} - \tfrac{\rho}{2p}\vec{u}^{\mathrm{T}}\vec{u},\ \tfrac{\rho}{p}\vec{u}^{\mathrm{T}},\ -\tfrac{\rho}{p}\right]^{\mathrm{T}}.$$

The entropy inequality and entropy variables satisfying the entropy pair conditions (8) have various interesting properties if pressure and density are positive. For instance, there is a one-to-one mapping between $\boldsymbol{\mathcal{U}}$ and $\boldsymbol{\mathcal{W}}$ due to the strict convexity of $\mathcal{S}(\boldsymbol{\mathcal{U}})$; when the Euler equations are written in terms of the entropy variables, they form a well-posed symmetric hyperbolic system of equations for Cauchy problems[9] [46,47]; and Dafermos [48] showed that a bound on the entropy $\mathcal{S}$ provides a bound on the solution $\boldsymbol{\mathcal{U}}$ for hyperbolic conservation laws. To appeal to the stability statement of Dafermos [48], in this work, we are interested in spatial discretization methods that can discretely mimic the entropy inequality.

We derive the flux terms of the entropy inequality (7) from those of the governing equations (6) to highlight the steps that must be followed at the semi-discrete level. We left-multiply the flux terms of the Euler equations by $\boldsymbol{\mathcal{W}}^{\mathrm{T}}$, integrate over the domain, and simplify as follows:

$$\int_\Omega \boldsymbol{\mathcal{W}}^{\mathrm{T}} \frac{\partial \boldsymbol{\mathcal{F}}_{x_i}}{\partial x_i}\,\mathrm{d}\Omega = \int_\Omega \boldsymbol{\mathcal{W}}^{\mathrm{T}} \frac{\partial \boldsymbol{\mathcal{F}}_{x_i}}{\partial \boldsymbol{\mathcal{U}}}\frac{\partial \boldsymbol{\mathcal{U}}}{\partial x_i}\,\mathrm{d}\Omega = \int_\Omega \frac{\partial \mathcal{G}_{x_i}}{\partial \boldsymbol{\mathcal{U}}}\cdot\frac{\partial \boldsymbol{\mathcal{U}}}{\partial x_i}\,\mathrm{d}\Omega = \int_\Omega \frac{\partial \mathcal{G}_{x_i}}{\partial x_i}\,\mathrm{d}\Omega = \int_{\partial\Omega} \mathcal{G}_{x_i} n_{x_i}\,\mathrm{d}\Gamma,$$

$\forall i \in \{1,...,d\}$, where we used the chain rule for the first and penultimate equalities, the contraction property (8b) for the second equality, and the divergence theorem for the last step. While the divergence theorem can be discretely mimicked using SBP operators, the chain rule does not necessarily hold at the discrete level. Fortunately, we can use numerical fluxes that conserve entropy in the sense of Tadmor [49] to recover $\int_\Omega \frac{\partial \mathcal{G}_{x_i}}{\partial x_i}\,\mathrm{d}\Omega$ from $\int_\Omega \boldsymbol{\mathcal{W}}^{\mathrm{T}} \frac{\partial \boldsymbol{\mathcal{F}}_{x_i}}{\partial x_i}\,\mathrm{d}\Omega$ without relying on the chain rule.

3.5 Entropy-conservative flux functions

As mentioned above, numerical flux functions that conserve entropy, named entropy-conservative fluxes, are essential for entropy-stable methods. We also require these fluxes to be symmetric in their arguments, consistent, and continuously differentiable. The last two requirements are needed for high-order accuracy [11]. Definition 3 formally summarizes these requirements.

Definition 3 (Entropy-conservative flux function) A two-point numerical flux function $\boldsymbol{\mathcal{F}}^*_{x_i}(\cdot,\cdot) : \mathcal{H}\times\mathcal{H} \to \mathbb{R}^m$ is said to be an entropy-conservative, symmetric, consistent, and continuously differentiable flux function in the x_i-direction if it satisfies the following conditions:

1. $\left(\boldsymbol{\mathcal{W}}(\boldsymbol{\mathcal{U}}_1) - \boldsymbol{\mathcal{W}}(\boldsymbol{\mathcal{U}}_2)\right)^{\mathrm{T}} \boldsymbol{\mathcal{F}}^*_{x_i}(\boldsymbol{\mathcal{U}}_1,\boldsymbol{\mathcal{U}}_2) = \psi_{x_i}(\boldsymbol{\mathcal{U}}_1) - \psi_{x_i}(\boldsymbol{\mathcal{U}}_2)$,
2. $\boldsymbol{\mathcal{F}}^*_{x_i}(\boldsymbol{\mathcal{U}}_1,\boldsymbol{\mathcal{U}}_2) = \boldsymbol{\mathcal{F}}^*_{x_i}(\boldsymbol{\mathcal{U}}_2,\boldsymbol{\mathcal{U}}_1)$,
3. $\boldsymbol{\mathcal{F}}^*_{x_i}(\boldsymbol{\mathcal{U}},\boldsymbol{\mathcal{U}}) = \boldsymbol{\mathcal{F}}_{x_i}(\boldsymbol{\mathcal{U}})$, and
4. $\boldsymbol{\mathcal{F}}^*_{x_i}(\cdot,\cdot) \in C^1(\mathcal{H},\mathcal{H})$

where $\psi_{x_i} \equiv \boldsymbol{\mathcal{W}}^{\mathrm{T}}\boldsymbol{\mathcal{F}}_{x_i} - \mathcal{G}_{x_i} \in \mathbb{R}$ is known as the potential flux in the x_i-direction, and $\boldsymbol{\mathcal{U}}_1$ and $\boldsymbol{\mathcal{U}}_2$ are two different states.

The first condition of the above definition is known as Tadmor's condition and was first derived by Tadmor in Ref. [49][10]. In this paper, we denote any flux function that satisfies Definition 3 as $\boldsymbol{\mathcal{F}}^{*,\mathrm{EC}}_{x_i}(\cdot,\cdot)$.

It is possible to use numerical flux functions to approximate the derivative of fluxes. At the continuous level, for any symmetric, consistent, and differentiable flux function, we can show that [9,10,11]

$$\frac{\partial \boldsymbol{\mathcal{F}}_{x_i}}{\partial x_i}(\boldsymbol{\mathcal{U}}) = 2\frac{\partial \boldsymbol{\mathcal{F}}^*_{x_i}}{\partial x_i}(\boldsymbol{\mathcal{C}},\boldsymbol{\mathcal{U}})\bigg|_{\boldsymbol{\mathcal{C}}=\boldsymbol{\mathcal{U}}}, \tag{9}$$

[9] Well posedness of the Euler equations is a complex subject: see, for example, Refs. [44,45].

[10] For the entropy pair of the Euler equations used in this paper, the potential flux is simply the momentum in the x_i-direction, i.e. $\psi_{x_i} = \rho u_i$.

where we assume $\boldsymbol{\mathcal{U}}$ is a function of x_i, i.e. $\boldsymbol{\mathcal{U}} = \boldsymbol{\mathcal{U}}(x_i)$, and $\boldsymbol{\mathcal{C}}$ is not. In words, the derivative of the actual flux is equal to twice the derivative of the numerical flux where we take only the second argument as a function of x_i. While in the finite-difference community, it is common to approximate the left-hand side of (9) as

$$\frac{\partial \boldsymbol{\mathcal{F}}_{x_i}}{\partial x_i}([\boldsymbol{u}_\kappa]_j) \approx \sum_{k=1}^{N_\kappa} [\mathsf{D}_{x_i}]_{jk} \boldsymbol{\mathcal{F}}_{x_i}([\boldsymbol{u}_\kappa]_k),\ \forall j \in \{1, ..., N_\kappa\},$$

for entropy-conservative methods, we must use entropy-conservative flux functions and approximate its right-hand side as

$$2\frac{\partial \boldsymbol{\mathcal{F}}^{*,\mathrm{EC}}_{x_i}}{\partial x_i}(\boldsymbol{c}, [\boldsymbol{u}_\kappa]_j)\bigg|_{\boldsymbol{c}=[\boldsymbol{u}_\kappa]_j} \approx 2\sum_{k=1}^{N_\kappa} [\mathsf{D}_{x_i}]_{jk} \boldsymbol{\mathcal{F}}^{*,\mathrm{EC}}_{x_i}([\boldsymbol{u}_\kappa]_j, [\boldsymbol{u}_\kappa]_k),\ \forall j \in \{1, ..., N_\kappa\}. \tag{10}$$

Linear combinations of two-point entropy-conservative fluxes, such as (10), were first used by LeFloch *et al.* [50] (and subsequently by other researchers such as Fisher and Carpenter [7]) to develop high-order entropy-conservative schemes.

To present the schemes in Section 4 in (compact) matrix form, we note that

$$\left[\left\{\tilde{\mathsf{A}} \circ \mathsf{F}_{x_i}(\boldsymbol{u}_\kappa, \boldsymbol{u}_\nu)\right\}\mathbf{1}_\nu\right]_j = \sum_{k=1}^{N_\nu} [\mathsf{A}]_{jk} \boldsymbol{\mathcal{F}}^{*,\mathrm{EC}}_{x_i}([\boldsymbol{u}_\kappa]_j, [\boldsymbol{u}_\nu]_k),\ \forall j \in \{1, ..., N_\kappa\},$$

where $\tilde{\mathsf{A}} \equiv \mathsf{A} \otimes \mathsf{I}_m$, $\mathsf{A} \in \mathbb{R}^{N_\kappa \times N_\nu}$ is a generic matrix and $\mathsf{F}_{x_i}(\cdot,\cdot) : \mathbb{R}^{m\cdot N_\kappa} \times \mathbb{R}^{m\cdot N_\nu} \to \mathbb{R}^{m\cdot N_\kappa \times m\cdot N_\nu}$ is defined as [11]

$$\mathsf{F}_{x_i}(\boldsymbol{u}_\kappa, \boldsymbol{u}_\nu) \equiv \begin{bmatrix} \mathrm{diag}\left[\boldsymbol{\mathcal{F}}^{*,\mathrm{EC}}_{x_i}([\boldsymbol{u}_\kappa]_1, [\boldsymbol{u}_\nu]_1)\right] & \cdots & \mathrm{diag}\left[\boldsymbol{\mathcal{F}}^{*,\mathrm{EC}}_{x_i}([\boldsymbol{u}_\kappa]_1, [\boldsymbol{u}_\nu]_{N_\nu})\right] \\ \vdots & \ddots & \vdots \\ \mathrm{diag}\left[\boldsymbol{\mathcal{F}}^{*,\mathrm{EC}}_{x_i}([\boldsymbol{u}_\kappa]_{N_\kappa}, [\boldsymbol{u}_\nu]_1)\right] & \cdots & \mathrm{diag}\left[\boldsymbol{\mathcal{F}}^{*,\mathrm{EC}}_{x_i}([\boldsymbol{u}_\kappa]_{N_\kappa}, [\boldsymbol{u}_\nu]_{N_\nu})\right] \end{bmatrix}.$$

The entropy-conservative fluxes are diagonally placed in this matrix and $\tilde{\mathsf{A}}$ is used in order to avoid coupling fluxes associated to different equations. Furthermore, the properties $\left(\mathsf{F}_{x_i}(\boldsymbol{u}_\kappa, \boldsymbol{u}_\nu)\right)^{\mathrm{T}} = \mathsf{F}_{x_i}(\boldsymbol{u}_\nu, \boldsymbol{u}_\kappa)$ and $\left(\mathsf{F}_{x_i}(\boldsymbol{u}_\kappa, \boldsymbol{u}_\kappa)\right)^{\mathrm{T}} = \mathsf{F}_{x_i}(\boldsymbol{u}_\kappa, \boldsymbol{u}_\kappa)$, which are a direct consequence of the structure of the matrices and the symmetry of entropy-conservative fluxes, are used extensively in the proofs of this paper.

3.6 Compact SBP matrices

Here we define some matrices to allow for a clear and concise presentation of the schemes and proofs in this paper. Important properties of these matrices are also shown.

We define $\mathsf{E}^{(\kappa\nu)}_{x_i} \in \mathbb{R}^{N_\kappa \times N_\nu}$, $\mathsf{E}^{(\kappa\kappa)}_{x_i} \in \mathbb{R}^{N_\kappa \times N_\kappa}$, and $\mathsf{E}^{(\kappa I)}_{x_i} \in \mathbb{R}^{N_\kappa \times N_I}$ as

$$\begin{aligned} \mathsf{E}^{(\kappa\nu)}_{x_i} &\equiv \mathsf{R}^{\mathrm{T}}_{\kappa\gamma} \mathsf{P}^{\mathrm{T}}_{\kappa\gamma\to I} \mathsf{B}_I \mathsf{N}^{(\kappa)}_{I,x_i} \mathsf{P}_{\nu\gamma\to I} \mathsf{R}_{\nu\gamma}, \\ \mathsf{E}^{(\kappa\kappa)}_{x_i} &\equiv \mathsf{R}^{\mathrm{T}}_{\kappa\gamma} \mathsf{P}^{\mathrm{T}}_{\kappa\gamma\to I} \mathsf{B}_I \mathsf{N}^{(\kappa)}_{I,x_i} \mathsf{P}_{\kappa\gamma\to I} \mathsf{R}_{\kappa\gamma}, \\ \mathsf{E}^{(\kappa I)}_{x_i} &\equiv \mathsf{R}^{\mathrm{T}}_{\kappa\gamma} \mathsf{P}^{\mathrm{T}}_{\kappa\gamma\to I} \mathsf{B}_I \mathsf{N}^{(\kappa)}_{I,x_i}, \end{aligned}$$

$\forall i \in \{1, ..., d\}$. We can easily demonstrate that $\mathsf{E}^{(\kappa\nu)}_{x_i} = -\left(\mathsf{E}^{(\nu\kappa)}_{x_i}\right)^{\mathrm{T}}$ (since $\mathsf{N}^{(\kappa)}_{I,x_i} = -\mathsf{N}^{(\nu)}_{I,x_i}$), and $\mathsf{E}_{x_i} = \sum_\kappa \mathsf{E}^{(\kappa\kappa)}_{x_i}$. Furthermore, since the extrapolation operators exactly extrapolate constant functions, the equalities $\mathsf{P}_{\kappa\gamma\to I}\mathsf{R}_{\kappa\gamma}\mathbf{1}_\kappa = \mathsf{P}_{\nu\gamma\to I}\mathsf{R}_{\nu\gamma}\mathbf{1}_\nu = \mathbf{1}_I$ hold and we can show that the properties $\mathsf{E}^{(\kappa\nu)}_{x_i}\mathbf{1}_\nu = \mathsf{E}^{(\kappa\kappa)}_{x_i}\mathbf{1}_\kappa$ and $\mathbf{1}^{\mathrm{T}}_\kappa \mathsf{E}^{(\kappa I)}_{x_i} = \mathbf{1}^{\mathrm{T}}_I \mathsf{B}_I \mathsf{N}^{(\kappa)}_{I,x_i}$ hold as well $\forall i \in \{1, ..., d\}$.

4 Non-conforming entropy-stable schemes

In this section, we introduce two entropy-conservative semi-discrete schemes applicable to non-conforming curvilinear grids with periodic boundary conditions. The first, is an extension of Crean *et al.*'s work [11] to non-conforming grids. The scheme is compatible with any diagonal-norm SBP operator equipped with facet quadrature rules of degree $2p$ or higher; however, for dense-E operators, it fully couples the volume nodes of neighbouring elements. Accordingly, we term this method the "dense-coupling entropy-conservative scheme". The second, named the "pointwise-coupling entropy-conservative scheme", uses the penalty term of Chan [10], which couples neighbouring elements in a pointwise manner via the shared interface nodes. We then introduce an entropy dissipative interface stabilization term which can augment both schemes to produce entropy-stable schemes. While both semi-discrete methods are entropy-conservative (or entropy-stable when augmented with the interface stabilization term), they rely on the assumption that certain quantities, such as density and pressure for the Euler equations, remain positive. Furthermore, we prove that the diagonal-E entropy-conservative scheme of Ref. [35] (which is an extension of the tensor-product scheme of Friedrich *et al.* [28] to general elements) is a subset of the dense-coupling entropy-conservative scheme on affine non-conforming meshes. Finally, we conclude this section by describing how to implement the algorithms in a step-by-step manner.

4.1 Dense-coupling entropy-conservative scheme

The strong form of the dense-coupling entropy-conservative scheme seeks, for an arbitrary element κ, the solution $\boldsymbol{u}_\kappa \in \mathbb{R}^{m\cdot N_\kappa}$ such that

$$\begin{aligned}\frac{\mathrm{d}\boldsymbol{u}_\kappa}{\mathrm{d}t} + \sum_{i=1}^{d}\left(2\tilde{\mathsf{D}}_{x_i}\circ\mathsf{F}_{x_i}(\boldsymbol{u}_\kappa,\boldsymbol{u}_\kappa)\right)\mathbf{1}_\kappa = &-\sum_{\kappa\gamma}\sum_{i=1}^{d}\tilde{\mathsf{H}}^{-1}\left\{\tilde{\mathsf{E}}_{x_i}^{(\kappa\nu)}\circ\mathsf{F}_{x_i}(\boldsymbol{u}_\kappa,\boldsymbol{u}_\nu)\right\}\mathbf{1}_\nu\\ &+\sum_{i=1}^{d}\tilde{\mathsf{H}}^{-1}\left\{\tilde{\mathsf{E}}_{x_i}\circ\mathsf{F}_{x_i}(\boldsymbol{u}_\kappa,\boldsymbol{u}_\kappa)\right\}\mathbf{1}_\kappa,\end{aligned} \tag{11}$$

where $\mathsf{E}_{x_i}^{(\kappa\nu)} \equiv \mathsf{R}_{\kappa\gamma}^{\mathrm{T}}\mathsf{P}_{\kappa\gamma\to I}^{\mathrm{T}}\mathsf{B}_I\mathsf{N}_{I,x_i}^{(\kappa)}\mathsf{P}_{\nu\gamma\to I}\mathsf{R}_{\nu\gamma}$ as defined in Section 3.6. The second term is an approximation of $\frac{\partial\boldsymbol{\mathcal{F}}_{x_i}}{\partial x_i}$ at the volume nodes (see Section 3.5), while the right-hand side is a penalty method that weakly imposes inter-element conditions. To populate $\mathsf{F}_{x_i}(\boldsymbol{u}_\kappa,\boldsymbol{u}_\nu)$ we require the evaluation of entropy-conservative fluxes between all volume nodes in S_{Ω_κ} and S_{Ω_ν}.

Remark 1 On a conforming grid, the interface extrapolation operators $\mathsf{P}_{\kappa\gamma\to I}$ and $\mathsf{P}_{\nu\gamma\to I}$ in $\mathsf{E}_{x_i}^{(\kappa\nu)} \equiv \mathsf{R}_{\kappa\gamma}^{\mathrm{T}}\mathsf{P}_{\kappa\gamma\to I}^{\mathrm{T}}\mathsf{B}_I\mathsf{N}_{I,x_i}^{(\kappa)}\mathsf{P}_{\nu\gamma\to I}\mathsf{R}_{\nu\gamma}$ and in $\mathsf{E}_{x_i}^{(\kappa\kappa)} \equiv \mathsf{R}_{\kappa\gamma}^{\mathrm{T}}\mathsf{P}_{\kappa\gamma\to I}^{\mathrm{T}}\mathsf{B}_I\mathsf{N}_{I,x_i}^{(\kappa)}\mathsf{P}_{\kappa\gamma\to I}\mathsf{R}_{\kappa\gamma}$ simplify to the identity matrices and the scheme in Crean *et al.* [11] is recovered.

The (algebraically equivalent) weak form of (11) is obtained by multiplying by a test function $\boldsymbol{v}_\kappa \in \mathbb{R}^{m\cdot N_\kappa}$ and integrating by parts (i.e. using $\mathsf{Q}_{x_i} = \mathsf{E}_{x_i} - \mathsf{Q}_{x_i}^{\mathrm{T}}$):

$$\begin{aligned}\boldsymbol{v}_\kappa^{\mathrm{T}}\tilde{\mathsf{H}}\frac{\mathrm{d}\boldsymbol{u}_\kappa}{\mathrm{d}t} - \sum_{i=1}^{d}\boldsymbol{v}_\kappa^{\mathrm{T}}\left(2\tilde{\mathsf{Q}}_{x_i}^{\mathrm{T}}\circ\mathsf{F}_{x_i}(\boldsymbol{u}_\kappa,\boldsymbol{u}_\kappa)\right)\mathbf{1}_\kappa = &-\sum_{\kappa\gamma}\sum_{i=1}^{d}\boldsymbol{v}_\kappa^{\mathrm{T}}\left\{\tilde{\mathsf{E}}_{x_i}^{(\kappa\nu)}\circ\mathsf{F}_{x_i}(\boldsymbol{u}_\kappa,\boldsymbol{u}_\nu)\right\}\mathbf{1}_\nu\\ &-\sum_{i=1}^{d}\boldsymbol{v}_\kappa^{\mathrm{T}}\left\{\tilde{\mathsf{E}}_{x_i}\circ\mathsf{F}_{x_i}(\boldsymbol{u}_\kappa,\boldsymbol{u}_\kappa)\right\}\mathbf{1}_\kappa,\ \forall\boldsymbol{v}_\kappa\in\mathbb{R}^{m\cdot N_\kappa}.\end{aligned} \tag{12}$$

Finally, using the skew-symmetric matrix $\mathsf{S}_{x_i} = -\mathsf{Q}_{x_i}^{\mathrm{T}} + \frac{1}{2}\mathsf{E}_{x_i}$ and removing $\boldsymbol{v}_\kappa$, a third equivalent, but more compact, form is obtained:

$$\tilde{\mathsf{H}}\frac{\mathrm{d}\boldsymbol{u}_\kappa}{\mathrm{d}t} + \sum_{i=1}^{d}\left(2\tilde{\mathsf{S}}_{x_i}\circ\mathsf{F}_{x_i}(\boldsymbol{u}_\kappa,\boldsymbol{u}_\kappa)\right)\mathbf{1}_\kappa = -\sum_{\kappa\gamma}\sum_{i=1}^{d}\left\{\tilde{\mathsf{E}}_{x_i}^{(\kappa\nu)}\circ\mathsf{F}_{x_i}(\boldsymbol{u}_\kappa,\boldsymbol{u}_\nu)\right\}\mathbf{1}_\nu. \tag{13}$$

4.2 Pointwise-coupling entropy-conservative scheme

To obtain the pointwise-coupling entropy-conservative scheme, we replace the inter-element coupling term of the dense-coupling entropy-conservative scheme by that of Chan [10][11]. Doing so, we enable a pointwise coupling between neighbouring elements. The strong form of the pointwise-coupling entropy-conservative scheme seeks, for an arbitrary element κ, the solution $\boldsymbol{u}_\kappa \in \mathbb{R}^{m\cdot N_\kappa}$ such that

$$\begin{aligned}\frac{\mathrm{d}\boldsymbol{u}_\kappa}{\mathrm{d}t} + \sum_{i=1}^{d}\left(2\tilde{\mathsf{D}}_{x_i}\circ\mathsf{F}_{x_i}(\boldsymbol{u}_\kappa,\boldsymbol{u}_\kappa)\right)\mathbf{1}_\kappa = &-\sum_{\kappa\gamma}\sum_{i=1}^{d}\tilde{\mathsf{H}}^{-1}\left\{\tilde{\mathsf{E}}_{x_i}^{(\kappa I)}\circ\mathsf{F}_{x_i}(\boldsymbol{u}_\kappa,\overline{\boldsymbol{u}}_{\kappa I})\right\}\mathbf{1}_I\\ &+\sum_{\kappa\gamma}\sum_{i=1}^{d}\tilde{\mathsf{H}}^{-1}\tilde{\mathsf{R}}_{\kappa\gamma}^{\mathrm{T}}\tilde{\mathsf{P}}_{\kappa\gamma\to I}^{\mathrm{T}}\left\{(\tilde{\mathsf{E}}_{x_i}^{(\kappa I)})^{\mathrm{T}}\circ\mathsf{F}_{x_i}(\overline{\boldsymbol{u}}_{\kappa I},\boldsymbol{u}_\kappa)\right\}\mathbf{1}_\kappa\\ &-\sum_{\kappa\gamma}\sum_{i=1}^{d}\tilde{\mathsf{H}}^{-1}\tilde{\mathsf{E}}_{x_i}^{(\kappa I)}\boldsymbol{f}_{x_i}^{*,\mathrm{EC}}(\overline{\boldsymbol{u}}_{\kappa I},\overline{\boldsymbol{u}}_{\nu I})\\ &+\sum_{i=1}^{d}\tilde{\mathsf{H}}^{-1}\left\{\tilde{\mathsf{E}}_{x_i}\circ\mathsf{F}_{x_i}(\boldsymbol{u}_\kappa,\boldsymbol{u}_\kappa)\right\}\mathbf{1}_\kappa,\end{aligned} \tag{14}$$

where $\mathsf{E}_{x_i}^{(\kappa I)} \equiv \mathsf{R}_{\kappa\gamma}^{\mathrm{T}}\mathsf{P}_{\kappa\gamma\to I}^{\mathrm{T}}\mathsf{B}_I\mathsf{N}_{I,x_i}^{(\kappa)}$ as defined in Section 3.6, and the entries of $\boldsymbol{f}_{x_i}^{*,\mathrm{EC}}(\overline{\boldsymbol{u}}_{\kappa I},\overline{\boldsymbol{u}}_{\nu I}) \in \mathbb{R}^{m\cdot N_I}$, $\overline{\boldsymbol{u}}_{\kappa I} \in \mathbb{R}^{m\cdot N_I}$, and $\overline{\boldsymbol{u}}_{\nu I} \in \mathbb{R}^{m\cdot N_I}$ are defined as

$$\begin{aligned}[\boldsymbol{f}_{x_i}^{*,\mathrm{EC}}(\overline{\boldsymbol{u}}_{\kappa I},\overline{\boldsymbol{u}}_{\nu I})]_l &= \boldsymbol{\mathcal{F}}_{x_i}^{*,\mathrm{EC}}([\overline{\boldsymbol{u}}_{\kappa I}]_l,[\overline{\boldsymbol{u}}_{\nu I}]_l),\ \forall li\in\{1,...,N_I\},\\ [\overline{\boldsymbol{u}}_{\kappa I}]_l &\equiv \boldsymbol{\mathcal{U}}\Big([\boldsymbol{w}_{\kappa I}]_l\Big),\quad [\overline{\boldsymbol{u}}_{\nu I}]_l \equiv \boldsymbol{\mathcal{U}}\Big([\boldsymbol{w}_{\nu I}]_l\Big),\ \forall li\in\{1,...,N_I\},\\ [\boldsymbol{w}_{\kappa I}]_l &\equiv [\tilde{\mathsf{P}}_{\kappa\gamma\to I}\tilde{\mathsf{R}}_{\kappa\gamma}\boldsymbol{w}_\kappa]_l,\quad \text{and}\quad [\boldsymbol{w}_{\nu I}]_l \equiv [\tilde{\mathsf{P}}_{\nu\gamma\to I}\tilde{\mathsf{R}}_{\nu\gamma}\boldsymbol{w}_\nu]_l,\ \forall li\in\{1,...,N_I\}.\end{aligned}$$

The entries of $\boldsymbol{w}_\kappa \in \mathbb{R}^{m\cdot N_\kappa}$ and $\boldsymbol{w}_\nu \in \mathbb{R}^{m\cdot N_\nu}$ are the entropy variables evaluated at the volume nodes of element κ and ν, respectively. In essence, $\overline{\boldsymbol{u}}_{\kappa I} \in \mathbb{R}^{m\cdot N_I}$ and $\overline{\boldsymbol{u}}_{\nu I} \in \mathbb{R}^{m\cdot N_I}$ are the conservative variables corresponding to the extrapolated entropy variables $\boldsymbol{w}_{\kappa I} \in \mathbb{R}^{m\cdot N_I}$ and $\boldsymbol{w}_{\nu I} \in \mathbb{R}^{m\cdot N_I}$, respectively[12]. These are important to ensure that Tadmor's condition (condition 1 of Definition 3) can be invoked when showing entropy conservation. The first two terms on the right-hand side of (14), which couple the volume nodes of element κ with the intermediate interface nodes, are nearly the negative of the transpose of each other. As it will be shown in Section 5, this structure is critical for the conservation and entropy conservation properties of the scheme and enables the scheme to couple neighbouring elements in a pointwise manner via the third term on the right-hand side of (14). Again, multiplying by a test function $\boldsymbol{v}_\kappa \in \mathbb{R}^{m\cdot N_\kappa}$ and integrating by parts, we obtain the weak form:

$$\begin{aligned}\boldsymbol{v}_\kappa^{\mathrm{T}}\tilde{\mathsf{H}}\frac{\mathrm{d}\boldsymbol{u}_\kappa}{\mathrm{d}t} - \sum_{i=1}^{d}\boldsymbol{v}_\kappa^{\mathrm{T}}\left(2\tilde{\mathsf{Q}}_{x_i}^{\mathrm{T}}\circ\mathsf{F}_{x_i}(\boldsymbol{u}_\kappa,\boldsymbol{u}_\kappa)\right)\mathbf{1}_\kappa = &-\sum_{\kappa\gamma}\sum_{i=1}^{d}\boldsymbol{v}_\kappa^{\mathrm{T}}\left\{\tilde{\mathsf{E}}_{x_i}^{(\kappa I)}\circ\mathsf{F}_{x_i}(\boldsymbol{u}_\kappa,\overline{\boldsymbol{u}}_{\kappa I})\right\}\mathbf{1}_I\\ &+\sum_{\kappa\gamma}\sum_{i=1}^{d}\boldsymbol{v}_\kappa^{\mathrm{T}}\tilde{\mathsf{R}}_{\kappa\gamma}^{\mathrm{T}}\tilde{\mathsf{P}}_{\kappa\gamma\to I}^{\mathrm{T}}\left\{(\tilde{\mathsf{E}}_{x_i}^{(\kappa I)})^{\mathrm{T}}\circ\mathsf{F}_{x_i}(\overline{\boldsymbol{u}}_{\kappa I},\boldsymbol{u}_\kappa)\right\}\mathbf{1}_\kappa\\ &-\sum_{\kappa\gamma}\sum_{i=1}^{d}\boldsymbol{v}_\kappa^{\mathrm{T}}\tilde{\mathsf{E}}_{x_i}^{(\kappa I)}\boldsymbol{f}_{x_i}^{*,\mathrm{EC}}(\overline{\boldsymbol{u}}_{\kappa I},\overline{\boldsymbol{u}}_{\nu I})\\ &-\sum_{i=1}^{d}\boldsymbol{v}_\kappa^{\mathrm{T}}\left\{\tilde{\mathsf{E}}_{x_i}\circ\mathsf{F}_{x_i}(\boldsymbol{u}_\kappa,\boldsymbol{u}_\kappa)\right\}\mathbf{1}_\kappa,\ \forall\boldsymbol{v}_\kappa\in\mathbb{R}^{m\cdot N_\kappa}.\end{aligned} \tag{15}$$

[11] In Ref. [10], the author uses "decoupled" SBP operators which can be viewed as a superset of the (collocated) SBP operators used in this paper.

[12] $\overline{\boldsymbol{u}}_{\kappa I}$ and $\overline{\boldsymbol{u}}_{\nu I}$ are generally not equal to the extrapolated conservative variables.

Finally, using $\mathsf{S}_{x_i} = -\mathsf{Q}_{x_i}^{\mathrm{T}} + \frac{1}{2}\mathsf{E}_{x_i}$ and removing $\boldsymbol{v}_\kappa$, the compact form is obtained:

$$\begin{aligned}\tilde{\mathsf{H}}\frac{\mathrm{d}\boldsymbol{u}_\kappa}{\mathrm{d}t} + \sum_{i=1}^{d}\left(2\tilde{\mathsf{S}}_{x_i} \circ \mathsf{F}_{x_i}(\boldsymbol{u}_\kappa, \boldsymbol{u}_\kappa)\right)\mathbf{1}_\kappa = &-\sum_{\kappa\gamma}\sum_{i=1}^{d}\left\{\tilde{\mathsf{E}}_{x_i}^{(\kappa I)} \circ \mathsf{F}_{x_i}(\boldsymbol{u}_\kappa, \overline{\boldsymbol{u}}_{\kappa I})\right\}\mathbf{1}_I \\ &+ \sum_{\kappa\gamma}\sum_{i=1}^{d}\tilde{\mathsf{R}}_{\kappa\gamma}^{\mathrm{T}}\tilde{\mathsf{P}}_{\kappa\gamma\to I}^{\mathrm{T}}\left\{(\tilde{\mathsf{E}}_{x_i}^{(\kappa I)})^{\mathrm{T}} \circ \mathsf{F}_{x_i}(\overline{\boldsymbol{u}}_{\kappa I}, \boldsymbol{u}_\kappa)\right\}\mathbf{1}_\kappa \\ &- \sum_{\kappa\gamma}\sum_{i=1}^{d}\tilde{\mathsf{E}}_{x_i}^{(\kappa I)}\boldsymbol{f}_{x_i}^{*,\mathrm{EC}}(\overline{\boldsymbol{u}}_{\kappa I}, \overline{\boldsymbol{u}}_{\nu I}).\end{aligned} \tag{16}$$

Remark 2 When using diagonal-E SBP operators, both (13) and (16) reduce to Carpenter *et al.*'s [20] or Chen and Shu's [9] schemes on conforming quadrilateral and simplex grids, respectively. This can be shown by using the Kronecker delta property of the extrapolation operators R_γ and by noting that the interface extrapolation operators $\mathsf{P}_{\gamma\to I}$ simplify to the identity matrix.

4.3 Entropy dissipative term

We follow the approach of Ref. [11] and add the following interface entropy dissipative term to the right-hand side of the entropy-conservative schemes (13) and (16) such that the resulting schemes are entropy stable:

$$-\sum_{\kappa\gamma}\tilde{\mathsf{R}}_{\kappa\gamma}^{\mathrm{T}}\tilde{\mathsf{P}}_{\kappa\gamma\to I}^{\mathrm{T}}\tilde{\mathsf{B}}_I\Lambda_I(\boldsymbol{u}_{\kappa I}, \boldsymbol{u}_{\nu I}; \boldsymbol{n}_I^{(\kappa)})(\boldsymbol{w}_{\kappa I} - \boldsymbol{w}_{\nu I}), \tag{17}$$

where the extrapolated solutions on the intermediate interface $\boldsymbol{u}_{\kappa I} \in \mathbb{R}^{m\cdot N_I}$ and $\boldsymbol{u}_{\nu I} \in \mathbb{R}^{m\cdot N_I}$ are defined as $\boldsymbol{u}_{\kappa I} \equiv \tilde{\mathsf{P}}_{\kappa\gamma\to I}\tilde{\mathsf{R}}_{\kappa\gamma}\boldsymbol{u}_\kappa$ and $\boldsymbol{u}_{\nu I} \equiv \tilde{\mathsf{P}}_{\nu\gamma\to I}\tilde{\mathsf{R}}_{\nu\gamma}\boldsymbol{u}_\nu$ respectively, $\boldsymbol{n}_I^{(\kappa)}$ holds the outward-pointing normal unit vector at each of the intermediate interface nodes in S_I (with respect to element κ), and $\Lambda_I(\boldsymbol{u}_{\kappa I}, \boldsymbol{u}_{\nu I}; \boldsymbol{n}_I^{(\kappa)}) \in \mathbb{R}^{m\cdot N_I \times m\cdot N_I}$ is a block-diagonal symmetric positive semidefinite matrix satisfying the property $\Lambda_I(\boldsymbol{u}_{\kappa I}, \boldsymbol{u}_{\nu I}; \boldsymbol{n}_I^{(\kappa)}) = \Lambda_I(\boldsymbol{u}_{\nu I}, \boldsymbol{u}_{\kappa I}; \boldsymbol{n}_I^{(\nu)})$.

4.4 Diagonal-E entropy-conservative scheme

In this subsection, we show that the non-conforming method of Refs. [28,35] on affine meshes is a subset of the dense-coupling entropy-conservative scheme. Using our notation, the diagonal-E entropy-conservative scheme used in Refs. [28,35] is written as

$$\begin{aligned}\tilde{\mathsf{H}}\frac{\mathrm{d}\boldsymbol{u}_\kappa}{\mathrm{d}t} - \sum_{i=1}^{d}\left(2\tilde{\mathsf{Q}}_{x_i}^{\mathrm{T}} \circ \mathsf{F}_{x_i}(\boldsymbol{u}_\kappa, \boldsymbol{u}_\kappa)\right)\mathbf{1}_\kappa = &-\sum_{\kappa\gamma}\sum_{i=1}^{d}\tilde{\mathsf{R}}_{\kappa\gamma}^{\mathrm{T}}\tilde{\mathsf{N}}_{\kappa\gamma,x_i}\tilde{\mathsf{B}}_{\kappa\gamma}\left(\tilde{\mathsf{P}}_{\nu\gamma\to\kappa\gamma} \circ \mathsf{F}_{x_i}(\boldsymbol{u}_{\kappa\gamma}, \boldsymbol{u}_{\nu\gamma})\right)\mathbf{1}_{\nu\gamma} \\ &- \sum_{\kappa\gamma}\sum_{i=1}^{d}\left((\tilde{\mathsf{R}}_{\kappa\gamma}^{\mathrm{T}}\tilde{\mathsf{N}}_{\kappa\gamma,x_i}\tilde{\mathsf{B}}_{\kappa\gamma}\tilde{\mathsf{R}}_{\kappa\gamma}) \circ \mathsf{F}_{x_i}(\boldsymbol{u}_\kappa, \boldsymbol{u}_\kappa)\right)\mathbf{1}_\kappa,\end{aligned} \tag{18}$$

for an arbitrary element κ, where $\boldsymbol{u}_{\kappa\gamma} \in \mathbb{R}^{m\cdot N_{\kappa\gamma}}$ and $\boldsymbol{u}_{\nu\gamma} \in \mathbb{R}^{m\cdot N_{\nu\gamma}}$ are the facet extrapolated solutions, $\mathsf{N}_{\kappa\gamma,x_i} \equiv n_{\gamma,x_i}\mathsf{I}_{N_{\kappa\gamma}}$, and $\mathsf{P}_{\nu\gamma\to\kappa\gamma} \in \mathbb{R}^{N_{\kappa\gamma}\times N_{\nu\gamma}}$ is an operator which projects functions from the facet nodal set $S_{\nu\gamma}$ onto the facet nodal set $S_{\kappa\gamma}$. These are defined as $\boldsymbol{u}_{\kappa\gamma} \equiv \tilde{\mathsf{R}}_{\kappa\gamma}\boldsymbol{u}_\kappa$, $\boldsymbol{u}_{\nu\gamma} \equiv \tilde{\mathsf{R}}_{\nu\gamma}\boldsymbol{u}_\nu$, and

$$\mathsf{P}_{\nu\gamma\to\kappa\gamma} \equiv \mathsf{P}_{I\to\kappa\gamma}\mathsf{P}_{\nu\gamma\to I}, \tag{19}$$

where $\mathsf{P}_{I\to\kappa\gamma} \in \mathbb{R}^{N_{\kappa\gamma}\times N_I}$ satisfies [33,26,27,28,35]

$$\mathsf{B}_{\kappa\gamma}\mathsf{P}_{I\to\kappa\gamma} = \mathsf{P}_{\kappa\gamma\to I}^{\mathrm{T}}\mathsf{B}_I. \tag{20}$$

Property (20) is crucial for the entropy conservation and element-wise conservation properties of the diagonal-E entropy-conservative scheme (18). Note that, unlike the entropy-conservative schemes (12) and (15) for which inter-element coupling is performed using the intermediate interface nodal set S_I, (18) uses the matrices $\mathsf{P}_{\nu\gamma\to\kappa\gamma}$ and $\mathsf{B}_{\kappa\gamma}$ to couple the element κ with its neighbours on its facet nodal set $S_{\kappa\gamma}$. Similarly, each of its neighbours, e.g. ν, perform the inter-element coupling on their facet nodal set, e.g. $S_{\nu\gamma}$.

Theorem 1 *When using SBP operators equipped with facet quadrature rules of degree $s_\kappa \geq 2r_\kappa (\geq 2p_\kappa)$, $\forall \Omega_\kappa \in \mathcal{T}_h$, the entropy-conservative scheme (18) is a subset of the dense-coupling entropy-conservative scheme (13) on affine meshes.*

Proof The proof is shown in Appendix B. □

4.5 Algorithm implementation

Here we summarize the steps that can be followed in order to implement the dense-coupling and pointwise-coupling semi-discrete schemes. For a given element κ:

1. Construct the degree p_κ reference SBP operators, namely $\hat{\mathsf{H}}$, $\mathsf{R}_{\kappa\gamma}$, $\hat{\mathsf{E}}_{\xi_i}$, and $\hat{\mathsf{Q}}_{\xi_i}$ in all spatial directions, as explained in Section 3.1.1.
2. For each neighbouring element ν with shared facet γ:
   (a) Construct the extrapolation operator $\mathsf{R}_{\nu\gamma}$ as explained in Section 3.1.1.
   (b) Construct the reference interface operators $\hat{\mathsf{B}}_I$, $\mathsf{P}_{\kappa\gamma\to I}$, and $\mathsf{P}_{\nu\gamma\to I}$ following Section 3.2's explanation.
3. Using the (defined) geometric polynomial mapping function, compute the physical SBP operators, namely B_I, $\mathsf{N}^{(\kappa)}_{I,x_i}$, E_{x_i}, H, and S_{x_i}, as explained in Section 3.3.
4. Store the volumetric discretization term in the spatial residual term $[\mathbf{r}_\kappa]_j \in \mathbb{R}^m,\ \forall j \in \{1, ..., N_\kappa\}$:

$$[\mathbf{r}_\kappa]_j = \frac{2}{[\mathsf{H}]_{jj}} \sum_{i=1}^{d} \sum_{k=1}^{N_\kappa} [\mathsf{S}_{x_i}]_{jk} \boldsymbol{\mathcal{F}}^{*,\mathrm{EC}}_{x_i}([\boldsymbol{u}_\kappa]_j, [\boldsymbol{u}_\kappa]_k).$$

5. For the dense-coupling scheme (13), add the inter-element coupling term to the residual term:

$$[\mathbf{r}_\kappa]_j = [\mathbf{r}_\kappa]_j + \frac{1}{[\mathsf{H}]_{jj}} \sum_{\kappa\gamma} \sum_{i=1}^{d} \sum_{l=1}^{N_\nu} [\mathsf{E}^{(\kappa\nu)}_{x_i}]_{jl} \boldsymbol{\mathcal{F}}^{*,\mathrm{EC}}_{x_i}([\boldsymbol{u}_\kappa]_j, [\boldsymbol{u}_\nu]_l),\ \forall j \in \{1, ..., N_\kappa\},$$

   where $\mathsf{E}^{(\kappa\nu)}_{x_i} \equiv \mathsf{R}^{\mathrm{T}}_{\kappa\gamma} \mathsf{P}^{\mathrm{T}}_{\kappa\gamma\to I} \mathsf{B}_I \mathsf{N}^{(\kappa)}_{I,x_i} \mathsf{P}_{\nu\gamma\to I} \mathsf{R}_{\nu\gamma}$.
   For the pointwise-coupling scheme (16), add the inter-element coupling term to the residual term:

$$\begin{aligned}
[\mathbf{r}_\kappa]_j = [\mathbf{r}_\kappa]_j &+ \frac{1}{[\mathsf{H}]_{jj}} \sum_{\kappa\gamma} \sum_{i=1}^{d} \sum_{l=1}^{N_I} [\mathsf{E}^{(\kappa I)}_{x_i}]_{jl} \boldsymbol{\mathcal{F}}^{*,\mathrm{EC}}_{x_i}([\boldsymbol{u}_\kappa]_j, [\overline{\boldsymbol{u}}_{\kappa I}]_l) \\
&- \frac{1}{[\mathsf{H}]_{jj}} \sum_{\kappa\gamma} \sum_{i=1}^{d} \sum_{l=1}^{N_I} \sum_{k=1}^{N_\kappa} [\mathsf{P}_{\kappa\gamma\to I} \mathsf{R}_{\kappa\gamma}]_{lj} [\mathsf{E}^{(\kappa I)}_{x_i}]_{kl} \boldsymbol{\mathcal{F}}^{*,\mathrm{EC}}_{x_i}([\overline{\boldsymbol{u}}_{\kappa I}]_l, [\boldsymbol{u}_\kappa]_k) \\
&+ \frac{1}{[\mathsf{H}]_{jj}} \sum_{\kappa\gamma} \sum_{i=1}^{d} \sum_{l=1}^{N_I} [\mathsf{E}^{(\kappa I)}_{x_i}]_{jl} \boldsymbol{\mathcal{F}}^{*,\mathrm{EC}}_{x_i}([\overline{\boldsymbol{u}}_{\kappa I}]_l, [\overline{\boldsymbol{u}}_{\nu I}]_l),\ \forall j \in \{1, ..., N_\kappa\},
\end{aligned}$$

   where $\mathsf{E}^{(\kappa I)}_{x_i} \equiv \mathsf{R}^{\mathrm{T}}_{\kappa\gamma} \mathsf{P}^{\mathrm{T}}_{\kappa\gamma\to I} \mathsf{B}_I \mathsf{N}^{(\kappa)}_{I,x_i}$ and the vectors $\overline{\boldsymbol{u}}_{\kappa I}$ and $\overline{\boldsymbol{u}}_{\nu I}$ are defined in Section 5.2.
6. If dissipation is required, augment the spatial residual term by the interface term (17):

$$[\mathbf{r}_\kappa]_j = [\mathbf{r}_\kappa]_j + \sum_{\kappa\gamma} \sum_{l=1}^{N_I} [\mathsf{P}_{\kappa\gamma\to I} \mathsf{R}_{\kappa\gamma}]_{lj} [\mathsf{B}_I]_{ll} \Lambda_I([\boldsymbol{u}_{\kappa I}]_l, [\boldsymbol{u}_{\nu I}]_l; [\boldsymbol{n}^{(\kappa)}_I]_l)([\boldsymbol{w}_{\kappa I}]_l - [\boldsymbol{w}_{\nu I}]_l),\ \forall j \in \{1, ..., N_\kappa\},$$

   where the matrix $\Lambda_I(\cdot, \cdot; \cdot)$ is positive semidefinite, the vectors $\boldsymbol{u}_{\kappa I}$ and $\boldsymbol{u}_{\nu I}$ are defined in Section 5.3, and the vectors $\boldsymbol{w}_{\kappa I}$ and $\boldsymbol{w}_{\nu I}$ in Section 5.2.

Once the spatial residual term has been computed for all elements in the tessellation, a time-marching method can be used to solve the resulting ordinary differential equations:

$$\frac{\mathrm{d}\boldsymbol{u}_\kappa}{\mathrm{d}t} + \mathbf{r}_\kappa = \mathbf{0}_\kappa,\ \forall \Omega_\kappa \in \mathcal{T}_h.$$

5 Theoretical analysis

In this section, we prove that both the dense-coupling and pointwise-coupling semi-discrete schemes locally and, consequently, globally conserve the conservative variables and entropy. Furthermore, we prove that the methods are design-order accurate. Finally, we demonstrate that the interface stabilization term dissipates entropy while maintaining the conservation and accuracy properties of the original schemes. We note that some of the proofs are the same as the ones shown in Crean *et al.* [11], while others follow their work and the work of Chan [10].

5.1 Dense-coupling entropy-conservative scheme

5.1.1 Conservation

For the schemes in this paper to accurately simulate flows with discontinuities, they must be consistent and conservative such that, if convergent, they converge to a weak solution as per the Lax-Wendroff theorem [51]. To show conservation of (13), we integrate over element κ by contracting the equation with the vector $\mathbf{1}_\kappa$ and deal with only one equation at a time. For instance, for the continuity equation, we have

$$\mathbf{1}_\kappa^{\mathrm{T}}\mathsf{H}\frac{\mathrm{d}\boldsymbol{\rho}_\kappa}{\mathrm{d}t}+\sum_{i=1}^{d}\mathbf{1}_\kappa^{\mathrm{T}}\left(2\mathsf{S}_{x_i}\circ\mathsf{F}_{x_i}^{(\rho)}(\boldsymbol{u}_\kappa,\boldsymbol{u}_\kappa)\right)\mathbf{1}_\kappa=-\sum_{\kappa\gamma}\sum_{i=1}^{d}\mathbf{1}_\kappa^{\mathrm{T}}\left\{\mathsf{E}_{x_i}^{(\kappa\nu)}\circ\mathsf{F}_{x_i}^{(\rho)}(\boldsymbol{u}_\kappa,\boldsymbol{u}_\nu)\right\}\mathbf{1}_\nu, \tag{21}$$

where $\boldsymbol{\rho}_\kappa\in\mathbb{R}^{N_\kappa}$ holds the density at the volume nodes of element κ and $\mathsf{F}_{x_i}^{(\rho)}(\cdot,\cdot)$ holds the rows and columns of $\mathsf{F}_{x_i}(\cdot,\cdot)$ associated to the continuity equation. Theorem 2 concerns the element-wise conservation property of the dense-coupling entropy-conservative scheme, while Theorem 3 concerns its global conservation property.

Theorem 2 *Scheme (13) is element-wise conservative. For instance, the discrete integral of the continuity equation over element κ is*

$$\mathbf{1}_\kappa^{\mathrm{T}}\mathsf{H}\frac{\mathrm{d}\boldsymbol{\rho}_\kappa}{\mathrm{d}t}=-\sum_{\kappa\gamma}\sum_{i=1}^{d}\mathbf{1}_\kappa^{\mathrm{T}}\left\{\mathsf{E}_{x_i}^{(\kappa\nu)}\circ\mathsf{F}_{x_i}^{(\rho)}(\boldsymbol{u}_\kappa,\boldsymbol{u}_\nu)\right\}\mathbf{1}_\nu,$$

which states that the time rate of change of mass inside element κ is equal to the net mass flow rate through its boundaries.

Proof The proof follows directly from Lemma 2 in Appendix C, and is similar to that given by Crean *et al.* [11] for their Theorem 3. □

Theorem 3 *Scheme (13) is globally conservative. For instance, with periodic boundary conditions, the discrete integral of the continuity equation over the domain simplifies to*

$$\sum_{\Omega_\kappa\in\mathcal{T}_h}\mathbf{1}_\kappa^{\mathrm{T}}\mathsf{H}_\kappa\frac{\mathrm{d}\boldsymbol{\rho}_\kappa}{\mathrm{d}t}=0.$$

Proof The proof is given in Appendix C. □

5.1.2 Entropy conservation

To show that scheme (13) conserves entropy, we left-multiply the PDEs by the entropy variables and integrate over element κ, which is equivalent to contracting (13) with the entropy variables $\boldsymbol{w}_\kappa$ to obtain

$$\boldsymbol{w}_\kappa^{\mathrm{T}}\tilde{\mathsf{H}}\frac{\mathrm{d}\boldsymbol{u}_\kappa}{\mathrm{d}t}+\sum_{i=1}^{d}\boldsymbol{w}_\kappa^{\mathrm{T}}\left(2\tilde{\mathsf{S}}_{x_i}\circ\mathsf{F}_{x_i}(\boldsymbol{u}_\kappa,\boldsymbol{u}_\kappa)\right)\mathbf{1}_\kappa=-\sum_{\kappa\gamma}\sum_{i=1}^{d}\boldsymbol{w}_\kappa^{\mathrm{T}}\left\{\tilde{\mathsf{E}}_{x_i}^{(\kappa\nu)}\circ\mathsf{F}_{x_i}(\boldsymbol{u}_\kappa,\boldsymbol{u}_\nu)\right\}\mathbf{1}_\nu. \tag{22}$$

Theorems 4 and 5 concern the element-wise and global entropy conservation properties of the scheme, respectively.

Theorem 4 *Scheme (13) is element-wise entropy conservative in the sense that (22) simplifies to*

$$\mathbf{1}_\kappa^{\mathrm{T}}\mathsf{H}\frac{\mathrm{d}\boldsymbol{s}_\kappa}{\mathrm{d}t} = -\sum_{\kappa\gamma}\sum_{i=1}^{d}\boldsymbol{w}_\kappa^{\mathrm{T}}\left\{\tilde{\mathsf{E}}_{x_i}^{(\kappa\nu)}\circ\mathsf{F}_{x_i}(\boldsymbol{u}_\kappa,\boldsymbol{u}_\nu)\right\}\mathbf{1}_\nu + \sum_{i=1}^{d}\mathbf{1}_\kappa^{\mathrm{T}}\mathsf{E}_{x_i}\boldsymbol{\psi}_{\kappa,x_i},$$

where $\boldsymbol{s}_\kappa \in \mathbb{R}^{N_\kappa}$ and $\boldsymbol{\psi}_{\kappa,x_i} \in \mathbb{R}^{N_\kappa}$ are the entropy and the potential flux in the x_i-direction at the volume nodes of element κ, respectively. Only the surface terms contribute to the net change of entropy, similar to the continuous case.

Proof The proof is shown in Crean *et al.* [11]. It also follows directly from Lemmas 3 and 4 in Appendix D. □

Theorem 5 *Scheme (13) globally conserves entropy. For instance, with periodic boundary conditions,*

$$\sum_{\Omega_\kappa\in\mathcal{T}_h}\mathbf{1}_\kappa^{\mathrm{T}}\mathsf{H}_\kappa\frac{\mathrm{d}\boldsymbol{s}_\kappa}{\mathrm{d}t} = 0.$$

Proof The proof directly follows from $\mathsf{E}_{x_i} = \sum_{\kappa\gamma}\mathsf{E}_{x_i}^{(\kappa\kappa)}$, Theorem 4 and Lemma 5 in Appendix D. □

5.1.3 Design-order accuracy

To show that the dense-coupling entropy-conservative scheme is design-order accurate, we deal with its strong form equation (11). We invoke Theorem 1 of Ref. [11] to prove that the spatial derivative term in (11) is design-order accurate. Theorem 6 concern the accuracy of the penalty term in (11).

Theorem 6 *The penalty term on the right-hand side of (11) is at least design-order accurate. More precisely, for $\boldsymbol{\mathcal{U}} \in C^{r_{\min}+1}(\Omega\times I,\mathbb{R}^m)$, the following relation is satisfied:*

$$\left[\left\{\tilde{\mathsf{E}}_{x_i}^{(\kappa\nu)}\circ\mathsf{F}_{x_i}(\boldsymbol{u}_\kappa,\boldsymbol{u}_\nu)\right\}\mathbf{1}_\nu - \left\{\tilde{\mathsf{E}}_{x_i}^{(\kappa\kappa)}\circ\mathsf{F}_{x_i}(\boldsymbol{u}_\kappa,\boldsymbol{u}_\kappa)\right\}\mathbf{1}_\kappa\right]_j = \mathcal{O}(h_{\max}^{r_{\min}}),\ \forall\ i\in\{1,...,d\},\ j\in\{1,...,N_\kappa\},$$

where $r_{\min}\equiv\min(r_\kappa,r_\nu)$, $h_{\max}\equiv\max(h_\kappa,h_\nu)$, $h_\kappa\equiv\max_{\boldsymbol{x}_j,\boldsymbol{x}_k\in S_\kappa}||\boldsymbol{x}_j-\boldsymbol{x}_k||_2$, and $h_\nu \equiv \max_{\boldsymbol{x}_j,\boldsymbol{x}_k\in S_\nu}||\boldsymbol{x}_j-\boldsymbol{x}_k||_2$.

Proof The proof is shown in Appendix E. □

5.2 Pointwise-coupling entropy-conservative scheme

5.2.1 Conservation

To show that (16) is conservative, similar to the dense-coupling entropy-conservative scheme, we contract it with the vector $\mathbf{1}_\kappa$ and deal with each equation separately. For the continuity equation, we have

$$\begin{aligned}\mathbf{1}_\kappa^{\mathrm{T}}\mathsf{H}\frac{\mathrm{d}\boldsymbol{\rho}_\kappa}{\mathrm{d}t} + \sum_{i=1}^{d}\mathbf{1}_\kappa^{\mathrm{T}}\left(2\mathsf{S}_{x_i}\circ\mathsf{F}_{x_i}^{(\rho)}(\boldsymbol{u}_\kappa,\boldsymbol{u}_\kappa)\right)\mathbf{1}_\kappa &= -\sum_{\kappa\gamma}\sum_{i=1}^{d}\mathbf{1}_\kappa^{\mathrm{T}}\left\{\mathsf{E}_{x_i}^{(\kappa I)}\circ\mathsf{F}_{x_i}^{(\rho)}(\boldsymbol{u}_\kappa,\overline{\boldsymbol{u}}_{\kappa I})\right\}\mathbf{1}_I\\ &\quad+\sum_{\kappa\gamma}\sum_{i=1}^{d}\mathbf{1}_\kappa^{\mathrm{T}}\mathsf{R}_{\kappa\gamma}^{\mathrm{T}}\mathsf{P}_{\kappa\gamma\to I}^{\mathrm{T}}\left\{(\mathsf{E}_{x_i}^{(\kappa I)})^{\mathrm{T}}\circ\mathsf{F}_{x_i}^{(\rho)}(\overline{\boldsymbol{u}}_{\kappa I},\boldsymbol{u}_\kappa)\right\}\mathbf{1}_\kappa\\ &\quad-\sum_{\kappa\gamma}\sum_{i=1}^{d}\mathbf{1}_\kappa^{\mathrm{T}}\mathsf{E}_{x_i}^{(\kappa I)}\boldsymbol{f}_{x_i}^{*,\mathrm{EC},\rho}(\overline{\boldsymbol{u}}_{\kappa I},\overline{\boldsymbol{u}}_{\nu I}),\end{aligned} \tag{23}$$

where $\boldsymbol{f}^{*,\mathrm{EC},\rho}(\cdot,\cdot)$ holds the elements in $\boldsymbol{f}^{*,\mathrm{EC}}(\cdot,\cdot)$ associated to the continuity equation. Theorem 7 addresses the element-wise conservation property of the pointwise-coupling entropy-conservative method, while theorem 8 addresses its global conservation property.

Theorem 7 *Scheme (16) is element-wise conservative. For instance, the discrete integral of the continuity equation over element κ is*

$$\mathbf{1}_\kappa^{\mathrm{T}}\mathsf{H}\frac{\mathrm{d}\boldsymbol{\rho}_\kappa}{\mathrm{d}t} = -\sum_{\kappa\gamma}\sum_{i=1}^{d}\mathbf{1}_\kappa^{\mathrm{T}}\mathsf{E}_{x_i}^{(\kappa I)}\boldsymbol{f}_{x_i}^{*,\mathrm{EC},\rho}(\overline{\boldsymbol{u}}_{\kappa I},\overline{\boldsymbol{u}}_{\nu I}).$$

Proof The proof is shown in Appendix F. □

Theorem 8 *Scheme (16) is globally conservative. For instance, with periodic boundary conditions, the discrete integral of the continuity equation over the domain simplifies to*

$$\sum_{\Omega_\kappa\in\mathcal{T}_h}\mathbf{1}_\kappa^{\mathrm{T}}\mathsf{H}_\kappa\frac{\mathrm{d}\boldsymbol{\rho}_\kappa}{\mathrm{d}t} = 0.$$

Proof The proof is shown in Appendix F. □

5.2.2 Entropy conservation

To show that (16) is entropy conservative, we contract it with the entropy variables $\boldsymbol{w}_\kappa$, which is equivalent to multiplying the PDEs by the entropy variables and integrating over element κ:

$$\begin{aligned}\boldsymbol{w}_\kappa^{\mathrm{T}}\tilde{\mathsf{H}}\frac{\mathrm{d}\boldsymbol{u}_\kappa}{\mathrm{d}t} + \sum_{i=1}^{d}\boldsymbol{w}_\kappa^{\mathrm{T}}\left(2\tilde{\mathsf{S}}_{x_i}\circ\mathsf{F}_{x_i}(\boldsymbol{u}_\kappa,\boldsymbol{u}_\kappa)\right)\mathbf{1}_\kappa = &-\sum_{\kappa\gamma}\sum_{i=1}^{d}\boldsymbol{w}_\kappa^{\mathrm{T}}\left\{\tilde{\mathsf{E}}_{x_i}^{(\kappa I)}\circ\mathsf{F}_{x_i}(\boldsymbol{u}_\kappa,\overline{\boldsymbol{u}}_{\kappa I})\right\}\mathbf{1}_I\\ &+\sum_{\kappa\gamma}\sum_{i=1}^{d}\boldsymbol{w}_\kappa^{\mathrm{T}}\tilde{\mathsf{R}}_{\kappa\gamma}^{\mathrm{T}}\tilde{\mathsf{P}}_{\kappa\gamma\to I}^{\mathrm{T}}\left\{(\tilde{\mathsf{E}}_{x_i}^{(\kappa I)})^{\mathrm{T}}\circ\mathsf{F}_{x_i}(\overline{\boldsymbol{u}}_{\kappa I},\boldsymbol{u}_\kappa)\right\}\mathbf{1}_\kappa\\ &-\sum_{\kappa\gamma}\sum_{i=1}^{d}\boldsymbol{w}_\kappa^{\mathrm{T}}\tilde{\mathsf{E}}_{x_i}^{(\kappa I)}\boldsymbol{f}_{x_i}^{*,\mathrm{EC}}(\overline{\boldsymbol{u}}_{\kappa I},\overline{\boldsymbol{u}}_{\nu I}).\end{aligned} \tag{24}$$

Theorems 9 and 10 concern the element-wise and global conservation properties of the scheme, respectively.

Theorem 9 *Scheme (16) is element-wise entropy conservative in the sense that (24) simplifies to*

$$\mathbf{1}_\kappa^{\mathrm{T}}\mathsf{H}\frac{\mathrm{d}\boldsymbol{s}_\kappa}{\mathrm{d}t} = -\sum_{\kappa\gamma}\sum_{i=1}^{d}\boldsymbol{w}_{\kappa I}^{\mathrm{T}}\tilde{\mathsf{N}}_{I,x_i}^{(\kappa)}\tilde{\mathsf{B}}_I\boldsymbol{f}_{x_i}^{*,\mathrm{EC}}(\overline{\boldsymbol{u}}_{\kappa I},\overline{\boldsymbol{u}}_{\nu I}) + \sum_{\kappa\gamma}\sum_{i=1}^{d}\mathbf{1}_I^{\mathrm{T}}\mathsf{N}_{I,x_i}^{(\kappa)}\mathsf{B}_I\overline{\boldsymbol{\psi}}_{\kappa I,x_i},$$

where $[\overline{\boldsymbol{\psi}}_{\kappa I,x_i}]_l \equiv \psi_{x_i}([\overline{\boldsymbol{u}}_{\kappa I}]_l)$, $\forall l\in\{1,...,N_I\}$ is the potential flux vector in the x_i-direction corresponding to the extrapolated entropy variables $\boldsymbol{w}_{\kappa I}$.

Proof The proof follows directly from Lemmas 3 and 4 in Appendix D, and Lemma 6 in Appendix G. □

Theorem 10 *Scheme (16) globally conserves entropy. For instance, with periodic boundary conditions,*

$$\sum_{\Omega_\kappa\in\mathcal{T}_h}\mathbf{1}_\kappa^{\mathrm{T}}\mathsf{H}_\kappa\frac{\mathrm{d}\boldsymbol{s}_\kappa}{\mathrm{d}t} = 0,$$

Proof The proof is shown in Appendix G. □

5.2.3 Design-order accuracy

For the accuracy proof of the pointwise-coupling entropy-conservative scheme, we deal with its strong form (14). We invoke Theorem 1 of Ref. [11] for the accuracy of the volumetric terms. Theorem 11 concerns the accuracy of the penalty term.

Theorem 11 *The penalty term on the right-hand side of (14) is at least design-order accurate. More precisely, for* $\boldsymbol{\mathcal{U}} \in C^{r_{\min}+1}(\Omega \times I, \mathbb{R}^m)$, $\boldsymbol{\mathcal{W}} \in C^{r_{\min}+1}(\mathcal{H}, \mathbb{R}^m)$, *the following relation holds:*

$$\Bigg[-\left\{\tilde{\mathsf{E}}^{(\kappa I)}_{x_i} \circ \mathsf{F}_{x_i}(\boldsymbol{u}_\kappa, \overline{\boldsymbol{u}}_{\kappa I})\right\}\mathbf{1}_I + \tilde{\mathsf{R}}^{\mathrm{T}}_{\kappa\gamma}\tilde{\mathsf{P}}^{\mathrm{T}}_{\kappa\gamma\to I}\left\{(\tilde{\mathsf{E}}^{(\kappa I)}_{x_i})^{\mathrm{T}} \circ \mathsf{F}_{x_i}(\overline{\boldsymbol{u}}_{\kappa I}, \boldsymbol{u}_\kappa)\right\}\mathbf{1}_\kappa$$
$$- \tilde{\mathsf{E}}^{(\kappa I)}_{x_i}\boldsymbol{f}^{*,\mathrm{EC}}_{x_i}(\overline{\boldsymbol{u}}_{\kappa I}, \overline{\boldsymbol{u}}_{\nu I}) + \left\{\tilde{\mathsf{E}}^{(\kappa\kappa)}_{x_i} \circ \mathsf{F}_{x_i}(\boldsymbol{u}_\kappa, \boldsymbol{u}_\kappa)\right\}\mathbf{1}_\kappa \Bigg]_j = \mathcal{O}(h^{r_{\min}}_{\max}),\ \forall\ i \in \{1, ..., d\},\ ji \in \{1, ..., N_\kappa\},$$

where, as previously defined, $r_{\min} \equiv \min(r_\kappa, r_\nu)$ *and* $h_{\max} \equiv \max(h_\kappa, h_\nu)$.

Proof The proof is shown in Appendix H. □

5.3 Entropy dissipative term

As previously mentioned, the dissipative interface term (17) can be added to the right-hand side of both entropy-conservative schemes (13) and (16) to obtain entropy-stable schemes. Here we show that the interface term (17) is conservative, entropy dissipative, and design-order accurate in Theorems 12, 13, and 14, respectively.

5.3.1 Conservation

Theorem 12 *The dissipative term (17) maintains the conservation property of the original schemes. For instance, for the continuity equation, at a given interface shared by two neighbouring elements* κ *and* ν,

$$\mathbf{1}^{\mathrm{T}}_\kappa \mathsf{R}^{\mathrm{T}}_{\kappa\gamma}\mathsf{P}^{\mathrm{T}}_{\kappa\gamma\to I}\Lambda_I(\boldsymbol{u}_{\kappa I}, \boldsymbol{u}_{\nu I}; \boldsymbol{n}^{(\kappa)}_I)^{(\rho)}\tilde{\mathsf{B}}_I(\boldsymbol{w}_{\kappa I} - \boldsymbol{w}_{\nu I}) +$$
$$\mathbf{1}^{\mathrm{T}}_\nu \mathsf{R}^{\mathrm{T}}_{\nu\gamma}\mathsf{P}^{\mathrm{T}}_{\nu\gamma\to I}\Lambda_I(\boldsymbol{u}_{\nu I}, \boldsymbol{u}_{\kappa I}; \mathsf{N}^{(\nu)}_I)^{(\rho)}\tilde{\mathsf{B}}_I(\boldsymbol{w}_{\nu I} - \boldsymbol{w}_{\kappa I}) = 0,$$

where $\Lambda_I(\boldsymbol{u}_{\kappa I}, \boldsymbol{u}_{\nu I}; \boldsymbol{n}^{(\kappa)}_I)^{(\rho)}$ *and* $\Lambda_I(\boldsymbol{u}_{\nu I}, \boldsymbol{u}_{\kappa I}; \mathsf{N}^{(\nu)}_I)^{(\rho)}$ *respectively hold the rows of* $\Lambda_I(\boldsymbol{u}_{\kappa I}, \boldsymbol{u}_{\nu I}; \boldsymbol{n}^{(\kappa)}_I)$ *and* $\Lambda_I(\boldsymbol{u}_{\nu I}, \boldsymbol{u}_{\kappa I}; \mathsf{N}^{(\nu)}_I)$ *corresponding to the continuity equation.*

Proof The proof is shown in Appendix I. □

5.3.2 Entropy dissipation

Theorem 13 *The term (17) dissipates entropy at each interface, i.e.*

$$-\boldsymbol{w}^{\mathrm{T}}_\kappa \tilde{\mathsf{R}}^{\mathrm{T}}_{\kappa\gamma}\tilde{\mathsf{P}}^{\mathrm{T}}_{\kappa\gamma\to I}\Lambda_I(\boldsymbol{u}_{\kappa I}, \boldsymbol{u}_{\nu I}; \boldsymbol{n}^{(\kappa)}_I)\tilde{\mathsf{B}}_I(\boldsymbol{w}_{\kappa I} - \boldsymbol{w}_{\nu I})$$
$$-\boldsymbol{w}^{\mathrm{T}}_\nu \tilde{\mathsf{R}}^{\mathrm{T}}_{\nu\gamma}\tilde{\mathsf{P}}^{\mathrm{T}}_{\nu\gamma\to I}\Lambda_I(\boldsymbol{u}_{\nu I}, \boldsymbol{u}_{\kappa I}; \mathsf{N}^{(\nu)}_I)\tilde{\mathsf{B}}_I(\boldsymbol{w}_{\nu I} - \boldsymbol{w}_{\kappa I}) \leq 0.$$

Proof The proof is shown in Appendix J and follows from the fact that the interface term penalizes the jump in entropy. □

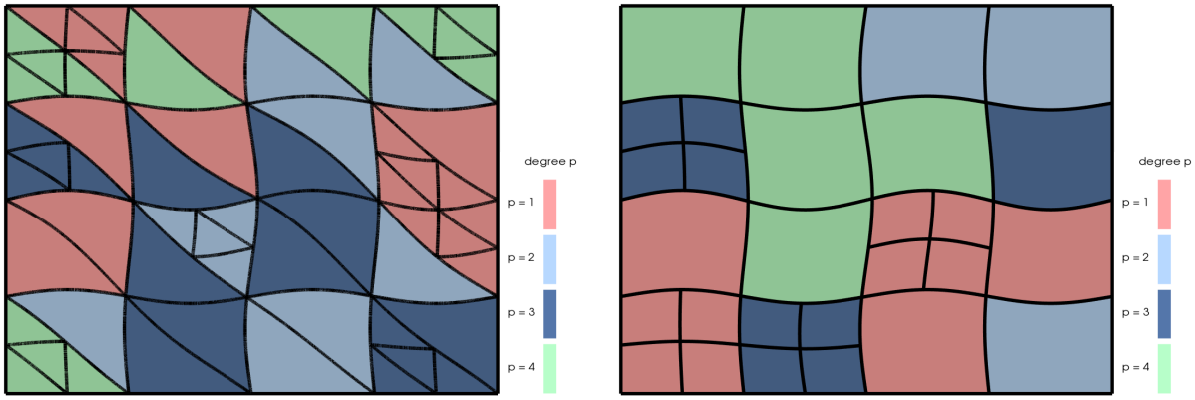

(a) Grid with triangles.

(b) Grid with quadrilaterals.

Fig. 3: 2 examples of coarse non-conforming curved grids with hanging nodes and different degree operators.

5.3.3 Design-order accuracy

Theorem 14 *The dissipative term (17) maintains the design-order accuracy of the original schemes. More precisely, for* $\boldsymbol{\mathcal{W}} \in C^{r_{\min}+1}(\mathcal{H}, \mathbb{R}^m)$*, the following relation holds:*

$$\tilde{\mathsf{R}}_{\kappa\gamma}^{\mathrm{T}} \tilde{\mathsf{P}}_{\kappa\gamma \to I} \Lambda_I(\boldsymbol{u}_{\kappa I}, \boldsymbol{u}_{\nu I}; \boldsymbol{n}_I^{(\kappa)}) \tilde{\mathsf{B}}_I(\boldsymbol{w}_{\kappa I} - \boldsymbol{w}_{\nu I}) = \mathcal{O}(h_{\max}^{r_{\min}}),$$

where, as previously defined, $r_{\min} \equiv \min(r_\kappa, r_\nu)$ *and* $h_{\max} \equiv \max(h_\kappa, h_\nu)$*.*

Proof The proof is shown in Appendix K. □

6 Results

In this section, we numerically validate the conservation, entropy conservation/dissipation, and design-order accuracy properties of both schemes. Furthermore, we compare the schemes in terms of robustness and efficiency.

6.1 Solver settings

The traditional explicit fourth-order Runge-Kutta time-marching method [52] is used to evolve the solution in time with a sufficiently small CFL condition to ensure that the temporal discretization errors are negligible compared to the spatial discretization errors. Ismail and Roe's [53] entropy-conservative flux is used with the extended Taylor series expansion proposed in Ref. [11] to compute logarithms of values near zero. This numerical flux satisfies Definition 3, as it was shown to be continuously differentiable in Ref. [11] for conservative variables with positive density and pressure. A matrix-type interface dissipation term is used by defining the symmetric positive semi-definite matrix of (17) as $\mathsf{R}^{\mathrm{T}}\mathsf{D}\mathsf{R}$, where R has as its columns the right eigenvectors of the Jacobian of the Ismail and Roe flux in the normal direction, and D is the diagonal matrix of the absolute values of the corresponding scaled eigenvalues (both of which are defined in Ref. [53]).

To generate a curvilinear grid with non-conforming interfaces, we first randomly assign different degree p operators (e.g. from $p = 1$ to $p = 4$) to the elements of a conforming affine mesh and then randomly isotropically subdivide some of the elements. Finally, we curve the grid using a geometric mapping function. An example of the outcome of this procedure is shown in Figure 3 for grids constructed with triangles and quadrilaterals. We use the Ω SBP operators of Ref. [31] on triangular elements and the tensor-product LG operators on quadrilateral and hexahedral elements.

6.2 Test cases

6.2.1 Two-dimensional isentropic vortex

A two-dimensional unsteady isentropic vortex problem with smooth solution is used for the convergence and efficiency studies, and to show that the schemes are conservative and entropy conservative/dissipative. The variant of the problem solved in this paper has the following analytical solution [54]:

$$u_1 = 1 - \frac{\alpha}{2\pi}(x_2 - x_2^{(c)})\mathrm{e}^{1-r^2}, \quad u_2 = \frac{\alpha}{2\pi}\Big(x_1 - (x_1^{(c)} + t)\Big)\mathrm{e}^{1-r^2},$$
$$\rho = \left(1 - \frac{\alpha^2(\gamma-1)}{16\gamma\pi^2}\mathrm{e}^{2(1-r^2)}\right)^{\frac{1}{\gamma-1}}, \quad p = \rho^\gamma,$$

where $r^2 = \Big(x_1 - (x_1^{(c)} + t)\Big)^2 + \Big(x_2 - x_2^{(c)}\Big)^2$. Here, we set the vortex strength to $\alpha = 3$, initially center the vortex at $(x_1^{(c)}, x_2^{(c)}) = (5, 0)$ on a $(0, 20) \times (-5, 5)$ domain, impose periodic boundary conditions, and numerically solve the test case until $t = T = 5$. Note that although the perturbation in the flow is not machine precision zero away from the vortex, the imposition of periodic boundary conditions introduces negligible error since the domain is relatively large (we refer the interested reader to Section IV.B. of Ref. [55] for further information).

The grids generated for this problem are curved using the perturbation function [32]

$$x_1 = \hat{x}_1 + \frac{1}{8}\cos\left(\frac{\pi}{20}(\hat{x}_1 - 10)\right)\cos\left(\frac{3\pi}{10}\hat{x}_2\right),$$
$$x_2 = \hat{x}_2 + \frac{1}{8}\sin\left(\frac{\pi}{5}(x_1 - 10)\right)\cos\left(\frac{\pi}{10}\hat{x}_2\right),$$

where $\vec{\hat{x}}$ represents the nodal coordinates of the affine meshes (i.e. before performing the curvilinear mapping). Using the aforementioned perturbation function, we perturb the elements at the nodal coordinates coinciding with the nodes of degree $l = 2$ multidimensional Lagrange finite elements. We then perform a degree $l = 2$ polynomial interpolation of these nodal sets to the nodes of the SBP operators. Finally, we follow the approach of Section 3.3 to construct the SBP operators on the physical elements. This procedure ensures that Assumption 1 holds.

6.2.2 Three-dimensional isentropic vortex

To verify the accuracy of the schemes for three-dimensional test cases, a three-dimensional unsteady isentropic vortex problem with smooth solution, obtained from an extrusion of its two-dimensional counterpart, is solved. In this work, the following analytical solution is used [56]:

$$\rho = \left(1 - \frac{\gamma-1}{2}\Pi^2\right)^{\frac{1}{\gamma-1}}, \quad \vec{u} = \vec{u}_0 + \Pi\vec{r}, \quad e = \frac{1}{\gamma-1}\left(1 - \frac{\gamma-1}{2}\Pi^2\right)^{\frac{\gamma}{\gamma-1}} + \frac{\rho}{2}\vec{u}^{\mathrm{T}}\vec{u},$$

where $\Pi = 0.4\mathrm{e}^{\frac{1-\vec{r}^{\mathrm{T}}\vec{r}}{2}}$, $\vec{v}_0 = \big[0,\, 1,\, 0\big]^{\mathrm{T}}$, and $\vec{r} = \big[-(x_2 - t),\, x_1,\, 0\big]^{\mathrm{T}}$. We impose periodic boundary conditions on a $\Omega \equiv (-10, 10)^3$ domain and numerically solve the test case until $t = T = 2.5$. The grid used for this problem is curved using the perturbation function

$$x_i = \hat{x}_i + 0.05\sin\left(\frac{\pi\hat{x}_i}{2}\right), \ \forall i \in \{1, 2, 3\},$$

at the nodes of degree $l = 2$ Lagrange elements, which satisfies Assumption 1 when all SBP operators are at least degree $p = 3$.

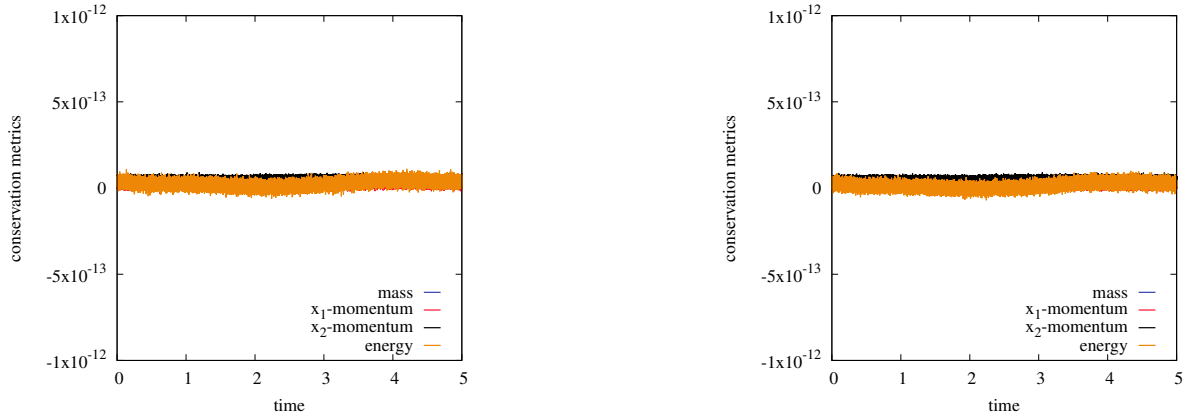

(a) Dense-coupling entropy-stable scheme.

(b) Pointwise-coupling entropy-stable scheme.

Fig. 4: Two-dimensional isentropic vortex test case. Conservation of mass, momentum, and energy on a coarse non-conforming curved grid.

6.2.3 Three-dimensional inviscid Taylor-Green vortex

The viscous Taylor-Green vortex is often studied in the turbulence community, while its inviscid counterpart is used to assess the robustness of discretization methods. The initial three-dimensional vortices stretch and, over time, generate small eddies which do not decay in the inviscid case due to the lack of viscosity. The flow is thus rendered under-resolved and can pose stability issues for some numerical methods. The initial condition is given by [57]

$$\rho = 1,\ u_1 = \sin(x_1)\cos(x_2)\cos(x_3),\ u_2 = -\cos(x_1)\sin(x_2)\cos(x_3),$$
$$u_3 = 0,\ p = \frac{1}{\gamma M_0^2} + \frac{1}{16}\Big(2\cos(2x_1) + 2\cos(2x_2) + \cos(2x_1)\cos(2x_3) + \cos(2x_2)\cos(2x_3)\Big),$$

on a $(-\pi,\pi)^3$ periodic domain. Here, the Mach number is set to $M_0 = 0.1$ and the solution is solved until $t = T = 20$. Furthermore, the grid is curved according to [40]

$$x_i = \hat{x}_i + \frac{1}{8}\sin(\hat{x}_1)\sin(\hat{x}_2)\sin(\hat{x}_3),\ \forall i \in \{1,2,3\},$$

at the nodes of degree $l = 2$ Lagrange elements, which satisfies Assumption 1 when all SBP operators are at least degree $p = 3$.

6.3 Conservation

As previously mentioned, it is important to ensure that the schemes developed in this work are conservative in the Lax-Wendroff sense [51] such that they can be used to simulate flows with discontinuities. In Figure 4, we plot the evolution of the conservation metrics defined as

$$\sum_{\Omega_\kappa \in \mathcal{T}_h} \mathbf{1}_\kappa^{\mathrm{T}} \mathsf{H}_\kappa \Big(\boldsymbol{\rho}_\kappa(t) - \boldsymbol{\rho}_\kappa(t=0)\Big),\ \sum_{\Omega_\kappa \in \mathcal{T}_h} \mathbf{1}_\kappa^{\mathrm{T}} \mathsf{H}_\kappa \Big((\boldsymbol{\rho u}_1)_\kappa(t) - (\boldsymbol{\rho u}_1)_\kappa(t=0)\Big),$$
$$\sum_{\Omega_\kappa \in \mathcal{T}_h} \mathbf{1}_\kappa^{\mathrm{T}} \mathsf{H}_\kappa \Big((\boldsymbol{\rho u}_2)_\kappa(t) - (\boldsymbol{\rho u}_2)_\kappa(t=0)\Big),\ \sum_{\Omega_\kappa \in \mathcal{T}_h} \mathbf{1}_\kappa^{\mathrm{T}} \mathsf{H}_\kappa \Big((\boldsymbol{e})_\kappa(t) - (\boldsymbol{e})_\kappa(t=0)\Big),\ \forall t \in I,$$

for the two-dimensional isentropic vortex test case, which are the discrete analogue to individually integrating the difference in the conservative variables over the domain. The results, obtained for a coarse curved grid with $4 \times 4 \times 2$ triangular elements (before the random *hp*-refinement procedure) with degree $p = 1$ to $p = 4$ operators, show that mass, momentum, and energy are conserved (up to machine precision zero) for both entropy-stable schemes on non-conforming curved grids. A coarse grid is used to emphasize that the conservation property of these schemes holds for arbitrarily coarse grids and not only in the limit of mesh refinement. Similar results were obtained for the entropy-conservative schemes.

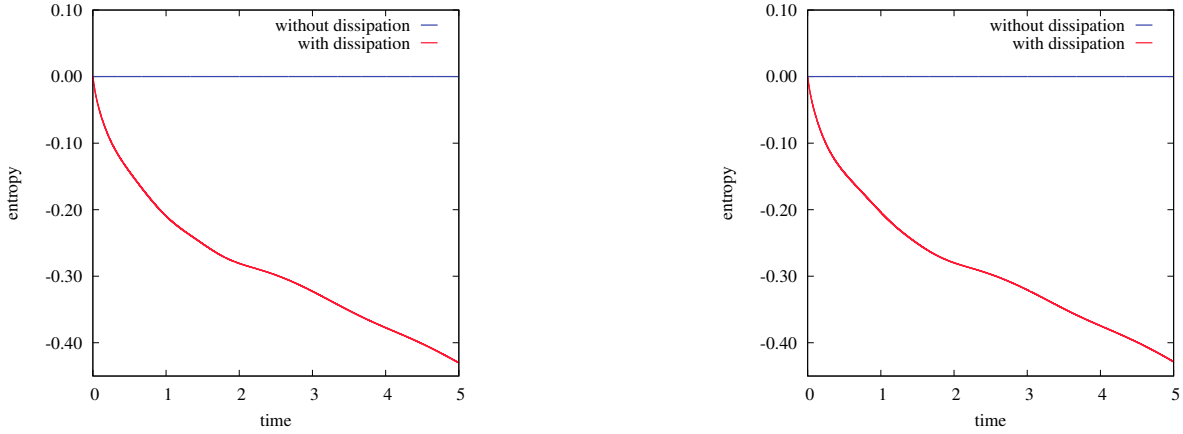

(a) Dense-coupling schemes.

(b) Pointwise-coupling schemes.

Fig. 5: Two-dimensional isentropic vortex test case. Conservation and dissipation of entropy on a coarse non-conforming curved grid.

Table 1: Two-dimensional isentropic vortex test case. Entropy generated by the dense- and pointwise-coupling entropy-stable schemes on coarse and fine curved grids.

Grid	Degree of operators	Entropy at time T	
		Dense-coupling	Pointwise-coupling
Coarse ($4 \times 4 \times 2$ elements)	1, 2, 3, 4	-0.430	-0.428
Fine ($10 \times 10 \times 2$ elements)	3, 4	-0.035	-0.030

6.4 Entropy conservation and dissipation

Figure 5 shows the evolution of the discrete approximation to the integral of the entropy computed as

$$\sum_{\Omega_\kappa \in \mathcal{T}_h} \mathbf{1}_\kappa^{\mathrm{T}} \mathsf{H}_\kappa \boldsymbol{s}_\kappa(t), \ \forall t \in I,$$

over time for the two-dimensional isentropic vortex problem on a curved grid with $4 \times 4 \times 2$ triangular elements (before the random hp-refinement procedure) and degree $p = 1$ to $p = 4$ operators. The results show that both entropy-conservative methods (13) and (16) conserve entropy and, when augmented with the interface stabilization term (17), dissipate entropy on non-conforming curved meshes. Both entropy-stable schemes dissipate entropy in a similar manner since they utilize the same dissipative term. Once again, a coarse grid is used to show that the entropy conservation and dissipation properties of these schemes hold for arbitrarily coarse grids. Furthermore, the significant dissipative behaviour is primarily because a coarse grid is used in which approximately half the elements are associated with relatively low-degree ($p = 1$ and $p = 2$) operators. On a finer curved grid with $10 \times 10 \times 2$ elements (before the random hp-refinement procedure) and only $p = 3$ and $p = 4$ operators, we observed a decay in entropy of 92% and 93% for the dense- and pointwise-coupling entropy-stable schemes, respectively (see Table 1).

While we observed in Figure 5 that the entropy-conservative methods conserve entropy, the entropy generated at the fully-discrete level is not machine precision zero since the fourth-order Runge-Kutta time-marching method is not entropy-conservative. Figure 6 shows the entropy generation on a non-conforming curved grid with $4 \times 4 \times 2$ triangular elements (before the random hp-refinement procedure) for both entropy-conservative schemes as a function of the CFL. The results demonstrate that the entropy generated by the time-marching method converges to zero at a rate of $\mathcal{O}(\Delta t^{4.9})$, where Δt is the time step. Similar convergence rates have also been observed for conforming schemes [11, 10, 40].

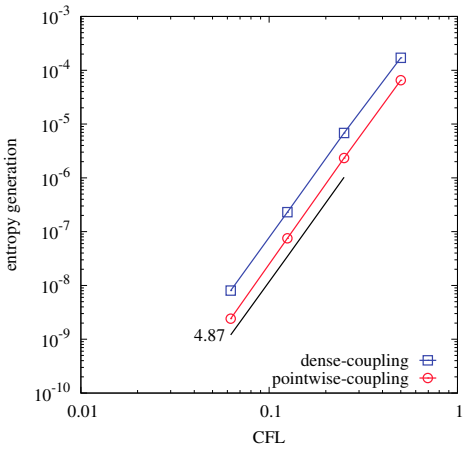

Fig. 6: Two-dimensional isentropic vortex test case. Convergence of entropy generation as a function of the CFL on a curved non-conforming grid (the convergence rates of the three smallest time steps are provided).

6.5 Accuracy and efficiency

6.5.1 Two-dimensional test cases

We test the accuracy of the schemes on non-conforming curved grids arising from *h*-, *p*-, and *hp*-refinement. We first generate a sequence of affine meshes with n element edges in each direction where $n \in \{25, 50, 75, 100, 125\}$. For *hp*-refinement, as before, we randomly assign different degree p operators to the elements (from $p = 1$ to $p = 4$), then randomly isotropically subdivide some of the elements, and curve the grids. For *p*-refinement, we randomly assign different degree p operators to the elements (from $p = 1$ to $p = 4$) and curve the grids. Finally, for *h*-refinement, we assign a constant degree p operator ($p = 1$, $p = 2$, $p = 3$, or $p = 4$), then randomly isotropically subdivide some of the elements, and curve the grids. This set of grids is then used to perform convergence studies of the entropy-conservative and entropy-stable schemes. Figures 7 and 8 show the L^2 error in the conservative variables, i.e.

$$\sqrt{\sum_{\Omega_\kappa \in \mathcal{T}_h} \left(||\boldsymbol{\rho}_\kappa - \boldsymbol{\rho}_{\kappa,\text{exact}}||_2^2 + ||\boldsymbol{e}_\kappa - \boldsymbol{e}_{\kappa,\text{exact}}||_2^2 + \sum_{i=1}^{d} ||(\boldsymbol{\rho u}_i)_\kappa - (\boldsymbol{\rho u}_i)_{\kappa,\text{exact}}||_2^2 \right)},$$

versus the mesh spacing $(1/n)$ for the two-dimensional isentropic vortex problem. To compute the L^2 solution error, we interpolate the solutions from the SBP nodes onto the nodes of a cubature rule of degree $3p_\kappa + 1$ for each element κ in the tessellation, and then integrate the square of the solution error over the domain. The convergence rates calculated from the least squares regression line of the 3 finest grids are also shown in the figures.

The results show that the entropy-stable schemes generally achieve $p_{\min} + 1$ asymptotic convergence rates, with the lowest convergence rate being $p_{\min} + 0.69$. The entropy-conservative schemes converge at rates between $p_{\min}$ and $p_{\min} + 1$ with the exception of the dense-coupling entropy-conservative scheme with $p = 4$ LG and Ω operators on the *h*-refinement grid, which converge at a rate slightly higher than $p_{\min} + 1$. Convergence rates between p and $p + 1$ have also been observed for entropy-conservative and entropy-stable schemes on conforming grids (e.g. [20,21,11]) and on staggered grids (e.g. [27]). Moreover, the dense-coupling and pointwise-coupling schemes achieve comparable errors on a given grid. Finally, the LG operators attain slightly lower errors than the Ω operators for a given mesh spacing.

The purpose of the efficiency study performed in this paper is simply to compare the dense-coupling scheme to the pointwise-coupling scheme (and not to compare tensor-product operators with multidimensional operators). Figure 9 shows the L^2 solution error as a function of the normalized average spatial residual computation time for one time step. In this plot, "EC" represents entropy-conservative, "SS" entropy-stable, "DC" dense-coupling scheme, and "PC" pointwise-coupling scheme. The results show that the pointwise-coupling scheme is computationally more efficient than the dense-coupling scheme: while both methods achieve similar errors, the pointwise-coupling scheme requires fewer entropy-conservative

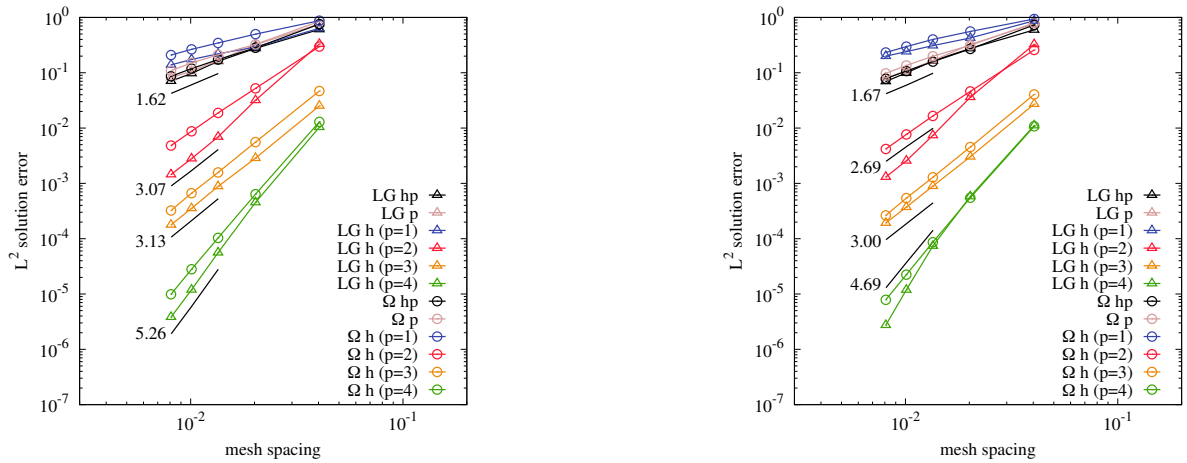

(a) Dense-coupling entropy-conservative scheme.

(b) Pointwise-coupling entropy-conservative scheme.

Fig. 7: Two-dimensional isentropic vortex test case. Convergence studies of the entropy-conservative schemes on curved non-conforming grids (the convergence rates of the three finest grids are provided).

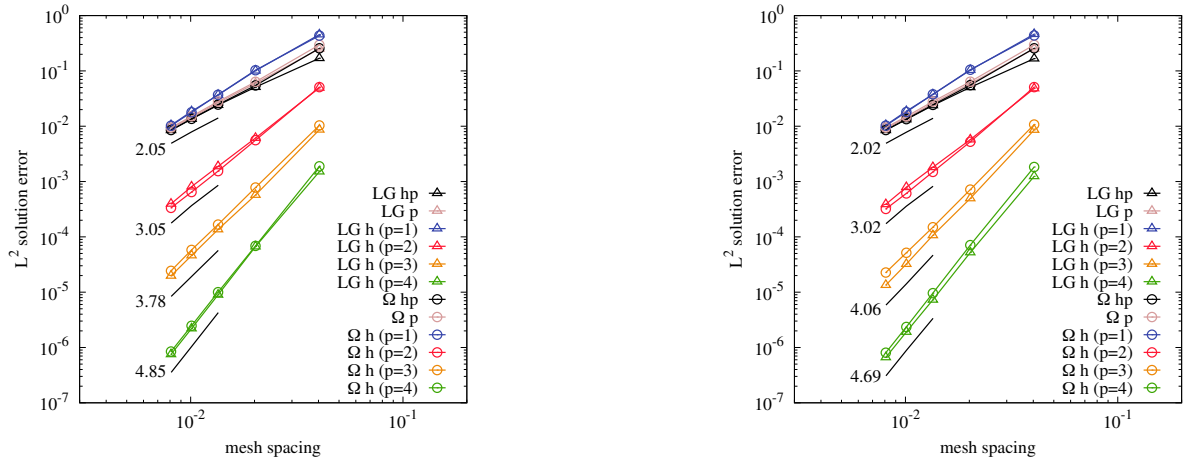

(a) Dense-coupling entropy-stable scheme.

(b) Pointwise-coupling entropy-stable scheme.

Fig. 8: Two-dimensional isentropic vortex test case. Convergence studies of the entropy-stable schemes on curved non-conforming grids (the convergence rates of the three finest grids are provided).

flux functions to couple neighbouring elements since it does not fully couple their volume nodes. The efficiency benefit provided by the pointwise-coupling scheme is even more pronounced for three-dimensional problems since the number of volume nodes per element for a given degree p scales as $\mathcal{O}(p^d)$, where d is the number of dimensions. Finally, augmenting the entropy-conservative schemes with the entropy dissipative term considerably improves the accuracy of the schemes with a negligible impact on computational time.

6.5.2 Three-dimensional test cases

We also verify that the accuracy properties of the schemes generalize to three-dimensional problems by randomly *hp*-refining a sequence of hexahedral curved grids with n element edges in each direction, where $n \in \{15, 25, 35, 45\}$, and degree $p = 3$ and $p = 4$ tensor-product LG operators for the three-dimensional isentropic vortex problem. Similar to the two-dimensional scenario, the convergence rate is between $p_{\min}$ and $p_{\min} + 1$ for the entropy-conservative schemes and approximately $p_{\min} + 1$ for the entropy-stable schemes as shown in Figure 10.

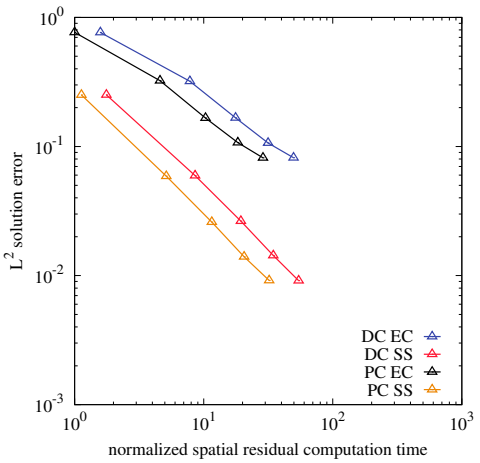

(a) LG SBP operators.

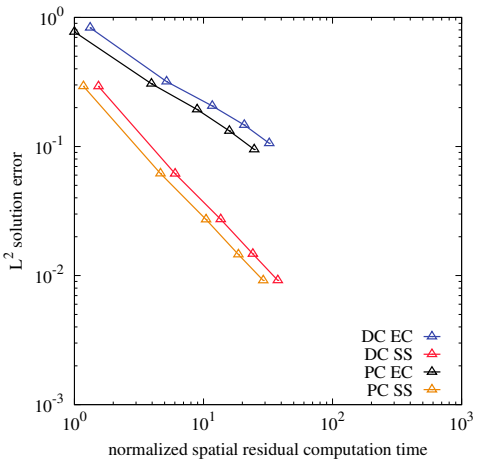

(b) Ω SBP operators.

Fig. 9: Two-dimensional isentropic vortex test case. Efficiency study of the entropy-conservative and entropy-stable schemes on curved non-conforming grids.

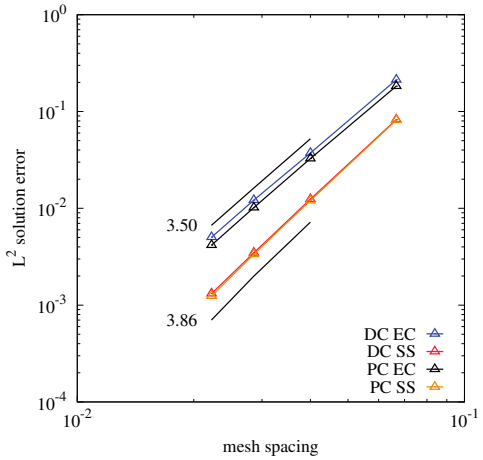

Fig. 10: Three-dimensional isentropic vortex test case. Convergence studies of the entropy-conservative and entropy-stable schemes on curved non-conforming grids (the convergence rates of the three finest grids are provided).

6.6 Robustness

Gassner *et al.* [21] numerically showed the robustness benefit of kinetic-energy-preserving, entropy-conservative, and entropy-stable methods over standard DG spectral-element methods. Figure 11(a) shows that both entropy-conservative methods (without interface dissipation) are stable for the inviscid Taylor-Green vortex test case on a coarse curved grid with $4 \times 4 \times 4$ hexahedral elements (before the random *hp*-refinement procedure) and degree $p = 3$ and $p = 4$ tensor-product LG operators, similar to the entropy-conservative schemes used in Ref. [21] on conforming grids. Since the schemes utilize the Ismail and Roe numerical flux, which is not kinetic-energy-preserving in the sense of Jameson [58], kinetic energy is not conserved as shown in Figure 11(b).

7 Conclusions

We presented two entropy-stable semi-discrete schemes for hyperbolic conservation laws applicable to curved non-conforming grids caused by *h*-, *p*-, or *hp*-adaptivity: one is characterized by dense coupling, the other by pointwise coupling. Both methods are compatible with any degree p diagonal-norm SBP operator equipped with degree $2p$ or higher interface quadrature rules, such as the collocated DG operators

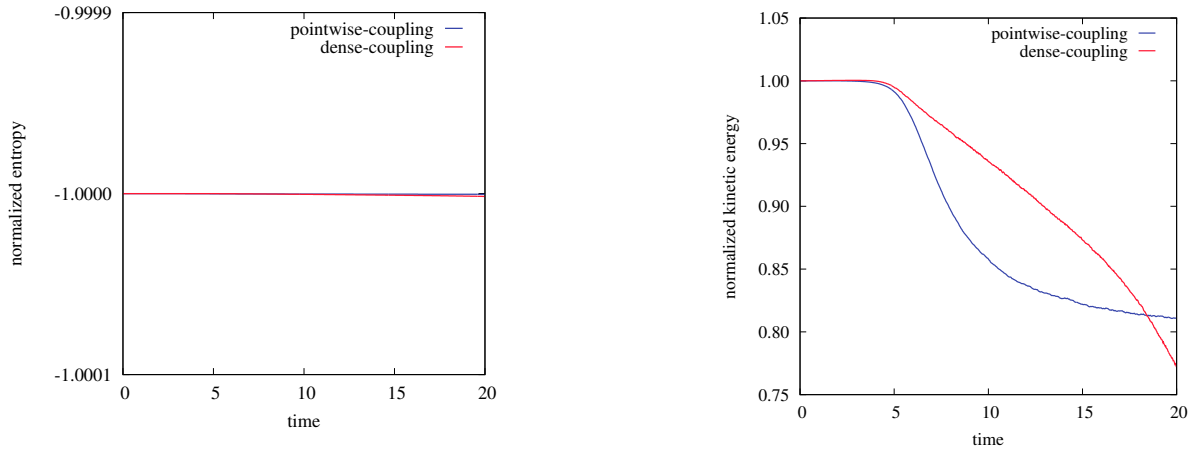

(a) Normalized entropy versus time.

(b) Normalized kinetic energy versus time.

Fig. 11: Inviscid Taylor-Green vortex test case. Evolution of entropy and kinetic energy over time using both entropy-conservative schemes on a coarse curved non-conforming grid.

constructed on the tensor-product LG nodes and the multidimensional Ω SBP operators of Ref. [31]. The conservation, entropy conservation/dissipation, and accuracy properties of the schemes were first theoretically proven and then numerically validated. Similar to their conforming counterparts, the non-conforming schemes are stable for the inviscid Taylor-Green vortex problem on a coarse curved grid without any interface dissipation. The "pointwise-coupling" scheme was shown to be computationally more efficient than the "dense-coupling" scheme, since the former couples neighbouring elements only at interface nodes, whereas the latter performs the coupling at the volume nodes. Furthermore, we showed that the entropy-conservative method of Friedrich *et al.* [28] applicable on non-conforming affine meshes and compatible with tensor-product SBP operators with boundary nodes is a subset of the dense-coupling entropy-conservative scheme (when the SBP operators are equipped with degree $2p$ or higher quadrature rules). While in this paper we assumed periodic boundary conditions, other entropy-stable boundary conditions developed primarily for tensor-product SBP operators with boundary nodes (e.g. the ones in Refs. [59,8]) are compatible with the pointwise-coupling scheme even when using SBP operators without boundary nodes. The underlying reason is that this scheme, similar to entropy-stable schemes compatible only with SBP operators with boundary nodes, can weakly impose boundary conditions in a pointwise manner. A critical assumption made in this work is the positivity of certain quantities, such as density and pressure for the Euler equations. Since this assumption can be violated in practice and thus undermine the robustness of the algorithms, a recommendation for future research is to carefully integrate positivity-preserving techniques, such as Zhang and Shu's [60], in these non-conforming methods such that the resulting schemes are both entropy stable and positivity preserving. Moreover, a natural extension of the current work is to expand the theory to include the compressible Navier-Stokes equations. The main challenge is to construct viscous inter-element coupling terms between non-conforming curved elements that are compatible with SBP operators without boundary nodes. Finally, we believe the results of this paper provide a sound foundation for the development of tensor-product and multidimensional entropy-stable *hp*-adaptive SBP methods driven by output-based *a posteriori* error estimates.

8 Acknowledgments

We wish to thank Masayuki Yano for insightful implementation recommendations about grids with hanging nodes and David Del Rey Fernández for helpful discussions regarding the pointwise-coupling term used in this paper. We also thank the Aerospace Computational Engineering Lab at the University of Toronto for the use of their software, the Automated PDE Solver (APS). Finally, we gratefully acknowledge the financial support provided by the governments of Ontario and Canada. Computations were performed on the Niagara supercomputer at the SciNet HPC Consortium [61]. SciNet is funded by: the Canada Foundation for Innovation; the Government of Ontario; Ontario Research Fund - Research Excellence; and the University of Toronto.

References

1. M. Yano and D. L. Darmofal, "An optimization-based framework for anisotropic simplex mesh adaptation," *Journal of Computational Physics*, vol. 231, pp. 7626–7649, Sept. 2012.
2. K. J. Fidkowski, "Output-based space-time mesh optimization for unsteady flows using continuous-in-time adjoints," *Journal of Computational Physics*, vol. 341, pp. 258–277, July 2017.
3. R. Hartmann, J. Held, T. Leicht, and F. Prill, "Error estimation and adaptive mesh refinement for aerodynamic flows," in *ADIGMA - A European Initiative on the Development of Adaptive Higher-Order Variational Methods for Aerospace Applications* (N. Kroll, H. Bieler, H. Deconinck, V. Couaillier, H. van der Ven, and K. Sorensen, eds.), pp. 339–353, Berlin, Heidelberg: Springer Berlin Heidelberg, 2010.
4. D. C. Del Rey Fernández, J. E. Hicken, and D. W. Zingg, "Review of summation-by-parts operators with simultaneous approximation terms for the numerical solution of partial differential equations," *Computers & Fluids*, vol. 95, pp. 171–196, 2014.
5. M. Svärd and J. Nordström, "Review of summation-by-parts schemes for initial-boundary-value problems," *Journal of Computational Physics*, vol. 268, pp. 17–38, July 2014.
6. T. C. Fisher, *High-order L2 stable multi-domain finite difference method for compressible flows.* PhD thesis, Purdue University, 2012.
7. T. C. Fisher and M. H. Carpenter, "High-order entropy stable finite difference schemes for nonlinear conservation laws: Finite domains," *Journal of Computational Physics*, vol. 252, pp. 518–557, 2013.
8. M. Parsani, M. H. Carpenter, and E. J. Nielsen, "Entropy stable wall boundary conditions for the three-dimensional compressible Navier-Stokes equations," *Journal of Computational Physics*, vol. 292, pp. 88–113, July 2015.
9. T. Chen and C.-W. Shu, "Entropy stable high order discontinuous Galerkin methods with suitable quadrature rules for hyperbolic conservation laws," *Journal of Computational Physics*, vol. 345, pp. 427–461, Sept. 2017.
10. J. Chan, "On discretely entropy conservative and entropy stable discontinuous Galerkin methods," *Journal of Computational Physics*, vol. 362, pp. 346–374, June 2018.
11. J. Crean, J. E. Hicken, D. C. Del Rey Fernández, D. W. Zingg, and M. H. Carpenter, "Entropy-stable summation-by-parts discretization of the Euler equations on general curved elements," *Journal of Computational Physics*, vol. 356, pp. 410–438, Mar. 2018.
12. K. Mattsson and M. H. Carpenter, "Stable and Accurate Interpolation Operators for High-Order Multiblock Finite Difference Methods," *SIAM Journal on Scientific Computing*, vol. 32, pp. 2298–2320, Jan. 2010.
13. D. A. Kopriva, "A Conservative Staggered-Grid Chebyshev Multidomain Method for Compressible Flows. II. A Semi-Structured Method," *Journal of Computational Physics*, vol. 128, pp. 475–488, Oct. 1996.
14. S. Wang, K. Virta, and G. Kreiss, "High Order Finite Difference Methods for the Wave Equation with Non-conforming Grid Interfaces," *Journal of Scientific Computing*, vol. 68, pp. 1002–1028, Sept. 2016.
15. J. E. Kozdon and L. C. Wilcox, "Stable Coupling of Nonconforming, High-Order Finite Difference Methods," *SIAM Journal on Scientific Computing*, vol. 38, pp. A923–A952, Jan. 2016.
16. T. Lundquist and J. Nordström, "On the suboptimal accuracy of summation-by-parts schemes with non-conforming block interfaces," tech. rep., Linköping University, 2015.
17. L. Friedrich, D. C. Del Rey Fernández, A. R. Winters, G. J. Gassner, D. W. Zingg, and J. Hicken, "Conservative and Stable Degree Preserving SBP Operators for Non-conforming Meshes," *Journal of Scientific Computing*, vol. 75, pp. 657–686, May 2018.
18. G. J. Gassner, "A Skew-Symmetric Discontinuous Galerkin Spectral Element Discretization and Its Relation to SBP-SAT Finite Difference Methods," *SIAM Journal on Scientific Computing*, vol. 35, pp. A1233–A1253, Jan. 2013.
19. D. A. Kopriva and G. J. Gassner, "An Energy Stable Discontinuous Galerkin Spectral Element Discretization for Variable Coefficient Advection Problems," *SIAM Journal on Scientific Computing*, vol. 36, pp. A2076–A2099, Jan. 2014.
20. M. H. Carpenter, T. C. Fisher, E. J. Nielsen, and S. H. Frankel, "Entropy Stable Spectral Collocation Schemes for the Navier–Stokes Equations: Discontinuous Interfaces," *SIAM Journal on Scientific Computing*, vol. 36, pp. B835–B867, Jan. 2014.
21. G. J. Gassner, A. R. Winters, and D. A. Kopriva, "Split form nodal discontinuous Galerkin schemes with summation-by-parts property for the compressible Euler equations," *Journal of Computational Physics*, vol. 327, pp. 39–66, 2016.
22. T. C. Fisher, M. H. Carpenter, J. Nordström, N. K. Yamaleev, and C. Swanson, "Discretely conservative finite-difference formulations for nonlinear conservation laws in split form: Theory and boundary conditions," *Journal of Computational Physics*, vol. 234, pp. 353–375, Feb. 2013.
23. G. J. Gassner, "A kinetic energy preserving nodal discontinuous Galerkin spectral element method: KEP-DGSEM," *International Journal for Numerical Methods in Fluids*, vol. 76, pp. 28–50, Sept. 2014.
24. Y. Abe, I. Morinaka, T. Haga, T. Nonomura, H. Shibata, and K. Miyaji, "Stable, non-dissipative, and conservative flux-reconstruction schemes in split forms," *Journal of Computational Physics*, vol. 353, pp. 193–227, Jan. 2018.
25. G. J. Gassner, A. R. Winters, and D. A. Kopriva, "A well balanced and entropy conservative discontinuous Galerkin spectral element method for the shallow water equations," *Applied Mathematics and Computation*, vol. 272, pp. 291–308, Jan. 2016.
26. M. H. Carpenter, M. Parsani, E. J. Nielsen, and T. C. Fisher, "Towards an Entropy Stable Spectral Element Framework for Computational Fluid Dynamics," in *54th AIAA Aerospace Sciences Meeting*, American Institute of Aeronautics and Astronautics, Jan. 2016.
27. M. Parsani, M. H. Carpenter, T. C. Fisher, and E. J. Nielsen, "Entropy Stable Staggered Grid Discontinuous Spectral Collocation Methods of any Order for the Compressible Navier–Stokes Equations," *SIAM Journal on Scientific Computing*, vol. 38, pp. A3129–A3162, Jan. 2016.
28. L. Friedrich, A. R. Winters, D. C. Del Rey Fernández, G. J. Gassner, M. Parsani, and M. H. Carpenter, "An Entropy Stable h/p Non-Conforming Discontinuous Galerkin Method with the Summation-by-Parts Property," *Journal of Scientific Computing*, vol. 77, pp. 689–725, May 2018.
29. D. C. Del Rey Fernández, *Generalized Summation-by-Parts Operators for First and Second Derivatives.* PhD thesis, University of Toronto (Canada), 2015.
30. J. E. Hicken, D. C. Del Rey Fernández, and D. W. Zingg, "Multidimensional Summation-by-Parts Operators: General Theory and Application to Simplex Elements," *SIAM Journal on Scientific Computing*, vol. 38, pp. A1935–A1958, Jan. 2016.

31. D. C. Del Rey Fernández, J. E. Hicken, and D. W. Zingg, "Simultaneous Approximation Terms for Multi-dimensional Summation-by-Parts Operators," *Journal of Scientific Computing*, vol. 75, pp. 83–110, Aug. 2017.
32. J. Chan, D. C. Del Rey Fernández, and M. H. Carpenter, "Efficient Entropy Stable Gauss Collocation Methods," *SIAM Journal on Scientific Computing*, vol. 41, pp. A2938–A2966, Oct. 2019.
33. M. H. Carpenter, M. Parsani, T. C. Fisher, and E. J. Nielsen, "Entropy Stable Staggered Grid Spectral Collocation for the Burgers and Compressible Navier-Stokes Equations," tech. rep., NASA, 2015.
34. D. C. Del Rey Fernández, J. Crean, M. H. Carpenter, and J. E. Hicken, "Staggered-grid entropy-stable multidimensional summation-by-parts discretizations on curvilinear coordinates," *Journal of Computational Physics (accepted)*, 2019.
35. S. Shadpey and D. W. Zingg, "Energy- and Entropy-Stable Multidimensional Summation-by-Parts Discretizations on Non-Conforming Grids," American Institute of Aeronautics and Astronautics, June 2019. AIAA-2019-3204.
36. F. Bassi and S. Rebay, "High-Order Accurate Discontinuous Finite Element Solution of the 2d Euler Equations," *Journal of Computational Physics*, vol. 138, pp. 251–285, Dec. 1997.
37. Z. J. Wang, "High-order computational fluid dynamics tools for aircraft design," *Philosophical Transactions of the Royal Society A: Mathematical, Physical and Engineering Sciences*, vol. 372, pp. 20130318–20130318, July 2014.
38. M. Vinokur, "Conservation equations of gasdynamics in curvilinear coordinate systems," *Journal of Computational Physics*, vol. 14, pp. 105–125, Feb. 1974.
39. P. D. Thomas and C. K. Lombard, "Geometric Conservation Law and Its Application to Flow Computations on Moving Grids," *AIAA Journal*, vol. 17, pp. 1030–1037, Oct. 1979.
40. J. Chan and L. C. Wilcox, "On discretely entropy stable weight-adjusted discontinuous Galerkin methods: curvilinear meshes," *Journal of Computational Physics*, vol. 378, pp. 366–393, Feb. 2019.
41. M. R. Visbal and D. V. Gaitonde, "On the Use of Higher-Order Finite-Difference Schemes on Curvilinear and Deforming Meshes," *Journal of Computational Physics*, vol. 181, pp. 155–185, Sept. 2002.
42. D. A. Kopriva, "Metric Identities and the Discontinuous Spectral Element Method on Curvilinear Meshes," *Journal of Scientific Computing*, vol. 26, pp. 301–327, Mar. 2006.
43. T. Hughes, L. Franca, and M. Mallet, "A new finite element formulation for computational fluid dynamics: I. Symmetric forms of the compressible Euler and Navier-Stokes equations and the second law of thermodynamics," *Computer Methods in Applied Mechanics and Engineering*, vol. 54, pp. 223–234, Feb. 1986.
44. E. Chiodaroli, "A counterexample to well-posedness of entropy solutions to the compressible euler system," *Journal of Hyperbolic Differential Equations*, vol. 11, no. 03, pp. 493–519, 2014.
45. E. Chiodaroli, C. De Lellis, and O. Kreml, "Global ill-posedness of the isentropic system of gas dynamics," *Communications on Pure and Applied Mathematics*, vol. 68, no. 7, pp. 1157–1190, 2015.
46. K. O. Friedrichs and P. D. Lax, "Systems of conservation equations with a convex extension," *Proceedings of the National Academy of Sciences*, vol. 68, no. 8, pp. 1686–1688, 1971.
47. A. Harten, "On the symmetric form of systems of conservation laws with entropy," *Journal of Computational Physics*, vol. 49, no. 1, pp. 151–164, 1983.
48. C. M. Dafermos, *Hyperbolic Conservation Laws in Continuum Physics*, vol. 325. Springer Berlin Heidelberg, 3 ed., 2010.
49. E. Tadmor, "The Numerical Viscosity of Entropy Stable Schemes for Systems of Conservation Laws. I," *Mathematics of Computation*, vol. 49, p. 91, July 1987.
50. P. G. LeFloch, J. M. Mercier, and C. Rohde, "Fully Discrete, Entropy Conservative Schemes of Arbitrary Order," *SIAM Journal on Numerical Analysis*, vol. 40, pp. 1968–1992, Jan. 2002.
51. P. Lax and B. Wendroff, "Systems of conservation laws," *Communications on Pure and Applied Mathematics*, vol. 13, no. 2, pp. 217–237, 1960.
52. J. Butcher, "A history of Runge-Kutta methods," *Applied Numerical Mathematics*, vol. 20, pp. 247–260, Mar. 1996.
53. F. Ismail and P. L. Roe, "Affordable, entropy-consistent euler flux functions ii: Entropy production at shocks," *Journal of Computational Physics*, vol. 228, no. 15, pp. 5410–5436, 2009.
54. G. Erlebacher, M. Y. Hussaini, and C.-W. Shu, "Interaction of a shock with a longitudinal vortex," *Journal of Fluid Mechanics*, vol. 337, pp. 129–153, Apr. 1997.
55. S. C. Spiegel, H. T. Huynh, J. R. DeBonis, and N. Glenn, "A survey of the isentropic euler vortex problem using high-order methods," in *22nd AIAA Computational Fluid Dynamics Conference, AIAA Aviation*, pp. 1–21, 2015.
56. D. M. Williams and A. Jameson, "Nodal Points and the Nonlinear Stability of High-Order Methods for Unsteady Flow Problems on Tetrahedral Meshes," in *21st AIAA Computational Fluid Dynamics Conference*, (San Diego, CA), American Institute of Aeronautics and Astronautics, June 2013. AIAA 2013-2830.
57. Z. J. Wang, K. Fidkowski, R. Abgrall, F. Bassi, D. Caraeni, A. Cary, H. Deconinck, R. Hartmann, K. Hillewaert, H. T. Huynh, N. Kroll, G. May, P.-O. Persson, B. van Leer, and M. Visbal, "High-order CFD methods: current status and perspective," *International Journal for Numerical Methods in Fluids*, vol. 72, pp. 811–845, July 2013.
58. A. Jameson, "Formulation of Kinetic Energy Preserving Conservative Schemes for Gas Dynamics and Direct Numerical Simulation of One-Dimensional Viscous Compressible Flow in a Shock Tube Using Entropy and Kinetic Energy Preserving Schemes," *Journal of Scientific Computing*, vol. 34, pp. 188–208, Feb. 2008.
59. M. Svärd and H. Özcan, "Entropy-Stable Schemes for the Euler Equations with Far-Field and Wall Boundary Conditions," *Journal of Scientific Computing*, vol. 58, pp. 61–89, Jan. 2014.
60. X. Zhang and C.-W. Shu, "On positivity-preserving high order discontinuous Galerkin schemes for compressible Euler equations on rectangular meshes," *Journal of Computational Physics*, vol. 229, pp. 8918–8934, Nov. 2010.
61. C. Loken, D. Gruner, L. Groer, R. Peltier, N. Bunn, M. Craig, T. Henriques, J. Dempsey, C.-H. Yu, J. Chen, L. J. Dursi, J. Chong, S. Northrup, J. Pinto, N. Knecht, and R. V. Zon, "SciNet: Lessons Learned from Building a Power-efficient Top-20 System and Data Centre," *Journal of Physics: Conference Series*, vol. 256, p. 012026, Nov. 2010.

Appendix A Condition 2 of Definition 2

Here we show that condition 2 of Definition 2, i.e.

$$\mathsf{R}_{\kappa\gamma}^{\mathrm{T}}\hat{\mathsf{B}}_{\kappa\gamma}\mathsf{R}_{\kappa\gamma} = \mathsf{R}_{\kappa\gamma}^{\mathrm{T}}\mathsf{P}_{\kappa\gamma\to I}^{\mathrm{T}}\hat{\mathsf{B}}_{I}\mathsf{P}_{\kappa\gamma\to I}\mathsf{R}_{\kappa\gamma},$$
$$\mathsf{R}_{\nu\gamma}^{\mathrm{T}}\hat{\mathsf{B}}_{\nu\gamma}\mathsf{R}_{\nu\gamma} = \mathsf{R}_{\nu\gamma}^{\mathrm{T}}\mathsf{P}_{\nu\gamma\to I}^{\mathrm{T}}\hat{\mathsf{B}}_{I}\mathsf{P}_{\nu\gamma\to I}\mathsf{R}_{\nu\gamma},$$

holds under mild assumptions. For simplicity we show the proof for an arbitrary element and thus drop the subscripts κ and ν.

Assumption 2 *We assume that the reference element's facet quadrature rule and the intermediate reference interface's facet quadrature rule exactly integrate polynomials of at least degree $s \geq 2r$. Furthermore, we assume that the volume nodal set $S_{\hat{\Omega}}$ and facet nodal set $S_{\hat{\gamma}}$ produce degree r full-column-rank Vandermonde matrices $\hat{\mathsf{V}}_\Omega \in \mathbb{R}^{N\times n_r}$ and $\hat{\mathsf{V}}_\gamma \in \mathbb{R}^{N_\gamma \times n_r}$, respectively.*

Lemma 1 *If Assumption 2 holds, then*

$$\mathsf{R}_\gamma^{\mathrm{T}}\hat{\mathsf{B}}_\gamma\mathsf{R}_\gamma = \mathsf{R}_\gamma^{\mathrm{T}}\mathsf{P}_{\gamma\to I}^{\mathrm{T}}\hat{\mathsf{B}}_I\mathsf{P}_{\gamma\to I}\mathsf{R}_\gamma.$$

Proof Let $\hat{\mathsf{V}}_I \in \mathbb{R}^{N_I\times n_r}$ be the degree r Vandermonde matrix evaluated at the nodal set $S_{\hat{I}}$ (which does not necessarily coincide with $S_{\hat{\gamma}}$). Since $\hat{\mathsf{B}}_I$ and $\hat{\mathsf{B}}_\gamma$ integrate polynomials of at least degree $s \geq 2r$ and the Vandermonde matrices $\hat{\mathsf{V}}_\gamma$ and $\hat{\mathsf{V}}_I$ are each of degree r, then

$$\hat{\mathsf{V}}_\gamma^{\mathrm{T}}\hat{\mathsf{B}}_\gamma\hat{\mathsf{V}}_\gamma = \hat{\mathsf{V}}_I^{\mathrm{T}}\hat{\mathsf{B}}_I\hat{\mathsf{V}}_I.$$

Left-multiplying the right-hand side by $(\hat{\mathsf{V}}_\gamma^\dagger\hat{\mathsf{V}}_\gamma)^{\mathrm{T}} = \mathsf{I}$ and right-multiplying it by $(\hat{\mathsf{V}}_\gamma^\dagger\hat{\mathsf{V}}_\gamma) = \mathsf{I}$, we obtain

$$\hat{\mathsf{V}}_\gamma^{\mathrm{T}}\hat{\mathsf{B}}_\gamma\hat{\mathsf{V}}_\gamma = (\hat{\mathsf{V}}_I\hat{\mathsf{V}}_\gamma^\dagger\hat{\mathsf{V}}_\gamma)^{\mathrm{T}}\hat{\mathsf{B}}_I(\hat{\mathsf{V}}_I\hat{\mathsf{V}}_\gamma^\dagger\hat{\mathsf{V}}_\gamma).$$

Left-multiplying both sides by $(\hat{\mathsf{V}}_\Omega^\dagger)^{\mathrm{T}}$ and right-multiplying them by $\hat{\mathsf{V}}_\Omega^\dagger$ gives

$$(\hat{\mathsf{V}}_\gamma\hat{\mathsf{V}}_\Omega^\dagger)^{\mathrm{T}}\hat{\mathsf{B}}_\gamma(\hat{\mathsf{V}}_\gamma\hat{\mathsf{V}}_\Omega^\dagger) = \Big((\hat{\mathsf{V}}_I\hat{\mathsf{V}}_\gamma^\dagger)(\hat{\mathsf{V}}_\gamma\hat{\mathsf{V}}_\Omega^\dagger)\Big)^{\mathrm{T}}\hat{\mathsf{B}}_I\Big((\hat{\mathsf{V}}_I\hat{\mathsf{V}}_\gamma^\dagger)(\hat{\mathsf{V}}_\gamma\hat{\mathsf{V}}_\Omega^\dagger)\Big).$$

Substituting $\mathsf{R}_\gamma \equiv \hat{\mathsf{V}}_\gamma\hat{\mathsf{V}}_\Omega^\dagger$ and $\mathsf{P}_{\gamma\to I} \equiv \hat{\mathsf{V}}_I\hat{\mathsf{V}}_\gamma^\dagger$ in the above equation leads to

$$\begin{aligned}\mathsf{R}_\gamma^{\mathrm{T}}\hat{\mathsf{B}}_\gamma\mathsf{R}_\gamma &= (\mathsf{P}_{\gamma\to I}\mathsf{R}_\gamma)^{\mathrm{T}}\hat{\mathsf{B}}_I(\mathsf{P}_{\gamma\to I}\mathsf{R}_\gamma),\\ \mathsf{R}_\gamma^{\mathrm{T}}\hat{\mathsf{B}}_\gamma\mathsf{R}_\gamma &= \mathsf{R}_\gamma^{\mathrm{T}}\mathsf{P}_{\gamma\to I}^{\mathrm{T}}\hat{\mathsf{B}}_I\mathsf{P}_{\gamma\to I}\mathsf{R}_\gamma,\end{aligned}$$

which is the desired result. □

Appendix B Proof of Theorem 1

To show that the diagonal-E entropy-conservative scheme (18) and the dense-coupling entropy-conservative scheme (13) are equivalent on affine meshes for SBP operators equipped with facet quadrature rules of degree $s \geq 2r \geq 2p$, we individually deal with the transient, volumetric, and inter-element coupling terms.

The transient terms in (18) and (13) are the same. Furthermore, noting that on affine meshes $\mathsf{N}_{\kappa\gamma,x_i} = n_{\gamma,x_i}\mathsf{I}_{N_{\kappa\gamma}}$ and invoking condition 2 of Definition 2, we can regain the volumetric terms of (13) from the volumetric terms of (18) as follows:

$$\begin{aligned}\left\{\left(-2\tilde{\mathsf{Q}}_{x_i}^{\mathrm{T}} + \sum_{\kappa\gamma}(\tilde{\mathsf{R}}_{\kappa\gamma}^{\mathrm{T}}\tilde{\mathsf{N}}_{\kappa\gamma,x_i}\tilde{\mathsf{B}}_{\kappa\gamma}\tilde{\mathsf{R}}_{\kappa\gamma})\right)\circ\mathsf{F}_{x_i}(\boldsymbol{u}_\kappa,\boldsymbol{u}_\kappa)\right\}\mathbf{1}_\kappa &= \left\{\left(-2\tilde{\mathsf{Q}}_{x_i}^{\mathrm{T}} + \sum_{\kappa\gamma}\tilde{\mathsf{E}}_{x_i}^{(\kappa\kappa)}\right)\circ\mathsf{F}_{x_i}(\boldsymbol{u}_\kappa,\boldsymbol{u}_\kappa)\right\}\mathbf{1}_\kappa\\ &= \left\{\left(-2\tilde{\mathsf{Q}}_{x_i}^{\mathrm{T}} + \tilde{\mathsf{E}}_{x_i}\right)\circ\mathsf{F}_{x_i}(\boldsymbol{u}_\kappa,\boldsymbol{u}_\kappa)\right\}\mathbf{1}_\kappa\\ &= \left\{\left(2\tilde{\mathsf{S}}_{x_i}\right)\circ\mathsf{F}_{x_i}(\boldsymbol{u}_\kappa,\boldsymbol{u}_\kappa)\right\}\mathbf{1}_\kappa,\end{aligned}$$

where we used the property $\mathsf{E}_{x_i} = \sum_{\kappa\gamma}\mathsf{E}_{x_i}^{(\kappa\kappa)}$ in the penultimate step and $\mathsf{S}_{x_i} = -2\mathsf{Q}_{x_i}^{\mathrm{T}} + \mathsf{E}_{x_i}$ in the last step. The last term to consider is the facet coupling terms of the two schemes. We start with the coupling term of the dense-coupling entropy-stable scheme and utilize the property $[\mathsf{R}_\gamma]_{lj} = \delta_{lj},\ \forall\ ji \in \{1,...,N\},\ li \in \{1,...,N_\gamma\}$ of diagonal-E SBP operators. For $ji \in \{1,...,N_\kappa\}$, we have

$$\begin{aligned}\left[\left(\tilde{\mathsf{E}}_{x_i}^{(\kappa\nu)} \circ \mathsf{F}_{x_i}(\boldsymbol{u}_\kappa, \boldsymbol{u}_\nu)\right)\mathbf{1}_\nu\right]_j &= \left[\left((\tilde{\mathsf{R}}_{\kappa\gamma}^{\mathrm{T}} \tilde{\mathsf{P}}_{\kappa\gamma\to I}^{\mathrm{T}} \tilde{\mathsf{N}}_{I,x_i}^{(\kappa)} \tilde{\mathsf{B}}_I \tilde{\mathsf{P}}_{\nu\gamma\to I} \tilde{\mathsf{R}}_{\nu\gamma}) \circ \mathsf{F}_{x_i}(\boldsymbol{u}_\kappa, \boldsymbol{u}_\nu)\right)\mathbf{1}_\nu\right]_j \\ &= \sum_{l=1}^{N_{\kappa\gamma}} \sum_{k=1}^{N_{\kappa I}} \sum_{m=1}^{N_{\nu\gamma}} \delta_{lj} [\mathsf{P}_{\kappa\gamma\to I}]_{kl} [\mathsf{N}_{I,x_i}^{(\kappa)}]_{kk} [\mathsf{B}_I]_{kk} [\mathsf{P}_{\nu\gamma\to I}]_{km} \sum_{n=1}^{N_\nu} \delta_{mn} \boldsymbol{\mathcal{F}}_{x_i}^{*,\mathrm{EC}}([\boldsymbol{u}_\kappa]_j, [\boldsymbol{u}_\nu]_n) \\ &= \sum_{l=1}^{N_{\kappa\gamma}} \sum_{k=1}^{N_{\kappa I}} \sum_{m=1}^{N_{\nu\gamma}} \delta_{lj} [\mathsf{P}_{\kappa\gamma\to I}]_{kl} [\mathsf{N}_{I,x_i}^{(\kappa)}]_{kk} [\mathsf{B}_I]_{kk} [\mathsf{P}_{\nu\gamma\to I}]_{km} \boldsymbol{\mathcal{F}}_{x_i}^{*,\mathrm{EC}}([\boldsymbol{u}_{\kappa\gamma}]_l, [\boldsymbol{u}_{\nu\gamma}]_m),\end{aligned}$$

where we used the properties of the Kronecker delta and substituted $\delta_{lj} \sum_{n=1}^{N_\nu} \delta_{mn} \boldsymbol{\mathcal{F}}_{x_i}^{*,\mathrm{EC}}([\boldsymbol{u}_\kappa]_j, [\boldsymbol{u}_\nu]_n) = \delta_{lj} \boldsymbol{\mathcal{F}}_{x_i}^{*,\mathrm{EC}}([\boldsymbol{u}_{\kappa\gamma}]_l, [\boldsymbol{u}_{\nu\gamma}]_m)$. On affine meshes $\mathsf{N}_{I,x_i}^{(\kappa)} = n_{\gamma,x_i} \mathsf{I}_{N_I}$ and we can write the above expression in matrix form as

$$\begin{aligned}\left(\tilde{\mathsf{E}}_{x_i}^{(\kappa\nu)} \circ \mathsf{F}_{x_i}(\boldsymbol{u}_\kappa, \boldsymbol{u}_\nu)\right)\mathbf{1}_\nu &= n_{\gamma,x_i} \tilde{\mathsf{R}}_{\kappa\gamma}^{\mathrm{T}} \left((\tilde{\mathsf{P}}_{\kappa\gamma\to I}^{\mathrm{T}} \tilde{\mathsf{B}}_I \tilde{\mathsf{P}}_{\nu\gamma\to I}) \circ \mathsf{F}_{x_i}(\boldsymbol{u}_{\kappa\gamma}, \boldsymbol{u}_{\nu\gamma})\right)\mathbf{1}_{\nu\gamma} \\ &= n_{\gamma,x_i} \tilde{\mathsf{R}}_{\kappa\gamma}^{\mathrm{T}} \left((\tilde{\mathsf{B}}_{\kappa\gamma} \tilde{\mathsf{P}}_{I\to\kappa\gamma} \tilde{\mathsf{P}}_{\nu\gamma\to I}) \circ \mathsf{F}_{x_i}(\boldsymbol{u}_{\kappa\gamma}, \boldsymbol{u}_{\nu\gamma})\right)\mathbf{1}_{\nu\gamma} \\ &= n_{\gamma,x_i} \tilde{\mathsf{R}}_{\kappa\gamma}^{\mathrm{T}} \left((\tilde{\mathsf{B}}_{\kappa\gamma} \tilde{\mathsf{P}}_{\nu\gamma\to\kappa\gamma}) \circ \mathsf{F}_{x_i}(\boldsymbol{u}_{\kappa\gamma}, \boldsymbol{u}_{\nu\gamma})\right)\mathbf{1}_{\nu\gamma},\end{aligned}$$

where we used (20), $\mathsf{P}_{\kappa\gamma\to I}^{\mathrm{T}} \mathsf{B}_I = \mathsf{B}_{\kappa\gamma} \mathsf{P}_{I\to\kappa\gamma}$, and (19), $\mathsf{P}_{\nu\gamma\to\kappa\gamma} \equiv \mathsf{P}_{I\to\kappa\gamma} \mathsf{P}_{\nu\gamma\to I}$, in the second and last steps, respectively. Finally, we can pull out the diagonal mass matrix and write the normal as a matrix to obtain

$$\left(\tilde{\mathsf{E}}_{x_i}^{(\kappa\nu)} \circ \mathsf{F}_{x_i}(\boldsymbol{u}_\kappa, \boldsymbol{u}_\nu)\right)\mathbf{1}_\nu = \tilde{\mathsf{R}}_{\kappa\gamma}^{\mathrm{T}} \tilde{\mathsf{N}}_{\kappa\gamma,x_i} \tilde{\mathsf{B}}_{\kappa\gamma} \left(\tilde{\mathsf{P}}_{\nu\gamma\to\kappa\gamma} \circ \mathsf{F}_{x_i}(\boldsymbol{u}_{\kappa\gamma}, \boldsymbol{u}_{\nu\gamma})\right)\mathbf{1}_{\nu\gamma},$$

which is exactly the coupling term in (18).

Appendix C Dense-coupling entropy-conservative scheme – conservation proof (Theorems 2 and 3)

C.1 Element-wise conservation

Lemma 2 *The spatial derivative term in (21) simplifies to*

$$\mathbf{1}_\kappa^{\mathrm{T}} \left(2\mathsf{S}_{x_i} \circ \mathsf{F}_{x_i}^{(\rho)}(\boldsymbol{u}_\kappa, \boldsymbol{u}_\kappa)\right)\mathbf{1}_\kappa = 0, \quad \forall\ i \in \{1, ..., d\}.$$

Proof Since S_{x_i} is a skew-symmetric matrix and $\mathsf{F}_{x_i}^{(\rho)}(\boldsymbol{u}_\kappa, \boldsymbol{u}_\kappa)$ is a symmetric matrix, their Hadamard product, i.e. $\mathsf{S}_{x_i} \circ \mathsf{F}_{x_i}^{(\rho)}(\boldsymbol{u}_\kappa, \boldsymbol{u}_\kappa)$, is a skew-symmetric matrix as well. Therefore, the term above is zero. □

C.2 Global conservation

The proof of Theorem 3 follows from the element-wise conservation theorem (Theorem 2), the symmetry of the flux functions, and the skew-symmetric property $\left(\mathsf{E}_{x_i}^{(\nu\kappa)}\right)^{\mathrm{T}} = -\mathsf{E}_{x_i}^{(\kappa\nu)}$. Using Theorem 2, we add the element-wise conservation equation for element κ to the equivalent equation for its neighbouring

element ν (and drop the terms not associated with the shared facet) to obtain

$$\begin{aligned}
\mathbf{1}_\kappa^{\mathrm{T}}\mathsf{H}_\kappa\frac{\mathrm{d}\boldsymbol{\rho}_\kappa}{\mathrm{d}t}+\mathbf{1}_\nu^{\mathrm{T}}\mathsf{H}_\nu\frac{\mathrm{d}\boldsymbol{\rho}_\nu}{\mathrm{d}t} &= \sum_{i=1}^{d}\mathbf{1}_\kappa^{\mathrm{T}}\left\{\mathsf{E}_{x_i}^{(\kappa\nu)}\circ\mathsf{F}_{x_i}^{(\rho)}(\boldsymbol{u}_\kappa,\boldsymbol{u}_\nu)\right\}\mathbf{1}_\nu+\mathbf{1}_\nu^{\mathrm{T}}\left\{\mathsf{E}_{x_i}^{(\nu\kappa)}\circ\mathsf{F}_{x_i}^{(\rho)}(\boldsymbol{u}_\nu,\boldsymbol{u}_\kappa)\right\}\mathbf{1}_\kappa\\
&= \sum_{i=1}^{d}\mathbf{1}_\kappa^{\mathrm{T}}\left\{\mathsf{E}_{x_i}^{(\kappa\nu)}\circ\mathsf{F}_{x_i}^{(\rho)}(\boldsymbol{u}_\kappa,\boldsymbol{u}_\nu)\right\}\mathbf{1}_\nu+\mathbf{1}_\kappa^{\mathrm{T}}\left\{\left(\mathsf{E}_{x_i}^{(\nu\kappa)}\right)^{\mathrm{T}}\circ\left(\mathsf{F}_{x_i}^{(\rho)}(\boldsymbol{u}_\nu,\boldsymbol{u}_\kappa)\right)^{\mathrm{T}}\right\}\mathbf{1}_\nu\\
&= \sum_{i=1}^{d}\mathbf{1}_\kappa^{\mathrm{T}}\left\{\mathsf{E}_{x_i}^{(\kappa\nu)}\circ\mathsf{F}_{x_i}^{(\rho)}(\boldsymbol{u}_\kappa,\boldsymbol{u}_\nu)\right\}\mathbf{1}_\nu-\mathbf{1}_\kappa^{\mathrm{T}}\left\{\mathsf{E}_{x_i}^{(\kappa\nu)}\circ\mathsf{F}_{x_i}^{(\rho)}(\boldsymbol{u}_\kappa,\boldsymbol{u}_\nu)\right\}\mathbf{1}_\nu\\
&= 0,
\end{aligned}$$

where we took the transpose of the second (scalar) term in the second step and used the properties $\left(\mathsf{F}_{x_i}^{(\rho)}(\boldsymbol{u}_\nu,\boldsymbol{u}_\kappa)\right)^{\mathrm{T}}=\mathsf{F}_{x_i}^{(\rho)}(\boldsymbol{u}_\kappa,\boldsymbol{u}_\nu)$ and $\left(\mathsf{E}_{x_i}^{(\nu\kappa)}\right)^{\mathrm{T}}=-\mathsf{E}_{x_i}^{(\kappa\nu)}$ in the penultimate step. Repeating these steps for all facets in $\Gamma_h=\Gamma_{h,i}$, we arrive at the desired result.

Appendix D Dense-coupling entropy-conservative scheme – entropy conservation proof (Theorems 4 and 5)

D.1 Element-wise entropy conservation

Lemma 3 *The transient term in (22) simplifies to*

$$\boldsymbol{w}_\kappa^{\mathrm{T}}\tilde{\mathsf{H}}\frac{\mathrm{d}\boldsymbol{u}_\kappa}{\mathrm{d}t}=\mathbf{1}_\kappa^{\mathrm{T}}\mathsf{H}\frac{\mathrm{d}\boldsymbol{s}_\kappa}{\mathrm{d}t}.$$

Proof Writing the term in index notation and noting that the H matrix is diagonal, we obtain

$$\boldsymbol{w}_\kappa^{\mathrm{T}}\tilde{\mathsf{H}}\frac{\mathrm{d}\boldsymbol{u}_\kappa}{\mathrm{d}t}=\sum_{j=1}^{N_\kappa}[\boldsymbol{w}_\kappa]_j^{\mathrm{T}}[\mathsf{H}]_{jj}[\frac{\mathrm{d}\boldsymbol{u}_\kappa}{\mathrm{d}t}]_j=\sum_{j=1}^{N_\kappa}[\mathsf{H}]_{jj}[\frac{\mathrm{d}\boldsymbol{s}_\kappa}{\mathrm{d}t}]_j=\mathbf{1}_\kappa^{\mathrm{T}}\mathsf{H}\frac{\mathrm{d}\boldsymbol{s}_\kappa}{\mathrm{d}t},$$

where, for the second equality, we invoked the relation $\boldsymbol{\mathcal{W}}^{\mathrm{T}}\frac{\mathrm{d}\boldsymbol{\mathcal{U}}}{\mathrm{d}t}=\frac{\partial\mathcal{S}}{\partial\boldsymbol{\mathcal{U}}}\cdot\frac{\mathrm{d}\boldsymbol{\mathcal{U}}}{\mathrm{d}t}=\frac{\mathrm{d}\mathcal{S}}{\mathrm{d}t}$ for each node $ji\in\{1,...,N_\kappa\}$. □

Lemma 4 *The spatial derivative term in (22) simplifies to*

$$\boldsymbol{w}_\kappa^{\mathrm{T}}\left(2\tilde{\mathsf{S}}_{x_i}\circ\mathsf{F}_{x_i}(\boldsymbol{u}_\kappa,\boldsymbol{u}_\kappa)\right)\mathbf{1}_\kappa=-\mathbf{1}_\kappa^{\mathrm{T}}\mathsf{E}_{x_i}\boldsymbol{\psi}_{\kappa,x_i},\ \forall\ i\in\{1,...,d\}.$$

Proof The proof relies on the SBP property, the symmetry and the entropy conservation property of the entropy-conservative flux function, and the exactness of the derivative operator for constant functions. Substituting $2\mathsf{S}_{x_i}=\mathsf{S}_{x_i}-\mathsf{S}_{x_i}^{\mathrm{T}}=\mathsf{Q}_{x_i}-\mathsf{Q}_{x_i}^{\mathrm{T}},\ \forall i\in\{1,...,d\}$, we obtain,

$$\begin{aligned}
\boldsymbol{w}_\kappa^{\mathrm{T}}\left(2\tilde{\mathsf{S}}_{x_i}\circ\mathsf{F}_{x_i}(\boldsymbol{u}_\kappa,\boldsymbol{u}_\kappa)\right)\mathbf{1}_\kappa &= \sum_{j=1}^{N_\kappa}\sum_{k=1}^{N_\kappa}2[\boldsymbol{w}_\kappa]_j^{\mathrm{T}}[\mathsf{S}_{x_i}]_{jk}\boldsymbol{\mathcal{F}}_{x_i}^{*,\mathrm{EC}}([\boldsymbol{u}_\kappa]_j,[\boldsymbol{u}_\kappa]_k)\\
&= \sum_{j=1}^{N_\kappa}\sum_{k=1}^{N_\kappa}[\boldsymbol{w}_\kappa]_j^{\mathrm{T}}\Big([\mathsf{Q}_{x_i}]_{jk}-[\mathsf{Q}_{x_i}]_{kj}\Big)\boldsymbol{\mathcal{F}}_{x_i}^{*,\mathrm{EC}}([\boldsymbol{u}_\kappa]_j,[\boldsymbol{u}_\kappa]_k)\\
&= \sum_{j=1}^{N_\kappa}\sum_{k=1}^{N_\kappa}[\boldsymbol{w}_\kappa]_j^{\mathrm{T}}[\mathsf{Q}_{x_i}]_{jk}\boldsymbol{\mathcal{F}}_{x_i}^{*,\mathrm{EC}}([\boldsymbol{u}_\kappa]_j,[\boldsymbol{u}_\kappa]_k)\\
&\quad-\sum_{j=1}^{N_\kappa}\sum_{k=1}^{N_\kappa}[\boldsymbol{w}_\kappa]_k^{\mathrm{T}}[\mathsf{Q}_{x_i}]_{jk}\boldsymbol{\mathcal{F}}_{x_i}^{*,\mathrm{EC}}([\boldsymbol{u}_\kappa]_k,[\boldsymbol{u}_\kappa]_j),
\end{aligned}$$

where we flipped the indices of the second (scalar) term in the last line. Invoking the symmetry of the entropy-conservative flux and Tadmor's condition (from Definition 3), we find

$$\begin{aligned}\boldsymbol{w}_\kappa^{\mathrm{T}}\left(2\tilde{\mathsf{S}}_{x_i}\circ\mathsf{F}_{x_i}(\boldsymbol{u}_\kappa,\boldsymbol{u}_\kappa)\right)\mathbf{1}_\kappa &= \sum_{j=1}^{N_\kappa}\sum_{k=1}^{N_\kappa}\left([\boldsymbol{w}_\kappa]_j-[\boldsymbol{w}_\kappa]_k\right)^{\mathrm{T}}\boldsymbol{\mathcal{F}}_{x_i}^{*,\mathrm{EC}}([\boldsymbol{u}_\kappa]_j,[\boldsymbol{u}_\kappa]_k)[\mathsf{Q}_{x_i}]_{jk}\\ &= \sum_{j=1}^{N_\kappa}\sum_{k=1}^{N_\kappa}\left([\boldsymbol{\psi}_{\kappa,x_i}]_j-[\boldsymbol{\psi}_{\kappa,x_i}]_k\right)[\mathsf{Q}_{x_i}]_{jk}\\ &= \mathbf{1}_\kappa^{\mathrm{T}}\mathsf{Q}_{x_i}^{\mathrm{T}}\boldsymbol{\psi}_{\kappa,x_i}-\mathbf{1}_\kappa^{\mathrm{T}}\mathsf{Q}_{x_i}\boldsymbol{\psi}_{\kappa,x_i}.\end{aligned}$$

Since SBP operators exactly differentiate constant functions, i.e. $\mathsf{Q}_{x_i}\mathbf{1}=\mathbf{0}$, we can drop the first term and add $-\mathbf{1}^{\mathrm{T}}\mathsf{Q}_{x_i}^{\mathrm{T}}\boldsymbol{\psi}_{\kappa,x_i}=0$ to obtain

$$\boldsymbol{w}_\kappa^{\mathrm{T}}\left(2\tilde{\mathsf{S}}_{x_i}\circ\mathsf{F}_{x_i}(\boldsymbol{u}_\kappa,\boldsymbol{u}_\kappa)\right)\mathbf{1}_\kappa=-\mathbf{1}_\kappa^{\mathrm{T}}(\mathsf{Q}_{x_i}^{\mathrm{T}}+\mathsf{Q}_{x_i})\boldsymbol{\psi}_{\kappa,x_i}=-\mathbf{1}_\kappa^{\mathrm{T}}\mathsf{E}_{x_i}\boldsymbol{\psi}_{\kappa,x_i},$$

where we used the SBP property for the last equality. □

D.2 Global entropy conservation

Lemma 5 *Adding the interface coupling term of two neighbouring elements κ and ν in each direction, we obtain*

$$\boldsymbol{w}_\kappa^{\mathrm{T}}\left\{\tilde{\mathsf{E}}_{x_i}^{(\kappa\nu)}\circ\mathsf{F}_{x_i}(\boldsymbol{u}_\kappa,\boldsymbol{u}_\nu)\right\}\mathbf{1}_\nu+\boldsymbol{w}_\nu^{\mathrm{T}}\left\{\tilde{\mathsf{E}}_{x_i}^{(\nu\kappa)}\circ\mathsf{F}_{x_i}(\boldsymbol{u}_\nu,\boldsymbol{u}_\kappa)\right\}\mathbf{1}_\kappa=\mathbf{1}_\kappa^{\mathrm{T}}\mathsf{E}_{x_i}^{(\kappa\kappa)}\boldsymbol{\psi}_{\kappa,x_i}+\mathbf{1}_\nu^{\mathrm{T}}\mathsf{E}_{x_i}^{(\nu\nu)}\boldsymbol{\psi}_{\nu,x_i},\ \forall i\in\{1,...,d\}.$$

Proof The proof relies on the property $\left(\mathsf{E}_{x_i}^{(\nu\kappa)}\right)^{\mathrm{T}}=-\mathsf{E}_{x_i}^{(\kappa\nu)}$, the symmetry and the entropy conservation property of the entropy-conservative flux function, and the exactness of the extrapolation operators for constant functions. Taking the transpose of the second (scalar) term on the left-hand side, we obtain

$$\begin{aligned}&\boldsymbol{w}_\kappa^{\mathrm{T}}\left\{\tilde{\mathsf{E}}_{x_i}^{(\kappa\nu)}\circ\mathsf{F}_{x_i}(\boldsymbol{u}_\kappa,\boldsymbol{u}_\nu)\right\}\mathbf{1}_\nu\\ +\boldsymbol{w}_\nu^{\mathrm{T}}&\left\{\tilde{\mathsf{E}}_{x_i}^{(\nu\kappa)}\circ\mathsf{F}_{x_i}(\boldsymbol{u}_\nu,\boldsymbol{u}_\kappa)\right\}\mathbf{1}_\kappa=\boldsymbol{w}_\kappa^{\mathrm{T}}\left\{\tilde{\mathsf{E}}_{x_i}^{(\kappa\nu)}\circ\mathsf{F}_{x_i}(\boldsymbol{u}_\kappa,\boldsymbol{u}_\nu)\right\}\mathbf{1}_\nu+\mathbf{1}_\kappa\left\{\left(\tilde{\mathsf{E}}_{x_i}^{(\nu\kappa)}\right)^{\mathrm{T}}\circ\left(\mathsf{F}_{x_i}(\boldsymbol{u}_\nu,\boldsymbol{u}_\kappa)\right)^{\mathrm{T}}\right\}\boldsymbol{w}_\nu\\ &=\boldsymbol{w}_\kappa^{\mathrm{T}}\left\{\tilde{\mathsf{E}}_{x_i}^{(\kappa\nu)}\circ\mathsf{F}_{x_i}(\boldsymbol{u}_\kappa,\boldsymbol{u}_\nu)\right\}\mathbf{1}_\nu-\mathbf{1}_\kappa\left\{\tilde{\mathsf{E}}_{x_i}^{(\kappa\nu)}\circ\mathsf{F}_{x_i}(\boldsymbol{u}_\kappa,\boldsymbol{u}_\nu)\right\}\boldsymbol{w}_\nu,\end{aligned}$$

where we used the properties $\left(\mathsf{F}_{x_i}(\boldsymbol{u}_\nu,\boldsymbol{u}_\kappa)\right)^{\mathrm{T}}=\mathsf{F}_{x_i}(\boldsymbol{u}_\kappa,\boldsymbol{u}_\nu)$ and $\left(\mathsf{E}_{x_i}^{(\nu\kappa)}\right)^{\mathrm{T}}=-\mathsf{E}_{x_i}^{(\kappa\nu)}$ in the last step. Switching to index notation and invoking Tadmor's condition, we obtain

$$\begin{aligned}&\boldsymbol{w}_\kappa^{\mathrm{T}}\left\{\tilde{\mathsf{E}}_{x_i}^{(\kappa\nu)}\circ\mathsf{F}_{x_i}(\boldsymbol{u}_\kappa,\boldsymbol{u}_\nu)\right\}\mathbf{1}_\nu+\\ &\boldsymbol{w}_\nu^{\mathrm{T}}\left\{\tilde{\mathsf{E}}_{x_i}^{(\nu\kappa)}\circ\mathsf{F}_{x_i}(\boldsymbol{u}_\nu,\boldsymbol{u}_\kappa)\right\}\mathbf{1}_\kappa=\sum_{j=1}^{N_\kappa}\sum_{k=1}^{N_\nu}\left([\boldsymbol{w}_\kappa]_j-[\boldsymbol{w}_\nu]_k\right)^{\mathrm{T}}\boldsymbol{\mathcal{F}}_{x_i}^{*,\mathrm{EC}}([\boldsymbol{u}_\kappa]_j,[\boldsymbol{u}_\nu]_k)\left[\mathsf{E}_{x_i}^{(\kappa\nu)}\right]_{jk}\\ &=\sum_{j=1}^{N_\kappa}\sum_{k=1}^{N_\nu}\left([\boldsymbol{\psi}_{\kappa,x_i}]_j-[\boldsymbol{\psi}_{\nu,x_i}]_k\right)\left[\mathsf{E}_{x_i}^{(\kappa\nu)}\right]_{jk}.\end{aligned}$$

Switching back to matrix notation and using the property $\left(\mathsf{E}_{x_i}^{(\kappa\nu)}\right)^{\mathrm{T}} = -\mathsf{E}_{x_i}^{(\nu\kappa)}$ again, we have

$$\begin{aligned}
\boldsymbol{w}_\kappa^{\mathrm{T}}\left\{\tilde{\mathsf{E}}_{x_i}^{(\kappa\nu)} \circ \mathsf{F}_{x_i}(\boldsymbol{u}_\kappa, \boldsymbol{u}_\nu)\right\}\mathbf{1}_\nu + \boldsymbol{w}_\nu^{\mathrm{T}}\left\{\tilde{\mathsf{E}}_{x_i}^{(\nu\kappa)} \circ \mathsf{F}_{x_i}(\boldsymbol{u}_\nu, \boldsymbol{u}_\kappa)\right\}\mathbf{1}_\kappa &= \boldsymbol{\psi}_{\kappa,x_i}^{\mathrm{T}}\mathsf{E}_{x_i}^{(\kappa\nu)}\mathbf{1}_\nu - \mathbf{1}_\kappa^{\mathrm{T}}\mathsf{E}_{x_i}^{(\kappa\nu)}\boldsymbol{\psi}_{\nu,x_i} \\
&= \boldsymbol{\psi}_{\kappa,x_i}^{\mathrm{T}}\mathsf{E}_{x_i}^{(\kappa\nu)}\mathbf{1}_\nu + \boldsymbol{\psi}_{\nu,x_i}^{\mathrm{T}}\mathsf{E}_{x_i}^{(\nu\kappa)}\mathbf{1}_\kappa \\
&= \boldsymbol{\psi}_{\kappa,x_i}^{\mathrm{T}}\mathsf{E}_{x_i}^{(\kappa\kappa)}\mathbf{1}_\kappa + \boldsymbol{\psi}_{\nu,x_i}^{\mathrm{T}}\mathsf{E}_{x_i}^{(\nu\nu)}\mathbf{1}_\nu \\
&= \mathbf{1}_\kappa^{\mathrm{T}}\mathsf{E}_{x_i}^{(\kappa\kappa)}\boldsymbol{\psi}_{\kappa,x_i} + \mathbf{1}_\nu^{\mathrm{T}}\mathsf{E}_{x_i}^{(\nu\nu)}\boldsymbol{\psi}_{\nu,x_i},
\end{aligned}$$

where we invoked the properties $\mathsf{E}_{x_i}^{(\kappa\nu)}\mathbf{1}_\nu = \mathsf{E}_{x_i}^{(\kappa\kappa)}\mathbf{1}_\kappa$ and $\mathsf{E}_{x_i}^{(\nu\kappa)}\mathbf{1}_\kappa = \mathsf{E}_{x_i}^{(\nu\nu)}\mathbf{1}_\nu$ (from Section 3.6) in the third line, and the symmetry of $\mathsf{E}_{x_i}^{(\kappa\kappa)}$ and $\mathsf{E}_{x_i}^{(\nu\nu)}$ in the last line. □

Adding the element-wise entropy conservation equation of Theorem 4 for 2 neighbouring elements and dropping the terms not associated with the shared facet, we obtain

$$\begin{aligned}
\mathbf{1}_\kappa^{\mathrm{T}}\mathsf{H}_\kappa\frac{\mathrm{d}s_\kappa}{\mathrm{d}t} + \mathbf{1}_\nu^{\mathrm{T}}\mathsf{H}_\nu\frac{\mathrm{d}s_\nu}{\mathrm{d}t} = \sum_{i=1}^{d} &- \boldsymbol{w}_\kappa^{\mathrm{T}}\left\{\tilde{\mathsf{E}}_{x_i}^{(\kappa\nu)} \circ \mathsf{F}_{x_i}(\boldsymbol{u}_\kappa, \boldsymbol{u}_\nu)\right\}\mathbf{1}_\nu - \boldsymbol{w}_\nu^{\mathrm{T}}\left\{\tilde{\mathsf{E}}_{x_i}^{(\nu\kappa)} \circ \mathsf{F}_{x_i}(\boldsymbol{u}_\nu, \boldsymbol{u}_\kappa)\right\}\mathbf{1}_\kappa \\
&+ \mathbf{1}_\kappa^{\mathrm{T}}\mathsf{E}_{x_i}^{(\kappa\kappa)}\boldsymbol{\psi}_{\kappa,x_i} + \mathbf{1}_\nu^{\mathrm{T}}\mathsf{E}_{x_i}^{(\nu\nu)}\boldsymbol{\psi}_{\nu,x_i}.
\end{aligned}$$

Invoking Lemma 5, we see that the right-hand side is zero. Repeating this step for all facets in $\Gamma_h = \Gamma_{h,i}$, we obtain the desired result of Theorem 5.

Appendix E Dense-coupling entropy-conservative scheme – design-order accuracy (Theorem 6)

To prove Theorem 6, it is sufficient to prove that the penalty term vanishes for $\boldsymbol{\mathcal{F}}_{x_i}^{*,\mathrm{EC}}(\boldsymbol{\mathcal{U}}(\cdot),\boldsymbol{\mathcal{U}}(\cdot)) \in \mathbb{P}_{r_{\min}}(\Omega_\kappa \cup \Omega_\nu)$ w.r.t. x_i, $\forall\, i \in \{1, ..., d\}$. Noting that $\mathsf{E}_{x_i}^{(\kappa\kappa)} = \mathsf{E}_{x_i}^{(\kappa I)}\mathsf{P}_{\kappa\gamma\to I}\mathsf{R}_{\kappa\gamma}$ and $\mathsf{E}_{x_i}^{(\kappa\nu)} = \mathsf{E}_{x_i}^{(\kappa I)}\mathsf{P}_{\nu\gamma\to I}\mathsf{R}_{\nu\gamma}$ (see Section 3.6), for $i \in \{1, ..., d\}$, we can show that

$$\begin{aligned}
&\left[\left\{\tilde{\mathsf{E}}_{x_i}^{(\kappa\nu)} \circ \mathsf{F}_{x_i}(\boldsymbol{u}_\kappa, \boldsymbol{u}_\nu)\right\}\mathbf{1}_\nu\right. \\
&\left. - \left\{\tilde{\mathsf{E}}_{x_i}^{(\kappa\kappa)} \circ \mathsf{F}_{x_i}(\boldsymbol{u}_\kappa, \boldsymbol{u}_\kappa)\right\}\mathbf{1}_\kappa\right]_j &= \left[\left\{(\tilde{\mathsf{E}}_{x_i}^{(\kappa I)}\tilde{\mathsf{P}}_{\nu\gamma\to I}\tilde{\mathsf{R}}_{\nu\gamma}) \circ \mathsf{F}_{x_i}(\boldsymbol{u}_\kappa, \boldsymbol{u}_\nu)\right\}\mathbf{1}_\nu - \right. \\
&&\left.\left\{(\tilde{\mathsf{E}}_{x_i}^{(\kappa I)}\tilde{\mathsf{P}}_{\kappa\gamma\to I}\tilde{\mathsf{R}}_{\kappa\gamma}) \circ \mathsf{F}_{x_i}(\boldsymbol{u}_\kappa, \boldsymbol{u}_\kappa)\right\}\mathbf{1}_\kappa\right]_j \\
&&= \sum_{l=1}^{N_I}[\mathsf{E}_{x_i}^{(\kappa I)}]_{jl}\sum_{k=1}^{N_\nu}[\mathsf{P}_{\nu\gamma\to I}\mathsf{R}_{\nu\gamma}]_{lk}\boldsymbol{\mathcal{F}}_{x_i}^{*,\mathrm{EC}}([\boldsymbol{u}_\kappa]_j, [\boldsymbol{u}_\nu]_k) \\
&&\quad - \sum_{l=1}^{N_I}[\mathsf{E}_{x_i}^{(\kappa I)}]_{jl}\sum_{m=1}^{N_\kappa}[\mathsf{P}_{\kappa\gamma\to I}\mathsf{R}_{\kappa\gamma}]_{lm}\boldsymbol{\mathcal{F}}_{x_i}^{*,\mathrm{EC}}([\boldsymbol{u}_\kappa]_j, [\boldsymbol{u}_\kappa]_m) \\
&&= \sum_{l=1}^{N_I}[\mathsf{E}_{x_i}^{(\kappa I)}]_{jl}\boldsymbol{\mathcal{F}}_{x_i}^{*,\mathrm{EC}}([\boldsymbol{u}_\kappa]_j, [\boldsymbol{u}_I]_l) \\
&&\quad - \sum_{l=1}^{N_I}[\mathsf{E}_{x_i}^{(\kappa I)}]_{jl}\boldsymbol{\mathcal{F}}_{x_i}^{*,\mathrm{EC}}([\boldsymbol{u}_\kappa]_j, [\boldsymbol{u}_I]_l) \\
&&= 0,
\end{aligned}$$

where we used the accuracy properties of $\mathsf{R}_{\kappa\gamma}$, $\mathsf{R}_{\nu\gamma}$, $\mathsf{P}_{\kappa\gamma\to I}$, and $\mathsf{P}_{\nu\gamma\to I}$ to arrive at the penultimate step.

Appendix F Pointwise-coupling entropy-conservative scheme – conservation proof (Theorems 7 and 8)

F.1 Element-wise conservation

The proof of Theorem 7 is as follows. Taking the transpose of the second term on the right-hand side of (23) and noting that $\mathsf{P}_{\kappa\gamma\to I}\mathsf{R}_{\kappa\gamma}\mathbf{1}_\kappa = \mathbf{1}_I$ and $\left(\mathsf{F}_{x_i}^{(\rho)}(\overline{\boldsymbol{u}}_{\kappa I}, \boldsymbol{u}_\kappa)\right)^{\mathrm{T}} = \mathsf{F}_{x_i}^{(\rho)}(\boldsymbol{u}_\kappa, \overline{\boldsymbol{u}}_{\kappa I})$, this term cancels out with the first term. Furthermore, invoking Lemma 2 for the volumetric terms, we arrive at the desired result.

F.2 Global conservation

The proof of Theorem 8 follows from the element-wise conservation theorem (Theorem 7) and the symmetry of the entropy-conservative numerical flux. Using Theorem 7, we add the element-wise conservation equation for two neighbouring elements κ and ν, drop the terms not associated with the shared facet, and use the properties $\mathbf{1}_\kappa^{\mathrm{T}}\mathsf{E}_{x_i}^{(\kappa I)} = \mathbf{1}_I^{\mathrm{T}}\mathsf{B}_I\mathsf{N}_{I,x_i}^{(\kappa)}$ and $\mathbf{1}_\nu^{\mathrm{T}}\mathsf{E}_{x_i}^{(\nu I)} = \mathbf{1}_I^{\mathrm{T}}\mathsf{B}_I\mathsf{N}_{I,x_i}^{(\nu)}$ (from Section 3.6) to obtain

$$\begin{aligned}
\mathbf{1}_\kappa^{\mathrm{T}}\mathsf{H}_\kappa\frac{\mathrm{d}\boldsymbol{\rho}_\kappa}{\mathrm{d}t} + \mathbf{1}_\nu^{\mathrm{T}}\mathsf{H}_\nu\frac{\mathrm{d}\boldsymbol{\rho}_\nu}{\mathrm{d}t} &= \sum_{i=1}^{d} -\mathbf{1}_\kappa^{\mathrm{T}}\mathsf{E}_{x_i}^{(\kappa I)}\boldsymbol{f}_{x_i}^{*,\mathrm{EC},\rho}(\overline{\boldsymbol{u}}_{\kappa I}, \overline{\boldsymbol{u}}_{\nu I}) - \sum_{i=1}^{d}\mathbf{1}_\nu^{\mathrm{T}}\mathsf{E}_{x_i}^{(\nu I)}\boldsymbol{f}_{x_i}^{*,\mathrm{EC},\rho}(\overline{\boldsymbol{u}}_{\nu I}, \overline{\boldsymbol{u}}_{\kappa I}) \\
&= \sum_{i=1}^{d} -\mathbf{1}_I^{\mathrm{T}}\mathsf{N}_{I,x_i}^{(\kappa)}\mathsf{B}_I\boldsymbol{f}_{x_i}^{*,\mathrm{EC},\rho}(\overline{\boldsymbol{u}}_{\kappa I}, \overline{\boldsymbol{u}}_{\nu I}) - \sum_{i=1}^{d}\mathbf{1}_I^{\mathrm{T}}\mathsf{N}_{I,x_i}^{(\nu)}\mathsf{B}_I\boldsymbol{f}_{x_i}^{*,\mathrm{EC},\rho}(\overline{\boldsymbol{u}}_{\nu I}, \overline{\boldsymbol{u}}_{\kappa I}) \\
&= 0,
\end{aligned}$$

where, to arrive at the last step, we used the symmetry of the numerical flux and $\mathsf{N}_{I,x_i}^{(\nu)} = -\mathsf{N}_{I,x_i}^{(\kappa)}$. Repeating these steps for all facets in $\Gamma_h = \Gamma_{h,i}$, we arrive at the desired result.

Appendix G Pointwise-coupling entropy-conservative scheme – entropy conservation proof (Theorems 9 and 10)

G.1 Element-wise entropy conservation

Lemma 6 *The first and second terms on the right-hand side of (24) simplify to*

$$\begin{aligned}
&\sum_{\kappa\gamma} -\boldsymbol{w}_\kappa^{\mathrm{T}}\left\{\tilde{\mathsf{E}}_{x_i}^{(\kappa I)} \circ \mathsf{F}_{x_i}(\boldsymbol{u}_\kappa, \overline{\boldsymbol{u}}_{\kappa I})\right\}\mathbf{1}_I + \\
&\boldsymbol{w}_\kappa^{\mathrm{T}}\tilde{\mathsf{R}}_{\kappa\gamma}^{\mathrm{T}}\tilde{\mathsf{P}}_{\kappa\gamma\to I}^{\mathrm{T}}\left\{(\tilde{\mathsf{E}}_{x_i}^{(\kappa I)})^{\mathrm{T}} \circ \mathsf{F}_{x_i}(\overline{\boldsymbol{u}}_{\kappa I}, \boldsymbol{u}_\kappa)\right\}\mathbf{1}_\kappa = -\mathbf{1}_\kappa^{\mathrm{T}}\mathsf{E}_{x_i}\boldsymbol{\psi}_{\kappa,x_i} + \sum_{\kappa\gamma}\mathbf{1}_I^{\mathrm{T}}\mathsf{N}_{I,x_i}^{(\kappa)}\mathsf{B}_I\overline{\boldsymbol{\psi}}_{\kappa I,x_i}, \quad \forall\ i \in \{1, ..., d\},
\end{aligned}$$

where, as previously defined, $[\overline{\boldsymbol{\psi}}_{\kappa I,x_i}]_l \equiv \psi_{x_i}([\overline{\boldsymbol{u}}_{\kappa I}]_l),\ \forall li \in \{1, ..., N_I\}$ *is the potential flux vector in the* x_i*-direction corresponding to the extrapolated entropy variables* $\boldsymbol{w}_{\kappa I}$*.*

Proof The proof relies on the symmetry and the entropy conservation property of the entropy-conservative flux function and the exactness of the extrapolation operators for constant functions. Using $\boldsymbol{w}_{\kappa I} \equiv$

$\tilde{\mathsf{P}}_{\kappa\gamma\to I}\tilde{\mathsf{R}}_{\kappa\gamma}\boldsymbol{w}_\kappa$, we can show that, for $i \in \{1, ..., d\}$,

$$
\begin{aligned}
&\sum_{\kappa\gamma} -\boldsymbol{w}_\kappa^{\mathrm{T}}\left\{\tilde{\mathsf{E}}_{x_i}^{(\kappa I)} \circ \mathsf{F}_{x_i}(\boldsymbol{u}_\kappa, \overline{\boldsymbol{u}}_{\kappa I})\right\}\mathbf{1}_I + \\
\boldsymbol{w}_\kappa^{\mathrm{T}}\tilde{\mathsf{R}}_{\kappa\gamma}^{\mathrm{T}}\tilde{\mathsf{P}}_{\kappa\gamma\to I}^{\mathrm{T}}\left\{(\tilde{\mathsf{E}}_{x_i}^{(\kappa I)})^{\mathrm{T}} \circ \mathsf{F}_{x_i}(\overline{\boldsymbol{u}}_{\kappa I}, \boldsymbol{u}_\kappa)\right\}\mathbf{1}_\kappa &= \sum_{\kappa\gamma} -\boldsymbol{w}_\kappa^{\mathrm{T}}\left\{\tilde{\mathsf{E}}_{x_i}^{(\kappa I)} \circ \mathsf{F}_{x_i}(\boldsymbol{u}_\kappa, \overline{\boldsymbol{u}}_{\kappa I})\right\}\mathbf{1}_I \\
&\quad + \boldsymbol{w}_{\kappa I}^{\mathrm{T}}\left\{(\tilde{\mathsf{E}}_{x_i}^{(\kappa I)})^{\mathrm{T}} \circ \mathsf{F}_{x_i}(\overline{\boldsymbol{u}}_{\kappa I}, \boldsymbol{u}_\kappa)\right\}\mathbf{1}_\kappa \\
&= \sum_{\kappa\gamma}\sum_{j=1}^{N_\kappa}\sum_{l=1}^{N_I}([\boldsymbol{w}_{\kappa I}]_l - [\boldsymbol{w}_\kappa]_j)^{\mathrm{T}}\boldsymbol{\mathcal{F}}_{x_i}^{*,\mathrm{EC}}([\overline{\boldsymbol{u}}_{\kappa I}]_l, [\boldsymbol{u}_\kappa]_j)[\mathsf{E}_{x_i}^{(\kappa I)}]_{jl} \\
&= \sum_{\kappa\gamma}\sum_{j=1}^{N_\kappa}\sum_{l=1}^{N_I}([\overline{\psi}_{\kappa I, x_i}]_l - [\psi_{\kappa, x_i}]_j)[\mathsf{E}_{x_i}^{(\kappa I)}]_{jl} \\
&= \sum_{\kappa\gamma}\mathbf{1}_\kappa^{\mathrm{T}}\mathsf{E}_{x_i}^{(\kappa I)}\overline{\boldsymbol{\psi}}_{\kappa I, x_i} - \mathbf{1}_I^{\mathrm{T}}(\mathsf{E}_{x_i}^{(\kappa I)})^{\mathrm{T}}\boldsymbol{\psi}_{\kappa, x_i},
\end{aligned}
$$

where we invoked the symmetry of the numerical flux in the second step, and Tadmor's condition in the penultimate step. Using $\mathbf{1}_\kappa^{\mathrm{T}}\mathsf{E}_{x_i}^{(\kappa I)} = \mathbf{1}_I^{\mathrm{T}}\mathsf{N}_{I,x_i}^{(\kappa)}\mathsf{B}_I$ and $\sum_{\kappa\gamma}\mathsf{E}_{x_i}^{(\kappa I)}\mathbf{1}_I = \mathsf{E}_{x_i}^{\mathrm{T}}\mathbf{1}_\kappa$, we obtain

$$
\begin{aligned}
&\sum_{\kappa\gamma} -\boldsymbol{w}_\kappa^{\mathrm{T}}\left\{\tilde{\mathsf{E}}_{x_i}^{(\kappa I)} \circ \mathsf{F}_{x_i}(\boldsymbol{u}_\kappa, \overline{\boldsymbol{u}}_{\kappa I})\right\}\mathbf{1}_I + \\
\boldsymbol{w}_\kappa^{\mathrm{T}}\tilde{\mathsf{R}}_{\kappa\gamma}^{\mathrm{T}}\tilde{\mathsf{P}}_{\kappa\gamma\to I}^{\mathrm{T}}\left\{(\tilde{\mathsf{E}}_{x_i}^{(\kappa I)})^{\mathrm{T}} \circ \mathsf{F}_{x_i}(\overline{\boldsymbol{u}}_{\kappa I}, \boldsymbol{u}_\kappa)\right\}\mathbf{1}_\kappa &= \sum_{\kappa\gamma}\mathbf{1}_I^{\mathrm{T}}\mathsf{N}_{I,x_i}^{(\kappa)}\mathsf{B}_I\overline{\boldsymbol{\psi}}_{\kappa I, x_i} - \mathbf{1}_\kappa^{\mathrm{T}}\mathsf{E}_{x_i}\boldsymbol{\psi}_{\kappa, x_i},
\end{aligned}
$$

which is the desired result. □

G.2 Global entropy conservation

The proof of Theorem 10 follows from the element-wise entropy conservation theorem (Theorem 9), and the symmetry and the entropy conservation property of the entropy-conservative numerical flux. Using Theorem 9, we add the element-wise entropy conservation equation for two neighbouring elements κ and ν and, dropping the terms not associated with the shared facet, we obtain

$$
\begin{aligned}
\mathbf{1}_\kappa^{\mathrm{T}}\mathsf{H}_\kappa\frac{\mathrm{d}\boldsymbol{s}_\kappa}{\mathrm{d}t} + \mathbf{1}_\nu^{\mathrm{T}}\mathsf{H}_\nu\frac{\mathrm{d}\boldsymbol{s}_\nu}{\mathrm{d}t} &= \sum_{i=1}^{d}\mathbf{1}_I^{\mathrm{T}}\mathsf{N}_{I,x_i}^{(\kappa)}\mathsf{B}_I\overline{\boldsymbol{\psi}}_{\kappa I, x_i} + \sum_{i=1}^{d}\mathbf{1}_I^{\mathrm{T}}\mathsf{N}_{I,x_i}^{(\nu)}\mathsf{B}_I\overline{\boldsymbol{\psi}}_{\nu I, x_i} \\
&\quad - \sum_{i=1}^{d}\boldsymbol{w}_{\kappa I}^{\mathrm{T}}\tilde{\mathsf{N}}_{I,x_i}^{(\kappa)}\tilde{\mathsf{B}}_I\boldsymbol{f}_{x_i}^{*,\mathrm{EC}}(\overline{\boldsymbol{u}}_{\kappa I}, \overline{\boldsymbol{u}}_{\nu I}) - \sum_{i=1}^{d}\boldsymbol{w}_{\kappa I}^{\mathrm{T}}\tilde{\mathsf{N}}_{I,x_i}^{(\nu)}\tilde{\mathsf{B}}_I\boldsymbol{f}_{x_i}^{*,\mathrm{EC}}(\overline{\boldsymbol{u}}_{\nu I}, \overline{\boldsymbol{u}}_{\kappa I}) \\
&= \sum_{i=1}^{d}\mathbf{1}_I^{\mathrm{T}}\mathsf{N}_{I,x_i}^{(\kappa)}\mathsf{B}_I(\overline{\boldsymbol{\psi}}_{\kappa I, x_i} - \overline{\boldsymbol{\psi}}_{\nu I, x_i}) - \sum_{i=1}^{d}(\boldsymbol{w}_{\kappa I} - \boldsymbol{w}_{\nu I})^{\mathrm{T}}\tilde{\mathsf{N}}_{I,x_i}^{(\kappa)}\tilde{\mathsf{B}}_I\boldsymbol{f}_{x_i}^{*,\mathrm{EC}}(\overline{\boldsymbol{u}}_{\kappa I}, \overline{\boldsymbol{u}}_{\nu I}),
\end{aligned}
$$

where we used $\mathsf{N}_{I,x_i}^{(\nu)} = -\mathsf{N}_{I,x_i}^{(\kappa)}$ and the symmetry of the numerical flux. Writing the last term in index notation and invoking Tadmor's condition, we see that

$$
\begin{aligned}
(\boldsymbol{w}_{\kappa I} - \boldsymbol{w}_{\nu I})^{\mathrm{T}}\tilde{\mathsf{N}}_{I,x_i}^{(\kappa)}\tilde{\mathsf{B}}_I\boldsymbol{f}_{x_i}^{*,\mathrm{EC}}(\overline{\boldsymbol{u}}_{\kappa I}, \overline{\boldsymbol{u}}_{\nu I}) &= \sum_{l=1}^{N_I}[\mathsf{N}_{I,x_i}^{(\kappa)}]_l[\mathsf{B}_I]_l([\boldsymbol{w}_{\kappa I}]_l - [\boldsymbol{w}_{\nu I}]_l)^{\mathrm{T}}\boldsymbol{\mathcal{F}}_{x_i}^{*,\mathrm{EC}}([\overline{\boldsymbol{u}}_{\kappa I}]_l, [\overline{\boldsymbol{u}}_{\nu I}]_l) \\
&= \sum_{l=1}^{N_I}[\mathsf{N}_{I,x_i}^{(\kappa)}]_l[\mathsf{B}_I]_l([\overline{\boldsymbol{\psi}}_{\kappa I, x_i}]_l - [\overline{\boldsymbol{\psi}}_{\nu I, x_i}]_l) \\
&= \mathbf{1}_I^{\mathrm{T}}\mathsf{N}_{I,x_i}^{(\kappa)}\mathsf{B}_I(\overline{\boldsymbol{\psi}}_{\kappa I, x_i} - \overline{\boldsymbol{\psi}}_{\nu I, x_i}).
\end{aligned}
$$

Plugging this back into the first equation gives

$$\mathbf{1}_\kappa^{\mathrm{T}}\mathsf{H}_\kappa\frac{\mathrm{d}\boldsymbol{s}_\kappa}{\mathrm{d}t}+\mathbf{1}_\nu^{\mathrm{T}}\mathsf{H}_\nu\frac{\mathrm{d}\boldsymbol{s}_\nu}{\mathrm{d}t}=0.$$

Repeating these steps for all facets in $\Gamma_h=\Gamma_{h,i}$, we arrive at the desired result:

$$\sum_{\Omega_\kappa\in\mathcal{T}_h}\mathbf{1}_\kappa^{\mathrm{T}}\mathsf{H}_\kappa\frac{\mathrm{d}\boldsymbol{s}_\kappa}{\mathrm{d}t}=0.$$

Appendix H Pointwise-coupling entropy-conservative scheme – design-order accuracy (Theorem 11)

To prove Theorem 11, it is sufficient to show that the penalty term of (14) vanishes for $\boldsymbol{\mathcal{F}}_{x_i}^{*,\mathrm{EC}}(\boldsymbol{\mathcal{U}}(\cdot),\boldsymbol{\mathcal{U}}(\cdot))$, $\boldsymbol{\mathcal{W}}(\boldsymbol{\mathcal{U}}(\cdot)),\boldsymbol{\mathcal{U}}(\cdot)\in\mathbb{P}_{r_{\min}}(\Omega_\kappa\cup\Omega_\nu)$ w.r.t. $x_i,\ \forall i\in\{1,...,d\}$. First, we show that the first and last terms in the right-hand side of (14) cancel each other. Using $\mathsf{E}_{x_i}^{(\kappa\kappa)}=\mathsf{E}_{x_i}^{(\kappa I)}\mathsf{P}_{\kappa\gamma\to I}\mathsf{R}_{\kappa\gamma}$, the first and last terms can be simplified as follows for $i\in\{1,...,d\}$:

$$\begin{aligned}
&\Bigg[-\left\{\tilde{\mathsf{E}}_{x_i}^{(\kappa I)}\circ\mathsf{F}_{x_i}(\boldsymbol{u}_\kappa,\overline{\boldsymbol{u}}_{\kappa I})\right\}\mathbf{1}_I\\
&+\left\{\tilde{\mathsf{E}}_{x_i}^{(\kappa\kappa)}\circ\mathsf{F}_{x_i}(\boldsymbol{u}_\kappa,\boldsymbol{u}_\kappa)\right\}\mathbf{1}_\kappa\Bigg]_j
=\left[-\left\{\tilde{\mathsf{E}}_{x_i}^{(\kappa I)}\circ\mathsf{F}_{x_i}(\boldsymbol{u}_\kappa,\overline{\boldsymbol{u}}_{\kappa I})\right\}\mathbf{1}_I+\left\{(\tilde{\mathsf{E}}_{x_i}^{(\kappa I)}\tilde{\mathsf{P}}_{\kappa\gamma\to I}\tilde{\mathsf{R}}_{\kappa\gamma})\circ\mathsf{F}_{x_i}(\boldsymbol{u}_\kappa,\boldsymbol{u}_\kappa)\right\}\mathbf{1}_\kappa\right]_j\\
&\quad=-\sum_{l=1}^{N_I}[\mathsf{E}_{x_i}^{(\kappa I)}]_{jl}\boldsymbol{\mathcal{F}}_{x_i}^{*,\mathrm{EC}}([\boldsymbol{u}_\kappa]_j,[\overline{\boldsymbol{u}}_{\kappa I}]_l)\\
&\qquad+\sum_{l=1}^{N_I}[\mathsf{E}_{x_i}^{(\kappa I)}]_{jl}\sum_{k=1}^{N_\kappa}(\mathsf{P}_{\kappa\gamma\to I}\mathsf{R}_{\kappa\gamma})_{lk}\boldsymbol{\mathcal{F}}_{x_i}^{*,\mathrm{EC}}([\boldsymbol{u}_\kappa]_j,[\boldsymbol{u}_\kappa]_k)\\
&\quad=-\sum_{l=1}^{N_I}[\mathsf{E}_{x_i}^{(\kappa I)}]_{jl}\boldsymbol{\mathcal{F}}_{x_i}^{*,\mathrm{EC}}([\boldsymbol{u}_\kappa]_j,[\overline{\boldsymbol{u}}_{\kappa I}]_l)\\
&\qquad+\sum_{l=1}^{N_I}[\mathsf{E}_{x_i}^{(\kappa I)}]_{jl}\boldsymbol{\mathcal{F}}_{x_i}^{*,\mathrm{EC}}([\boldsymbol{u}_\kappa]_j,[\boldsymbol{u}_I]_l),
\end{aligned}$$

where we used the accuracy properties of the extrapolation operators $\mathsf{R}_{\kappa\gamma}$ and $\mathsf{P}_{\kappa\gamma\to I}$ in the last step. Furthermore, since both $\boldsymbol{\mathcal{W}}(\boldsymbol{\mathcal{U}}(\cdot))$ and $\boldsymbol{\mathcal{U}}(\cdot)$ are in the degree $r_{\min}$ polynomial space, the conservative variables evaluated at the extrapolated entropy variables are equal to the extrapolated conservative variables, i.e. $\overline{\boldsymbol{u}}_{\kappa I}=\boldsymbol{u}_I$. Therefore, the two terms in the last line above cancel each other.

Continuing, the second and third term in the right-hand side of (14) simplify, for $i \in \{1, ..., d\}$, to

$$\begin{aligned}
&\left[\tilde{\mathsf{R}}_{\kappa\gamma}^{\mathrm{T}}\tilde{\mathsf{P}}_{\kappa\gamma\to I}^{\mathrm{T}}\left\{(\tilde{\mathsf{E}}_{x_i}^{(\kappa I)})^{\mathrm{T}}\circ\mathsf{F}_{x_i}(\overline{\boldsymbol{u}}_{\kappa I},\boldsymbol{u}_\kappa)\right\}\mathbf{1}_\kappa\right.\\
&\qquad\left.-\tilde{\mathsf{E}}_{x_i}^{(\kappa I)}\boldsymbol{f}_{x_i}^{*,\mathrm{EC}}(\overline{\boldsymbol{u}}_{\kappa I},\overline{\boldsymbol{u}}_{\nu I})\right]_j &&= \left[\tilde{\mathsf{R}}_{\kappa\gamma}^{\mathrm{T}}\tilde{\mathsf{P}}_{\kappa\gamma\to I}^{\mathrm{T}}\left\{(\tilde{\mathsf{R}}_{\kappa\gamma}^{\mathrm{T}}\tilde{\mathsf{P}}_{\kappa\gamma\to I}^{\mathrm{T}}\tilde{\mathsf{N}}_{I,x_i}^{(\kappa)}\tilde{\mathsf{B}}_I)^{\mathrm{T}}\circ\mathsf{F}_{x_i}(\overline{\boldsymbol{u}}_{\kappa I},\boldsymbol{u}_\kappa)\right\}\mathbf{1}_\kappa\right.\\
&&&\qquad\left.-\tilde{\mathsf{R}}_{\kappa\gamma}^{\mathrm{T}}\tilde{\mathsf{P}}_{\kappa\gamma\to I}^{\mathrm{T}}\tilde{\mathsf{N}}_{I,x_i}^{(\kappa)}\tilde{\mathsf{B}}_I\boldsymbol{f}_{x_i}^{*,\mathrm{EC}}(\overline{\boldsymbol{u}}_{\kappa I},\overline{\boldsymbol{u}}_{\nu I})\right]_j\\
&&&= \sum_{l=1}^{N_I}[\mathsf{P}_{\kappa\gamma\to I}\mathsf{R}_{\kappa\gamma}]_{lj}[\mathsf{N}_{I,x_i}^{(\kappa)}\mathsf{B}_I]_{ll}\sum_{k=1}^{N_\kappa}[\mathsf{P}_{\kappa\gamma\to I}\mathsf{R}_{\kappa\gamma}]_{lk}\boldsymbol{\mathcal{F}}_{x_i}^{*,\mathrm{EC}}([\overline{\boldsymbol{u}}_{\kappa I}]_l,[\boldsymbol{u}_\kappa]_k)\\
&&&\quad-\sum_{l=1}^{N_I}[\mathsf{P}_{\kappa\gamma\to I}\mathsf{R}_{\kappa\gamma}]_{lj}[\mathsf{N}_{I,x_i}^{(\kappa)}\mathsf{B}_I]_{ll}\boldsymbol{\mathcal{F}}_{x_i}^{*,\mathrm{EC}}([\overline{\boldsymbol{u}}_{\kappa I}]_l,[\overline{\boldsymbol{u}}_{\nu I}]_l)\\
&&&= \sum_{l=1}^{N_I}[\mathsf{P}_{\kappa\gamma\to I}\mathsf{R}_{\kappa\gamma}]_{lj}[\mathsf{N}_{I,x_i}^{(\kappa)}\mathsf{B}_I]_{ll}\boldsymbol{\mathcal{F}}_{x_i}^{*,\mathrm{EC}}([\overline{\boldsymbol{u}}_{\kappa I}]_l,[\boldsymbol{u}_I]_l)\\
&&&\quad-\sum_{l=1}^{N_I}[\mathsf{P}_{\kappa\gamma\to I}\mathsf{R}_{\kappa\gamma}]_{lj}[\mathsf{N}_{I,x_i}^{(\kappa)}\mathsf{B}_I]_{ll}\boldsymbol{\mathcal{F}}_{x_i}^{*,\mathrm{EC}}([\overline{\boldsymbol{u}}_{\kappa I}]_l,[\overline{\boldsymbol{u}}_{\nu I}]_l),
\end{aligned}$$

where we used the accuracy properties of $\mathsf{R}_{\kappa\gamma}$ and $\mathsf{P}_{\kappa\gamma\to I}$ in the last step. Again, noting that $\overline{\boldsymbol{u}}_{\kappa I} = \overline{\boldsymbol{u}}_{\nu I} = \boldsymbol{u}_I$ (since both $\boldsymbol{\mathcal{W}}(\boldsymbol{\mathcal{U}}(\cdot))$ and $\boldsymbol{\mathcal{U}}(\cdot)$ are in the degree $r_{\min}$ polynomial space), the last line sums to zero.

Appendix I Entropy dissipative term – conservation proof (Theorem 12)

The proof of Theorem 12 is as follows. Invoking the exactness of the extrapolation operators for constant functions (i.e. $\mathsf{P}_{\kappa\gamma\to I}\mathsf{R}_{\kappa\gamma}\mathbf{1}_\kappa = \mathsf{P}_{\nu\gamma\to I}\mathsf{R}_{\nu\gamma}\mathbf{1}_\nu = \mathbf{1}_I$) and the symmetry $\Lambda_I(\boldsymbol{u}_{\kappa I},\boldsymbol{u}_{\nu I};\boldsymbol{n}_I^{(\kappa)}) = \Lambda_I(\boldsymbol{u}_{\nu I},\boldsymbol{u}_{\kappa I};\mathsf{N}_I^{(\nu)})$, we show that

$$\begin{aligned}
&\mathbf{1}_\kappa^{\mathrm{T}}\mathsf{R}_{\kappa\gamma}^{\mathrm{T}}\mathsf{P}_{\kappa\gamma\to I}^{\mathrm{T}}\Lambda_I(\boldsymbol{u}_{\kappa I},\boldsymbol{u}_{\nu I};\boldsymbol{n}_I^{(\kappa)})^{(\rho)}\tilde{\mathsf{B}}_I(\boldsymbol{w}_{\kappa I}-\boldsymbol{w}_{\nu I})+\\
&\mathbf{1}_\nu^{\mathrm{T}}\mathsf{R}_{\nu\gamma}^{\mathrm{T}}\mathsf{P}_{\nu\gamma\to I}^{\mathrm{T}}\Lambda_I(\boldsymbol{u}_{\nu I},\boldsymbol{u}_{\kappa I};\mathsf{N}_I^{(\nu)})^{(\rho)}\tilde{\mathsf{B}}_I(\boldsymbol{w}_{\nu I}-\boldsymbol{w}_{\kappa I}) &&= \mathbf{1}_I^{\mathrm{T}}\Lambda_I(\boldsymbol{u}_{\kappa I},\boldsymbol{u}_{\nu I};\boldsymbol{n}_I^{(\kappa)})^{(\rho)}\tilde{\mathsf{B}}_I\Big[(\boldsymbol{w}_{\kappa I}-\boldsymbol{w}_{\nu I})+(\boldsymbol{w}_{\nu I}-\boldsymbol{w}_{\kappa I})\Big]\\
&&&= 0,
\end{aligned}$$

which is the desired result.

Appendix J Entropy dissipative term – entropy dissipation proof (Theorem 13)

The proof of Theorem 13 is as follows. Using the definitions $\boldsymbol{w}_{\kappa I} \equiv \tilde{\mathsf{P}}_{\kappa\gamma\to I}\tilde{\mathsf{R}}_{\kappa\gamma}\boldsymbol{w}_\kappa$ and $\boldsymbol{w}_{\nu I} \equiv \tilde{\mathsf{P}}_{\nu\gamma\to I}\tilde{\mathsf{R}}_{\nu\gamma}\boldsymbol{w}_\nu$ and $\Lambda_I(\boldsymbol{u}_{\kappa I},\boldsymbol{u}_{\nu I};\boldsymbol{n}_I^{(\kappa)}) = \Lambda_I(\boldsymbol{u}_{\nu I},\boldsymbol{u}_{\kappa I};\mathsf{N}_I^{(\nu)})$, we show that

$$\begin{aligned}
&-\boldsymbol{w}_\kappa^{\mathrm{T}}\tilde{\mathsf{R}}_{\kappa\gamma}^{\mathrm{T}}\tilde{\mathsf{P}}_{\kappa\gamma\to I}^{\mathrm{T}}\Lambda_I(\boldsymbol{u}_{\kappa I},\boldsymbol{u}_{\nu I};\boldsymbol{n}_I^{(\kappa)})\tilde{\mathsf{B}}_I(\boldsymbol{w}_{\kappa I}-\boldsymbol{w}_{\nu I})\\
&-\boldsymbol{w}_\nu^{\mathrm{T}}\tilde{\mathsf{R}}_{\nu\gamma}^{\mathrm{T}}\tilde{\mathsf{P}}_{\nu\gamma\to I}^{\mathrm{T}}\Lambda_I(\boldsymbol{u}_{\nu I},\boldsymbol{u}_{\kappa I};\mathsf{N}_I^{(\nu)})\tilde{\mathsf{B}}_I(\boldsymbol{w}_{\nu I}-\boldsymbol{w}_{\kappa I}) &&= -(\boldsymbol{w}_{\kappa I}-\boldsymbol{w}_{\nu I})^{\mathrm{T}}\Lambda_I(\boldsymbol{u}_{\kappa I},\boldsymbol{u}_{\nu I};\boldsymbol{n}_I^{(\kappa)})\tilde{\mathsf{B}}_I(\boldsymbol{w}_{\kappa I}-\boldsymbol{w}_{\nu I})\\
&&&\leq 0,
\end{aligned}$$

since the matrix $\Lambda_I(\boldsymbol{u}_{\kappa I},\boldsymbol{u}_{\nu I};\boldsymbol{n}_I^{(\kappa)})\tilde{\mathsf{B}}_I$ is symmetric positive semi-definite.

Appendix K Entropy dissipative term – design-order accuracy proof (Theorem 14)

To prove Theorem 14, it is sufficient to show that the interface penalty term (17) vanishes for $\boldsymbol{\mathcal{W}}(\boldsymbol{\mathcal{U}}(\cdot)) \in \mathbb{P}_{r_{\min}}(\Omega_\kappa \cup \Omega_\nu)$ w.r.t. $x_i,\ \forall i \in \{1, ..., d\}$. For $li \in \{1, ..., N_I\}$, we can show that

$$\begin{aligned}
[\boldsymbol{w}_{\kappa I} - \boldsymbol{w}_{\nu I}]_l &= \sum_{j=1}^{N_\kappa} [\mathsf{P}_{\kappa\gamma\to I}\mathsf{R}_{\kappa\gamma}]_{lj}[\boldsymbol{w}_\kappa]_j - \sum_{k=1}^{N_\nu} [\mathsf{P}_{\nu\gamma\to I}\mathsf{R}_{\nu\gamma}]_{lk}[\boldsymbol{w}_\nu]_k \\
&= [\boldsymbol{w}_I]_l - [\boldsymbol{w}_I]_l \\
&= 0,
\end{aligned}$$

where we used the accuracy properties of $\mathsf{R}_{\kappa\gamma}$, $\mathsf{R}_{\nu\gamma}$, $\mathsf{P}_{\kappa\gamma\to I}$, and $\mathsf{P}_{\nu\gamma\to I}$.